

# Enzymatic synthesis of natural and artificial polyprenols

## Dissertation

zur Erlangung des Doktorgrades der Naturwissenschaften  
(Dr. rer. nat.)

der

Naturwissenschaftliche Fakultät II  
Chemie, Physik und Mathematik

der Martin-Luther-Universität  
Halle-Wittenberg

vorgelegt von

Frau M. Sc. Pia Schöne  
geboren am 04.02.1989 in Halle (Saale)

Die vorliegende Arbeit wurde im Zeitraum zwischen November 2013 und Dezember 2017 am Leibniz-Institut für Pflanzenbiochemie in Halle (Saale), in der Abteilung Natur- und Wirkstoffchemie unter der Betreuung von Prof. Dr. Ludger A. Wessjohann angefertigt.



Eingereicht am: 05.09.2018

Verteidigt am: 24.04.2019

Gutachter: 1. Prof. Dr. Ludger A. Wessjohann  
2. Prof. Dr. Ewa Swieżewska

Ich widme diese Arbeit meinen Eltern und meiner Familie, die mir so vieles ermöglicht und mich immer unterstützt haben.

Zwei Dinge sind zu unserer Arbeit nötig: Unermüdliche Ausdauer und die Bereitschaft, etwas, in das man viel Zeit und Arbeit gesteckt hat, wieder wegzuwerfen.

Albert Einstein (1879-1955)

## Table of contents

I.	List of abbreviations .....	v
II.	List of figures .....	ix
III.	List of tables .....	xiv
IV.	Formula directory.....	xvi
1.	Introduction .....	1
1.1.	Objective.....	1
1.2.	Isoprenoids .....	3
1.3.	Polyisoprenoids .....	6
1.4.	Prenyltransferases.....	7
1.4.1.	<i>trans</i> -Prenyltransferases (TPTs) .....	9
1.4.2.	<i>cis</i> -Prenyltransferases (CPTs) .....	10
1.4.2.1.	Medium-chain <i>cis</i> -prenyltransferases .....	12
1.4.2.2.	Long-chain <i>cis</i> -prenyltransferases .....	13
2.	Materials and methods .....	16
2.1.	Materials.....	16
2.1.1.	Chemicals.....	16
2.1.2.	Prenyl diphosphates .....	18
2.1.3.	Solutions, culture media and buffers .....	19
2.1.4.	Consumables .....	23
2.1.5.	Instruments .....	24
2.1.6.	Proteins .....	26
2.1.7.	Oligonucleotides.....	27
2.1.8.	Plasmids.....	28
2.1.9.	<i>E. coli</i> strains.....	28
2.1.10.	Software .....	29
2.2.	Microbiological methods.....	30
2.2.1.	Cultivation of bacteria .....	30
2.3.	Molecular biological methods.....	31
2.3.1.	Plasmid preparation from <i>E. coli</i> .....	31
2.3.2.	Determination of DNA concentration .....	31
2.3.3.	Agarose gel electrophoresis .....	31

2.3.4.	Sequencing of plasmid DNA .....	31
2.3.5.	Transformation .....	32
2.3.6.	Polymerase chain reaction (PCR) .....	32
2.3.6.1.	Site-directed mutagenesis .....	32
2.3.6.2.	Colony PCR.....	33
2.3.6.3.	Truncation of AtCPT .....	34
2.4.	Protein biochemical methods .....	36
2.4.1.	Recombinant protein production.....	36
2.4.1.1.	Recombinant protein production in microtiter plates (MTP) .....	37
2.4.2.	Cell lysis by ultrasonic treatment .....	37
2.4.3.	Cell lysis by osmotic shock.....	37
2.4.3.1.	Cell lysis by osmotic shock in microtiter plates (MTP) .....	38
2.4.4.	Protein purification via immobilized metal ion affinity chromatography (IMAC).....	38
2.4.5.	Protein purification via preparation of periplasmic extracts (AtCPT) .....	39
2.4.6.	Buffer exchange of protein samples via size-exclusion chromatography.....	40
2.4.7.	Dialysis.....	40
2.4.8.	Concentrating of protein samples.....	41
2.4.9.	Determination of the protein concentration .....	41
2.4.10.	Sodium dodecyl sulfate polyacrylamide gel electrophoresis (SDS-PAGE) .....	42
2.4.11.	In-solution tryptic digestion of protein samples .....	43
2.4.12.	In-gel tryptic digestion of protein samples .....	43
2.4.13.	Desalting of peptide fragments.....	44
2.5.	Analytical methods.....	45
2.5.1.	Activity assay for <i>cis</i> -prenyltransferases .....	45
2.5.1.1.	ThkCPT activity assay in a biphasic system.....	46
2.5.1.2.	ThkCPT activity assay with alternative bivalent cations.....	46
2.5.1.3.	ThkCPT activity assay with crude extracts.....	46
2.5.1.4.	Activity assay in microtiter plates (MTP).....	47
2.5.2.	Thin layer chromatography (TLC) for chain length determination .....	47
2.5.3.	High performance liquid chromatography (HPLC) analytics .....	47
2.5.3.1.	HPLC analysis of polyprenols with MANT-O-GPP as starter substrate.....	48
2.5.3.2.	Fractionation of products .....	49
2.5.4.	Sample preparation via solid phase extraction (SPE).....	50
2.5.5.	HR-ESI-MS analysis .....	50
2.5.6.	Analysis of peptide fragments via LC-ESI-MS (AtCPT) .....	51

---

3.	<i>Thermococcus kodakaraensis</i> CPT .....	52
3.1.	General information .....	52
3.2.	Results and discussion .....	52
3.2.1.	Removal of C-terminal poly-histidine tag in ThkCPT .....	52
3.2.2.	Production and purification of recombinant ThkCPT protein .....	53
3.2.3.	MANT-O-GPP as fluorescence marker for HPLC analyses .....	54
3.2.3.1.	Emission spectrum of MANT-O-GPP .....	54
3.2.3.2.	HPLC analysis with MANT-O-GPP .....	55
3.2.4.	Natural and artificial substrates .....	55
3.2.4.1.	Current issue .....	55
3.2.4.2.	Substrate conversion .....	56
3.2.5.	Modulation of the product chain-length .....	60
3.2.5.1.	Adjustment of assay conditions .....	60
3.2.5.2.	Challenges in the elongation of prenyl diphosphates with BPP .....	69
3.2.5.3.	Generation of variants .....	72
3.2.6.	Adaption of the assay to high-throughput conditions .....	81
3.2.7.	HR-ESI-MS analysis of reaction products .....	83
3.3.	Conclusions .....	85
4.	<i>Arabidopsis thaliana</i> CPT .....	88
4.1.	General information .....	88
4.2.	Results and discussion .....	88
4.2.1.	Truncation of AtCPT .....	88
4.2.2.	Production and purification of recombinant AtCPT protein .....	89
4.2.2.1.	Preparation of periplasmic extracts .....	89
4.2.2.2.	Cell lysis by ultrasonic treatment and purification of full-length and truncated AtCPT via IMAC .....	90
4.2.3.	Analysis of AtCPT peptide fragments .....	92
4.2.4.	Substrate conversion with full-length AtCPT .....	93
4.3.	Conclusions .....	95
5.	Summary .....	97
6.	Zusammenfassung .....	99
7.	List of References .....	xvi
8.	Appendix .....	xxxix
8.1.	MANT-O-Geraniol calibration line (calculations) .....	xxxix
8.2.	Amino acid sequences .....	xxxix

## Table of contents

---

8.3.	Characteristics of the used bivalent cations.....	xxxv
8.4.	Proportion of full-length AtCPT in gel bands and in solution.....	xxxv
8.5.	HPLC analyses (fractions after SPE).....	xxxvi
8.6.	HR-ESI-MS analyses .....	xxxviii
8.7.	In-house designation of experiments.....	xlix
Acknowledgement .....		li
Curriculum vitae .....		liii
Statutory declaration/Eidesstattliche Erklärung.....		lvi

## I. List of abbreviations

1-BuOH	1-Butanol
4HB	4-Hydroxybenzoate
AACT	Acetoacetyl-CoA thiolase
AGC	Acquired gain control
AI	Auto induction
APS	Ammonium peroxodisulfate
AtCPT	<i>Arabidopsis thaliana cis</i> -prenyltransferase
BPP	3-Butenyl diphosphate
Br-BPP	3-Bromo-3-butenyl diphosphate
BSA	Bovine serum albumin
Calc.	Calculated
CBP	CPT-binding protein
CDP-ME	4-Diphosphocytidyl-2-C-methyl-D-erythritol
CDP-MEP	4-Diphosphocytidyl-2-C-methyl-D-erythritol 2-phosphate
Cl-BPP	3-Chloro-3-butenyl diphosphate
CMK	4-(Cytidine 5'-diphospho)-2-C-methyl-D-erythritol kinase
CoA	Coenzyme A
CPT	<i>cis</i> -Prenyltransferase
DDA	Data dependent acquisition
DDPP	Dehydrololichyl diphosphate
DDPPS	Dehydrololichyl diphosphate synthase
DMAPP	Dimethylallyl diphosphate
DNA	Deoxyribonucleic acid
dNTP	Deoxynucleotide triphosphate
DPMD	5-Diphosphomevalonate decarboxylase
DPP	Decaprenyl diphosphate
DPPS	Decaprenyl diphosphate synthase
DRL	1-Deoxy-D-xylulose 5-phosphate reductoisomerase-like enzyme
DTT	Dithiothreitol
DXP	1-Deoxy-D-xylulose 5-phosphate



DXR	1-Deoxy-D-xylulose 5-phosphate reductoisomerase
DXS	1-Deoxy-D-xylulose 5-phosphate synthase
<i>E. coli</i>	<i>Escherichia coli</i>
EDTA	Ethylenediaminetetraacetic acid
ESI	Electrospray ionization
FDR	False discovery rate
FMN	Flavine mononucleotide
FPP	Farnesyl diphosphate
FPPS	Farnesyl diphosphate synthase
FTMS	Fourier transform mass spectrometry
fw	Forward
GAP	D-Glyceraldehyde 3-phosphate
GFPP	Geranylarnesyl diphosphate
GFPPS	Geranylarnesyl diphosphate synthase
GGPP	Geranylgeranyl diphosphate
GGPPS	Geranylgeranyl diphosphate synthase
GPP	Geranyl diphosphate
GPPS	Geranyl diphosphate synthase
GTP	Guanosine triphosphate
HDR	4-Hydroxy-3-methylbut-2-enyl diphosphate reductase
HDS	4-Hydroxy-3-methylbut-2-enyl diphosphate synthase
HEPES	4-(2-Hydroxyethyl)-1-piperazineethanesulfonic acid
HepPP	Heptaprenyl diphosphate
HepPPS	Heptaprenyl diphosphate synthase
HexPP	Hexaprenyl diphosphate
HexPPS	Hexaprenyl diphosphate synthase
HMBPP	4-Hydroxy-3-methylbut-2-enyl diphosphate
HMG-CoA	3-Hydroxy-3-methylglutaryl-CoA
HMGR	3-Hydroxy-3-methylglutaryl-CoA reductase
HMGS	3-Hydroxy-3-methylglutaryl-CoA synthase
HPLC	High performance liquid chromatography
HR	High resolution

HESI	Heated electrospray ionization
HTS	High-throughput screening
IDI	IPP/DMAPP isomerase
IMAC	Immobilized metal ion affinity chromatography
IPTG	Isopropyl $\beta$ -D-1-thiogalactopyranoside
IPP	Isopentenyl diphosphate
LB	Lysogeny broth
LTQ	Linear trap quadrupole
LU	Luminescence units
MANT-O-GPP	(2 <i>E</i> ,6 <i>E</i> )-8- <i>O</i> -( <i>N</i> -Methylanthranyl)-3,7-dimethyl-2,6-octandien-1-diphosphate
MANT-O-nor FPP	(2 <i>E</i> ,6 <i>E</i> ,10 <i>Z</i> )-12- <i>O</i> -( <i>N</i> -Methylanthranyl)-7,11-dimethyl-2,6,10-dodecatrien-1-diphosphate
MaxIT	Maximal injection time
MCT	2- <i>C</i> -Methyl- <i>D</i> -erythritol 4-phosphate cytidyltransferase
MDS	2- <i>C</i> -Methyl- <i>D</i> -erythritol 2,4-cyclodiphosphate synthase
MEcPP	2- <i>C</i> -Methyl- <i>D</i> -erythritol 2,4-cyclodiphosphate
MeOH	Methanol
MEP	2- <i>C</i> -Methyl- <i>D</i> -erythritol 4-phosphate
MS	Mass spectrometry
MTP	Microtiter plate
MVA	Mevalonate
MVK	Mevalonate kinase
MVP	5-Phosphomevalonate
MVPP	5-Diphosphomevalonate
<i>m/z</i>	Mass-to-charge ratio
NADPH	Nicotinamide adenine dinucleotide phosphate
NTA	Nitrilotriacetic acid
OD	Optical density
OPP	Octaprenyl diphosphate
OPPS	Octaprenyl diphosphate synthase
PD	Protein desalting

PMSF	Phenylmethane sulfonyl fluoride
PMVK	5-Phosphomevalonate kinase
ppm	Parts per million
PPP	Polyprenyl diphosphate
PPPS	Polyprenyl diphosphate synthase
PSM	Peptide spectrum match
PT	Prenyltransferase
re	Reverse
RP	Reversed phase
SDS	Sodium dodecyl sulfate
SDS-PAGE	Sodium dodecyl sulfate polyacrylamide gel electrophoresis
SEC	Size-exclusion chromatography
SOC	Super optimal broth with catabolite repression
SPE	Solid phase extraction
SPP	Solanesyl diphosphate
SPPS	Solanesyl diphosphate synthase
SV	Solvent
TEMED	Tetramethylethylenediamine
ThkCPT	<i>Thermococcus kodakaraensis cis</i> -prenyltransferase
TLC	Thin layer chromatography
T <sub>m</sub>	Melting temperature
TPT	<i>trans</i> -Prenyltransferase
Tris	Tris(hydroxymethyl)aminomethane
UPP	Undecaprenyl diphosphate
UPPS	Undecaprenyl diphosphate synthase
v/v	Volume per volume
w/v	Weight per volume
WT	Wild type

## II. List of figures

<b>Figure 1</b> The fundamental building blocks DMAPP and IPP which can be interconverted by the IPP/DMAPP isomerase (IDI). .....	3
<b>Figure 2</b> MEP (left) and MVA (right) pathway.....	4
<b>Figure 3</b> Classification of linear prenyltransferases. ....	9
<b>Figure 4</b> Sequential ionization-condensation-elimination mechanism. ....	10
<b>Figure 5</b> Comparison of the crystal structures from a TPT (left, avian FPPS <sup>[58]</sup> , PDB code: 1FPS) and a CPT (right, <i>M. luteus</i> B-P 26 UPPS <sup>[69]</sup> , PDB code: 1F75).....	11
<b>Figure 6</b> Concerted condensation-elimination mechanism.....	11
<b>Figure 7</b> Comparison of the crystal structures of the open (PDB code: 3QAS <sup>[74]</sup> , yellow) and the closed (PDB code: 1X06 <sup>[73]</sup> , blue) form of the EcUPPS in complex with Mg <sup>2+</sup> (magenta sphere) and the substrate analogue farnesyl thiopyrophosphate (shown as sticks, carbon: green, sulfur: yellow, phosphate: orange, oxygen: red). ....	12
<b>Figure 8</b> Schematic presentation of the transition state during the enzymatic condensation of IPP with FPP including the proposed catalytic diad Asn74 and Glu73.....	13
<b>Figure 9</b> Proposed model of long-chain rubber CPT and CBP complex on the surface of rubber particles. ....	15
<b>Figure 10</b> Schematic representation of the poly-histidine (blue) binding to Ni <sup>2+</sup> -NTA (red)...	39
<b>Figure 11</b> SDS-PAGE gel with Coomassie staining of the purification steps of ThkCPT.....	54
<b>Figure 12</b> Excitation (black line) and emission (dashed black line) spectra of MANT-O-Geraniol in MeOH.....	54
<b>Figure 13</b> HPLC analysis of MANT-O-Geraniol using stocks with different concentrations. ...	55
<b>Figure 14</b> Reaction scheme of the enzymatic conversion of MANT-O-GPP and different elongation substrates (as stated in the picture), leading to fluorescent labeled polyprenols with distinct chain lengths. ....	57
<b>Figure 15</b> HPLC chromatograms of the products of a ThkCPT reaction with MANT-O-GPP and (A) IPP, (B) BPP, (C) Br-BPP or (D) Cl-BPP as elongation substrates.....	58
<b>Figure 16</b> Comparison of the used homoallylic substrates which are shown in ball & stick presentation. ....	59
<b>Figure 17</b> HPLC chromatograms of the products of a ThkCPT reaction with MANT-O-GPP and IPP with (black) or without (blue) Triton X-100. ....	61

<b>Figure 18</b> HPLC chromatograms of the products of a ThkCPT reaction at different incubation times with MANT-O-GPP and (A) IPP or (B) Cl-BPP as elongation substrates. ....	61
<b>Figure 19</b> HPLC chromatograms of the products of a ThkCPT reaction in a purely aqueous system or in a biphasic system with MANT-O-GPP and (A) IPP or (B) Cl-BPP as elongation substrates. ....	63
<b>Figure 20</b> HPLC chromatograms of the products of a ThkCPT reaction with MANT-O-GPP and IPP using different bivalent cations. ....	66
<b>Figure 21</b> HPLC chromatograms of the products of a ThkCPT reaction with MANT-O-GPP and Cl-BPP using different bivalent cations. ....	68
<b>Figure 22</b> Model of the active site during catalysis showing (A) the first attachment of BPP to MANT-O-GPP and (B) the problematic further addition of BPP units to the first formed product which contains a less voluminous substituent at the C3 position. ....	70
<b>Figure 23</b> Conversion of the alternative allylic substrate MANT-O-nor FPP with BPP or IPP..	70
<b>Figure 24</b> HPLC chromatograms of the products of a ThkCPT reaction with MANT-O-nor FPP and BPP (red) or IPP (yellow and blue) as elongation substrates. ....	71
<b>Figure 25</b> Comparison of the homology model of ThkCPT (green) and the crystal structure of EcUPPS (PDB code: 1X06 <sup>[73]</sup> , yellow). ....	72
<b>Figure 26</b> Active sites in the homology models (green) of ThkCPT variants achieved by site-directed mutagenesis in complex with Mg <sup>2+</sup> (magenta sphere) and IPP (shown as sticks, carbon: grey, phosphate: orange, oxygen: red). ....	74
<b>Figure 27</b> HPLC chromatograms of the products of the reaction with MANT-O-GPP and IPP or BPP catalyzed by different ThkCPT variants. ....	75
<b>Figure 28</b> Comparison of the structures of the hydrophobic tunnels in the homology models of ThkCPT variants. ....	77
<b>Figure 29</b> HPLC chromatograms of the products of the reaction with MANT-O-GPP and IPP or Cl-BPP catalyzed by different ThkCPT variants. ....	78
<b>Figure 30</b> Schematic representation of the HTS procedure including enzyme production and substrate conversion in microtiter plates. ....	81
<b>Figure 31</b> SDS-PAGE gel with Coomassie staining indicating ThkCPT production in AI medium in MTPs. ....	82
<b>Figure 32</b> TLC analysis of the products formed by ThkCPT expressed in MTPs with FPP and IPP as substrates. ....	82

<b>Figure 33</b> SDS-PAGE gel with Coomassie staining of the periplasmic preparation steps for enrichment of AtCPT. ....	90
<b>Figure 34</b> SDS-PAGE gel with Coomassie staining of the purification steps of AtCPT. ....	91
<b>Figure 35</b> SDS-PAGE gel with Coomassie staining of the purification steps of AtCPT_Δ33.....	92
<b>Figure 36</b> SDS-PAGE gel with Coomassie staining of the enriched AtCPT fraction.....	92
<b>Figure 37</b> Reaction scheme of the enzymatic conversion of FPP and IPP, leading to polyprenols with distinct chain lengths. ....	93
<b>Figure 38</b> TLC analysis of the products formed by AtCPT with FPP and IPP as substrates.....	94
<b>Figure 39</b> HPLC chromatogram of the products of an AtCPT reaction with MANT-O-GPP and IPP.....	95
<b>Figure A1</b> Amino acid sequences of the used <i>cis</i> -prenyltransferases. ....	xxxiv
<b>Figure A2</b> HPLC chromatogram of ThkCPT products recovered from SPE extraction. ....	xxxvi
<b>Figure A3</b> HPLC chromatogram of ThkCPT products recovered from SPE extraction. ....	xxxvii
<b>Figure A4</b> HR-ESI-MS spectrum of SPE product fraction 1 of the ThkCPT reaction with MANT-O-GPP and IPP which shows the $[M+H]^+$ ion ( $C_{23}H_{34}O_3N$ ) corresponding to the 1-fold elongated reaction product. ....	xxxviii
<b>Figure A5</b> HR-ESI-MS spectrum of SPE product fraction 2 of the ThkCPT reaction with MANT-O-GPP and IPP which shows the $[M+H]^+$ ion ( $C_{28}H_{42}O_3N$ ) corresponding to the 2-fold elongated reaction product. ....	xxxviii
<b>Figure A6</b> HR-ESI-MS spectrum of SPE product fraction 3 of the ThkCPT reaction with MANT-O-GPP and IPP which shows the $[M+H]^+$ ion ( $C_{33}H_{50}O_3N$ ) corresponding to the 3-fold elongated reaction product. ....	xxxix
<b>Figure A7</b> HR-ESI-MS spectrum of SPE product fraction 4 of the ThkCPT reaction with MANT-O-GPP and IPP which shows the $[M+H]^+$ ion ( $C_{38}H_{58}O_3N$ ) corresponding to the 4-fold elongated reaction product. ....	xxxix
<b>Figure A8</b> HR-ESI-MS spectrum of SPE product fraction 5 of the ThkCPT reaction with MANT-O-GPP and IPP which shows the $[M+H]^+$ ion ( $C_{43}H_{66}O_3N$ ) corresponding to the 5-fold elongated reaction product. ....	xl
<b>Figure A9</b> HR-ESI-MS spectrum of SPE product fraction 6 of the ThkCPT reaction with MANT-O-GPP and IPP which shows the $[M+H]^+$ ion ( $C_{48}H_{74}O_3N$ ) corresponding to the 6-fold elongated reaction product. ....	xl

- Figure A10** HR-ESI-MS spectrum of SPE product fraction 7 of the ThkCPT reaction with MANT-O-GPP and IPP which shows the  $[M+H]^+$  ion ( $C_{53}H_{82}O_3N$ ) corresponding to the 7-fold elongated reaction product. ....xli
- Figure A11** HR-ESI-MS spectrum of SPE product fraction 8 of the ThkCPT reaction with MANT-O-GPP and IPP which shows the  $[M+H]^+$  ion ( $C_{58}H_{90}O_3N$ ) corresponding to the 8-fold elongated reaction product. ....xli
- Figure A12** HR-ESI-MS spectrum of SPE product fraction 9 of the ThkCPT reaction with MANT-O-GPP and IPP which shows the  $[M+H]^+$  ion ( $C_{63}H_{98}O_3N$ ) corresponding to the 9-fold elongated reaction product. ....xlii
- Figure A13** HR-ESI-MS spectrum of SPE product fraction 10 of the ThkCPT reaction with MANT-O-GPP and IPP which shows the  $[M+H]^+$  ion ( $C_{68}H_{106}O_3N$ ) corresponding to the 10-fold elongated reaction product. ....xlii
- Figure A14** HR-ESI-MS spectrum of SPE product fraction 11 of the ThkCPT reaction with MANT-O-GPP and IPP which shows the  $[M+H]^+$  ion ( $C_{73}H_{114}O_3N$ ) corresponding to the 11-fold elongated reaction product. ....xliii
- Figure A15** HR-ESI-MS spectrum of SPE product fraction 12 of the ThkCPT reaction with MANT-O-GPP and IPP which shows the  $[M+H]^+$  ion ( $C_{78}H_{122}O_3N$ ) corresponding to the 12-fold elongated reaction product. ....xliii
- Figure A16** HR-ESI-MS spectrum of SPE product fraction 13 of the ThkCPT reaction with MANT-O-GPP and IPP which shows the  $[M+H]^+$  ion ( $C_{83}H_{130}O_3N$ ) corresponding to the 13-fold elongated reaction product.. ....xliv
- Figure A17** HR-ESI-MS spectrum of the  $[M+H]^+$  ion ( $C_{22}H_{31}O_3NCl$ ) of the ThkCPT reaction with MANT-O-GPP and Cl-BPP constituting the 1-fold elongated product. ....xlv
- Figure A18** HR-ESI-MS spectrum of the  $[M+H]^+$  ion ( $C_{26}H_{36}O_3NCl_2$ ) of the ThkCPT reaction with MANT-O-GPP and Cl-BPP constituting the 2-fold elongated product. ....xlv
- Figure A19** HR-ESI-MS spectrum of the  $[M+H]^+$  ion ( $C_{30}H_{41}O_3NCl_3$ ) of the ThkCPT reaction with MANT-O-GPP and Cl-BPP constituting the 3-fold elongated product. ....xlvi
- Figure A20** HR-ESI-MS spectrum of the  $[M+H]^+$  ion ( $C_{34}H_{46}O_3NCl_4$ ) of the ThkCPT reaction with MANT-O-GPP and Cl-BPP constituting the 4-fold elongated product. ....xlvi
- Figure A21** HR-ESI-MS spectrum of the  $[M+H]^+$  ion ( $C_{38}H_{51}O_3NCl_5$ ) of the ThkCPT reaction with MANT-O-GPP and Cl-BPP constituting the 5-fold elongated product. ....xlvii

- Figure A22** HR-ESI-MS spectrum of the  $[M+H]^+$  ion ( $C_{42}H_{56}O_3NCl_6$ ) of the ThkCPT reaction with MANT-O-GPP and Cl-BPP constituting the 6-fold elongated product. ....xlvi
- Figure A23** HR-ESI-MS spectrum of the  $[M+H]^+$  ion ( $C_{46}H_{61}O_3NCl_7$ ) of the ThkCPT reaction with MANT-O-GPP and Cl-BPP constituting the 7-fold elongated product. ....xlvii
- Figure A24** HR-ESI-MS spectrum of the  $[M+H]^+$  ion ( $C_{50}H_{65}O_3NCl_8$ ) of the ThkCPT reaction with MANT-O-GPP and Cl-BPP constituting the 8-fold elongated product. ....xlviii



### III. List of tables

<b>Table 1</b> Used chemicals.....	16
<b>Table 2</b> Used prenyl diphosphates.....	18
<b>Table 3</b> Compositions of used solutions, culture media and buffers. ....	20
<b>Table 4</b> Used consumables.....	23
<b>Table 5</b> Used devices.....	24
<b>Table 6</b> Used proteins. FDU: FastDigest unit. ....	26
<b>Table 7</b> Used oligonucleotides for site-directed mutagenesis and sequencing. ....	27
<b>Table 8</b> Used plasmids.....	28
<b>Table 9</b> Used <i>E. coli</i> strains.....	28
<b>Table 10</b> Used software. ....	29
<b>Table 11</b> Components used in the site-directed mutagenesis PCR reactions. ....	32
<b>Table 12</b> PCR program for site-directed mutagenesis. ....	33
<b>Table 13</b> Components used in the colony PCR reactions. ....	33
<b>Table 14</b> Cycling program for colony PCR. ....	34
<b>Table 15</b> Components used in the PCR to truncate the AtCPT gene. ....	34
<b>Table 16</b> PCR program used to truncate the AtCPT gene.....	35
<b>Table 17</b> Components used in enzymatic restriction digestion.....	35
<b>Table 18</b> Components used for the ligation of fragment and vector. ....	36
<b>Table 19</b> Composition of the gels for SDS-PAGE (description for 2 gels). ....	42
<b>Table 20</b> Summary of the results obtained by medium engineering. ....	69
<b>Table 21</b> Summary of the results obtained by genetic engineering.....	80
<b>Table 22</b> HR-ESI-MS analysis of the product alcohols (ThkCPT reaction with MANT-O-GPP and the homoallylic substrate IPP at 65°C reaction temperature after diphosphate hydrolysis) in the positive ion mode. ....	84
<b>Table 23</b> HR-ESI-MS analysis of the product alcohols (ThkCPT reaction with MANT-O-GPP and the homoallylic substrate Cl-BPP at 65°C reaction temperature after diphosphate hydrolysis) in the positive ion mode.....	85
<b>Table A1</b> Values used for preparation of the MANT-O-Geraniol calibration line.....	xxx
<b>Table A2</b> Values of the terms used (for description see section 2.5.3.1.).....	xxx

<b>Table A3</b> Calculated values for $\hat{y}_i$ , $y_i - \hat{y}_i$ and $(y_i - \hat{y}_i)^2$ .....	xxxii
<b>Table A4</b> Summary of the characteristics of the used bivalent cations and the most abundant chain length of products as stated in the corresponding text in section 3.2.5.1. ....	xxxv
<b>Table A5</b> Proportion of AtCPT in gel band 2 and in solution. ....	xxxv
<b>Table A6</b> Overview of the experiments carried out and their in-house code. ....	xlix

## IV. Formula directory

<b>Equation 1</b> Determination of the protein concentration on the basis of a BSA calibration line. .....	41
<b>Equation 2</b> MANT-O-Geraniol calibration line. ....	48
<b>Equation 3</b> Determination of the limit of detection $x_{LOD}$ . ....	49
<b>Equation 4</b> Determination of the method detection limit $x_{MDL}$ . ....	49
<b>Equation A1</b> Determination of the residual standard deviation. ....	xxxii
<b>Equation A2</b> Determination of the ordinary least squares of x values of the calibration....	xxxii
<b>Equation A3</b> Determination of the limit of detection $x_{LOD}$ . ....	xxxiii
<b>Equation A4</b> Determination of the method detection limit $x_{MDL}$ . ....	xxxiii

# 1. Introduction

## 1.1. Objective

The chemical syntheses of complex carbon compounds often require multistep reactions which can be time-consuming accompanied by high financial expenditure. Furthermore, it can be quite challenging to achieve selective conversions, e.g. in terms of stereo-/regioselectivity or *cis-/trans*-selectivity. However, enzymatic syntheses generally occur under mild conditions, compared to many chemical syntheses, and enable the application of natural-like production processes. Among the various and versatile enzyme classes used in biotechnology, alkylating enzymes play an important role. They are able to catalyze challenging C-C-bond formation which is one of the crucial steps in the biosynthesis of many natural products.<sup>[1]</sup> Alkylating enzymes comprise glycosyltransferases, methyltransferases as well as prenylating enzymes.<sup>[1]</sup> The latter can be subdivided into terpene synthases and prenyltransferases.<sup>[1]</sup> The two isomers dimethylallyl diphosphate (DMAPP) and isopentenyl diphosphate (IPP) are the fundamental building blocks for the biosynthesis of isoprenoids formed by these enzymes. While terpene synthases catalyze intramolecular reactions, prenyltransferases transfer the allylic prenyl group to acceptor molecules like cysteine residues in proteins (protein prenyltransferases)<sup>[2]</sup>, aromatic substrates (aromatic prenyltransferases)<sup>[2]</sup> or to the homoallylic prenyl diphosphate IPP (polyprenyl diphosphate synthase)<sup>[2]</sup>.

Within the presented thesis the medium-chain *cis*-prenyltransferase from *Thermococcus kodakaraensis* (ThkCPT, EC 2.5.1.87) was investigated concerning the conversion of natural and artificial substrates, modulation of the chain length of products (by varying the assay conditions and the generation of variants) and improvement of the analytics (HPLC, HR-ESI-MS). It was shown in previous studies that the ThkCPT constitutes a suitable model system to examine the enzymatic formation of (artificial) polyisoprenoids<sup>[3]</sup> and therefore can be used for gaining further knowledge. Moreover, a long-chain *cis*-prenyltransferase from *Arabidopsis thaliana* (AtCPT, EC 2.5.1.87) was studied as it has been described that it forms products with up to 120 carbon atoms and can be heterologously expressed in bacteria<sup>[4]</sup>. The obtained *cis*-polyisoprenoids with varying chain lengths could be promising materials in chemical and pharmaceutical fields for the development of valuable

compounds, such as functional polymer molecules or for the synthesis of even longer-chained polyisoprenoids.

## 1.2. Isoprenoids

Isoprenoids comprise more than 50,000 different compounds with diverse structures and thus form one of the most widespread structural classes of biomolecules. Nearly one half are terpenoids (including steroids) and the other half comprises compounds with moieties originating from other biosynthetic origins coupled to isoprenoids (so called meroterpenoids, e.g. cytokinins and phenylpropanoids).<sup>[5, 6]</sup> All isoprenoids are derived from two simple C<sub>5</sub> precursors, IPP and its isomer DMAPP (Figure 1).

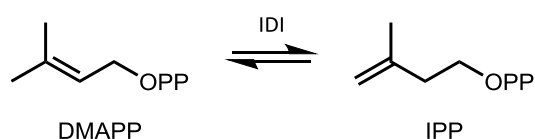


**Figure 1** The fundamental building blocks DMAPP and IPP which can be interconverted by the IPP/DMAPP isomerase (IDI).

These universal compounds are synthesized via two different pathways (Figure 2): on one hand the mevalonate pathway (MVA) which occurs universally in plants, bacteria, fungi and animals and on the other hand the non-mevalonate pathway (MEP) which occurs only in bacteria, algae and plants.<sup>[7-9]</sup> In plants, both pathways exist spatially separated. While the MVA pathway occurs in the cytosol to provide sterols, many sesquiterpenes and the prenyl chains of ubiquinones, the MEP pathway takes place in the plastids, giving rise to the production of hemi-, mono- and diterpenes, carotenoids and the side chain of plastoquinone<sup>[10, 11]</sup>. In the 1960s, Bloch and Lynen identified the MVA pathway for cholesterol biosynthesis<sup>[12-14]</sup>. Since then, the functional and structural basis for this metabolism was investigated until recent years<sup>[15]</sup>. For a long time, MVA was believed to be the only natural precursor for IPP and DMAPP. Finally, in the nineties, an alternative non-mevalonate pathway was discovered by Rohmer<sup>[16, 17]</sup>. As the MEP pathway is absent in humans it became an interesting target for the development of inhibitors as potential antibacterial drugs<sup>[18-20]</sup>.

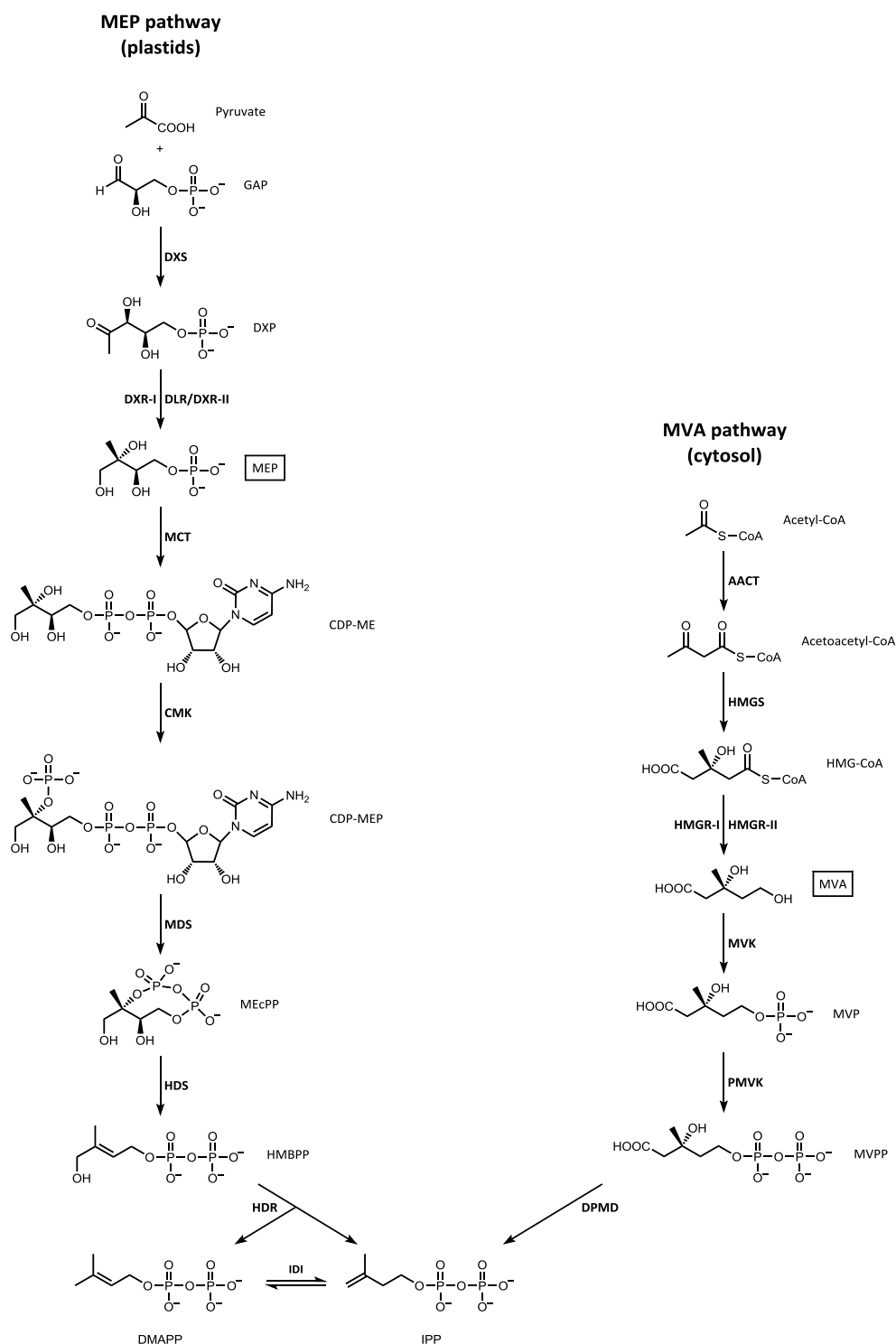


**Figure 2** MEP (left) and MVA (right) pathway. Figure was adapted from Pérez-Gil & Rodríguez-Concepción (2013)<sup>[21]</sup>.

AACT: acetoacetyl-CoA thiolase, CDP-ME: 4-diphosphocytidyl-2-C-methyl-D-erythritol, CDP-MEP: 4-diphosphocytidyl-2-C-methyl-D-erythritol 2-phosphate, CMK: 4-(cytidine 5'-diphospho)-2-C-methyl-D-erythritol kinase, DMAPP: dimethylallyl diphosphate, DPMD: 5-diphosphomevalonate decarboxylase, DRL: DXR-like enzyme, DXP: 1-deoxy-D-xylulose 5-phosphate, DXR: DXP reductoisomerase, DXS: DXP synthase, GAP: D-glyceraldehyde 3-phosphate, HDR: HMBPP reductase, HDS: HMBPP synthase, HMBPP: 4-hydroxy-3-methylbut-2-enyl diphosphate, HMGR: HMG-CoA reductase, HMGS: HMG-CoA synthase, IDI: IPP/DMAPP isomerase, IPP: isopentenyl diphosphate, MCT: MEP cytidyltransferase, MDS: MEcPP synthase, MEcPP: 2-C-methyl-D-erythritol 2,4-cyclodiphosphate, MEP: 2-C-methyl-D-erythritol 4-phosphate, MVA: mevalonate, MVK: mevalonate kinase, MVP: 5-phosphomevalonate, MVPP: 5-diphosphomevalonate, PMVK: MVP kinase.

Terpenes are classified concerning the number of isoprene (five-carbon) units they contain: hemiterpenes (C<sub>5</sub>: isoprene), monoterpenes (C<sub>10</sub>: volatile essences, essential oils), sesquiterpenes (C<sub>15</sub>: essential oils, phytoalexins), diterpenes (C<sub>20</sub>: gibberellin hormones, phytoalexins), sesterterpenes (C<sub>25</sub>), triterpenes (C<sub>30</sub>: brassinosteroids, phytosterols), sesquaterpenes (C<sub>35</sub>), tetraterpenes (C<sub>40</sub>: carotenoids) and polyterpenes (>C<sub>40</sub>: ubiquinone, dolichols).<sup>[6, 22]</sup> Terpenoids are biosynthetically derived from these hydrocarbons, and cover terpenes with incorporation of other functional groups, e.g. hydroxyl or glycosyl groups.

Isoprenoids play an important role in all living organisms. In plants they participate in both the primary and the secondary metabolism. As primary metabolites they are necessary for growth and development, e.g. gibberellins, brassinosteroids or abscisic acid<sup>[23]</sup>. Steroids serve as membrane components and are important for permeability and fluidity control<sup>[24]</sup>. They also act as steroid hormones<sup>[5]</sup>. Additionally, the lipid-soluble vitamins A, D, E and K are also vital agents belonging to the terpenoid family<sup>[25]</sup>. Other notable metabolites are the carotenoids which are essential for light harvesting and photoprotection<sup>[5, 24]</sup>. Furthermore, ubiquinones, menaquinones as well as plastoquinones are involved in the photosynthetic electron transport<sup>[5, 24]</sup>. Secondary metabolic terpenoids are for example involved in plant defense mechanisms (as toxins or antibiotics), serve as precursors to bioactive compounds or act as attractants<sup>[5, 26]</sup>.

Furthermore, isoprenoids are highly significant for commercial, pharmaceutical and agricultural purposes. Readily volatile terpenes and terpenoids (essential oils) are used in flavor and fragrance industries, e.g. linalool (floral/wood), menthol (mint), D-limonene (citron) and citronellol (rose)<sup>[27]</sup>. Some isoprenoids are also known for their biocidal activity, for example against cancer cells<sup>[28, 29]</sup> or malaria parasites<sup>[30]</sup>. A very well-known cancer therapeutic is paclitaxel, alias Taxol<sup>®</sup>. It was first isolated in 1971 by Wani and coworkers from the stem bark of the pacific yew, *Taxus brevifolia*<sup>[31]</sup>. As the yield from yew is very low and insufficient to cover commercial demands, alternative sources were investigated - also because the isolation from bark destroyed large yew stocks. So far, Taxol<sup>®</sup> is produced semi-synthetically from a precursor (10-deacetylbaocatin III) which can be found in the more readily accessible leaves of the European yew, *Taxus baccata*.<sup>[32]</sup> Another medically and commercially important agent is artemisinin from *Artemisia annua*, which possesses anti-malaria activity<sup>[30]</sup>. The compound can be isolated from the plant material or can be obtained from *in vitro* tissue culture<sup>[33]</sup>.



### 1.3. Polyisoprenoids

High molecular weight polyisoprenoids like natural rubber (*cis*-1,4-polyisoprene) or gutta-percha (*trans*-1,4-polyisoprene) are of high commercial interest due to their properties as elastic materials. Polyprenyl diphosphate synthases are able to synthesize such long-chain polyisoprenes by condensing more than 5000 isoprene units, as the rubber transferase (EC 2.5.1.20) does<sup>[34]</sup>. Natural rubber is harvested mainly from the rubber tree *Hevea brasiliensis* as latex, containing about 44 % (w/v) polyisoprene<sup>[35]</sup>. In 2016 the total rubber production reached about 27 million tonnes worldwide, from which nearly 55 % are produced synthetically and 45 % are made from natural rubber<sup>[36]</sup>. By vulcanization an elastic and resilient rubber results which is also abrasion- and shock-resistant<sup>[37]</sup>. The major part (75 %) of natural rubber is used for the manufacturing of tires<sup>[35]</sup> but it is also utilized for the production of surgical gloves, condoms, balloons or even mattresses and carpet backings<sup>[38]</sup>. As rubber is highly demanded, high molecular *cis*-polyisoprenes are also synthesized chemically. Synthetic rubber is made from various mineral oil-based monomers. The most distributed one is styrene-butadiene rubber derived from the copolymerization of styrene and 1,3-butadiene.<sup>[39]</sup> Other common synthetic rubbers are for example 1,4-*cis*-polyisoprene, polybutadiene or polychloroprene (neoprene®). Synthetic polyisoprene is applied to tire treads, belts, footwear, rubber filaments and bands, medical supplies and even goods for the food industry.<sup>[39]</sup>

Unfortunately, the allergic reactions to the proteins in the latex of *H. brasiliensis* increased dramatically in the past<sup>[40]</sup>. Therefore, there is considerable motivation to develop alternative natural rubber sources. The *cis*-1,4-polyisoprene can also be produced from other plant sources<sup>[40, 41]</sup>. As a source of hypoallergenic latex guayule (*Parthenium argentatum*) was focused as it has a much lower protein content than the *H. brasiliensis*-based product<sup>[40]</sup>. Rubber particle-associated proteins of guayule do not cross-react with immunoglobulin (Ig)E (Type I latex allergy) and IgG antibodies to *H. brasiliensis* latex proteins<sup>[42]</sup> what makes allergic reactions to guayule rubber by consumers sensitized to *H. brasiliensis* rubber unlikely. Another potential source is the Russian dandelion *Taraxacum koksaghyz*. The root is a source of high quality rubber which exhibits extraordinarily high molecular weight.<sup>[40]</sup> A big disadvantage of *T. koksaghyz* is that its rubber particles contain even more associated proteins than *H. brasiliensis* rubber. This increases the risk that people might be sensitized to rubber from Russian dandelion, as has

happened with the latex from the rubber tree. Therefore, it should be considered for conventional, non-medical applications.<sup>[40]</sup> However, *H. brasiliensis* is still the main source because of its larger production than guayule or dandelion.

As mentioned before, there are also *trans*-isomers of polyisoprene, e.g. balata<sup>[43, 44]</sup> or, better known, gutta-percha<sup>[45]</sup>. In contrast to the latex of *H. brasiliensis*, gutta-percha is inelastic and rigid but softens when heated. Therefore, it was used for the production of golf balls but also in medicine or as insulating medium in the laying of underground seawater cables<sup>[45]</sup>. The use of gutta-percha in dentistry was developed since the mid of 19<sup>th</sup> century and it remains to be the main core material used for root canal fillings.<sup>[45, 46]</sup>

## 1.4. Prenyltransferases

As already mentioned before, there are different types of prenyltransferases (PTs)<sup>[2]</sup>. Protein PTs transfer the allyl chains of farnesyl diphosphate (FPP) or geranylgeranyl diphosphate (GGPP) via a thio-ether linkage to a conserved cysteine residue in a CaaX (Cys-aliphatic-aliphatic-variable) motif near the C-terminus of proteins or peptides (the type of amino acid X specifies whether a FPP or a GGPP residue is attached). This modification is important for the functionality of various proteins, e.g. Ras, Rab, protein kinases, nuclear lamins, trimeric G-protein  $\gamma$  subunits and small Ras-related GTP-binding proteins. Due to the attachment of a geranylgeranyl group the proteins can anchor in cell membranes. Farnesylated proteins require a second signal for stable membrane interaction. Interestingly, the inhibition of the Ras farnesyltransferases became interesting in anticancer therapy as prenylated Ras proteins take part in cell cycle control which is upregulated in tumor cells.<sup>[47-49]</sup>

Aromatic PTs catalyze the transfer of prenyl groups to aromatic acceptor molecules which produces a huge diversity of metabolites. The prenylation occurs at C-, O- or N-atoms. For example, ubiquinones are formed by the attachment of prenyl moieties to 4-hydroxybenzoate (4HB).<sup>[50]</sup> A prominent example for such a 4HB polyprenyltransferase is the UbiA from *Escherichia coli* which has also been successfully used for the chemoenzymatic synthesis of prenylated aromatic compounds<sup>[51]</sup>. In fungi, the prenylation of indole moieties leads to a huge variety of alkaloids. These PTs are able to perform regular and reverse C- and N-prenylations. In plants, prenylated flavonoids and isoflavonoids are important in defense mechanisms. Prenylation is carried out by membrane bound PTs localized in plastids. Membrane bound aromatic PTs exhibit an aspartate-rich motif (e.g.

NDxxDxxxD) and are magnesium-dependent. In contrast, soluble aromatic PTs are not necessarily dependent on bivalent cations and do not contain an aspartate-rich motif. They show a  $\beta/\alpha$  fold with antiparallel strands and because of the  $\alpha$ - $\beta$ - $\beta$ - $\alpha$  architecture they are also known as ABBA PTs.<sup>[50]</sup>

Polyprenyl diphosphate synthases form linear isoprenoids by sequential condensation of IPP with allylic diphosphates. According to the geometry of the prenyl chain units in the product, these prenyltransferases are classified into two groups, *cis*-prenyltransferases (CPT) and *trans*-prenyltransferases (TPT). The catalyzed reactions are similar as they both use the same substrates for the prenyl chain elongation. The only difference is the prochirality of the proton, which is eliminated from the 2-position of IPP, *pro*-R for TPT and *pro*-S for CPT, respectively<sup>[2, 52]</sup>. So, the formation of the *trans* or *cis* double bond during the reaction depends on the spatial arrangement of the substrates<sup>[47]</sup>. Short-chain allylic diphosphates like geranyl diphosphate (GPP: C<sub>10</sub>), farnesyl diphosphate (FPP: C<sub>15</sub>) and geranylgeranyl diphosphate (GGPP: C<sub>20</sub>) are formed by TPTs. They are then applied as allylic primer substrates for further IPP condensation.<sup>[2]</sup> Originating from FPP or GGPP, a large number of different-chain-length products are generated by different synthases (Figure 3)<sup>[2, 47]</sup>. The products formed by PTs show specific chain lengths which are important for their biological function<sup>[47]</sup>. Several *cis*-prenyltransferases are responsible for forming side chains of ubiquinone in different species<sup>[47]</sup>. The product of the bacterial undecaprenyl diphosphate synthase (C<sub>55</sub>) acts as a lipid carrier in cell wall peptidoglycan biosynthesis<sup>[47]</sup>. In eukaryotes, the equivalent dehydrololichyl diphosphate synthase catalyzes the formation of C<sub>55</sub>-C<sub>100</sub> dolichols for glycoprotein biosynthesis.<sup>[53]</sup> *Arabidopsis thaliana* possesses a CPT which is able to form an even longer C<sub>120</sub> polymer<sup>[4, 54]</sup>.

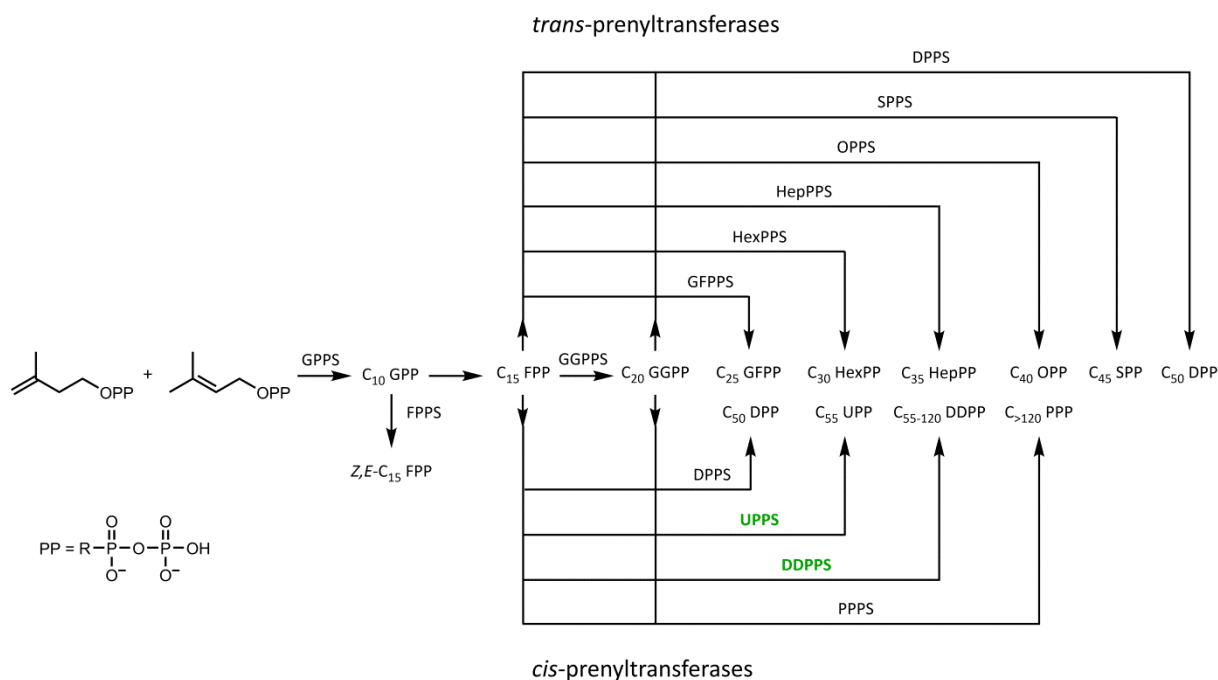


**Figure 3** Classification of linear prenyltransferases. Besides FPP, GGPP can also serve as an initiator of polyisoprenoids chains. Figure modified according to Liang et al. 2002<sup>[47]</sup>. Enzymes used in this study are marked in green.

DDPP: dehydrodolichyl diphosphate, DDPPS: DDPP synthase, DPP: decaprenyl diphosphate, DPPS: DPP synthase, FPP: farnesyl diphosphate, FPPS: FPP synthase, GFPP: geranylgeranyl diphosphate, GFPPS: GFPP synthase, GGPP: geranylgeranyl diphosphate, GGPPS: GGPP synthase, GPP: geranyl diphosphate, GPPS: GPP synthase, HepPP: heptaprenyl diphosphate, HepPPS: HepPP synthase, HexPP: hexaprenyl diphosphate, HexPPS: HexPP synthase, OPP: octaprenyl diphosphate, OPPS: OPP synthase, PPP: polyprenyl diphosphate, PPPS: PPP synthase, SPP: solanesyl diphosphate, SPPS: SPP synthase, UPP: undecaprenyl diphosphate, UPPS: UPP synthase.

### 1.4.1. *trans*-Prenyltransferases (TPTs)

The first cDNA cloning of rat liver FPP synthase was carried out by Clarke et al. in 1987<sup>[55]</sup>. Since then, many genes from TPTs were cloned from different organisms and characterized<sup>[34, 56, 57]</sup>. The catalytic mechanism of TPTs has been studied by X-ray crystal structural analysis<sup>[58, 59]</sup> as well as by site-directed mutagenesis<sup>[60-63]</sup>. Seven highly conserved regions and two aspartate-rich motifs, DDXXD in regions II and IV, were found in all TPTs<sup>[2]</sup>. The first aspartate-rich motif binds the allylic substrate and the second binds IPP via Mg<sup>2+</sup>, respectively<sup>[52, 59]</sup>. Mutagenesis studies showed that the 5<sup>th</sup> amino acid residue upstream from the first aspartate-rich motif (Tyr81) is significant for controlling the chain length of the final product formed in the reaction catalyzed by FPP synthase from *Geobacillus stearothermophilus* (basonym *Bacillus stearothermophilus*), whereas the average chain length of products is inversely proportional to the accessible surface area of the substituted amino acid<sup>[64]</sup>. For the TPT reaction a sequential ionization-condensation-

elimination mechanism has been suggested (Figure 4). Here, the diphosphate group is split off from the allylic substrate that thereupon becomes ionized. Thereby a carbocation is formed which is then attacked nucleophilically by the double bond of IPP. At this, the allylic substrate is added to the *si* face of the double bond of IPP. The elimination of the *pro-R* proton at C2 of the intermediate leads to the formation of a new double bond with *trans* configuration.<sup>[47, 65]</sup>

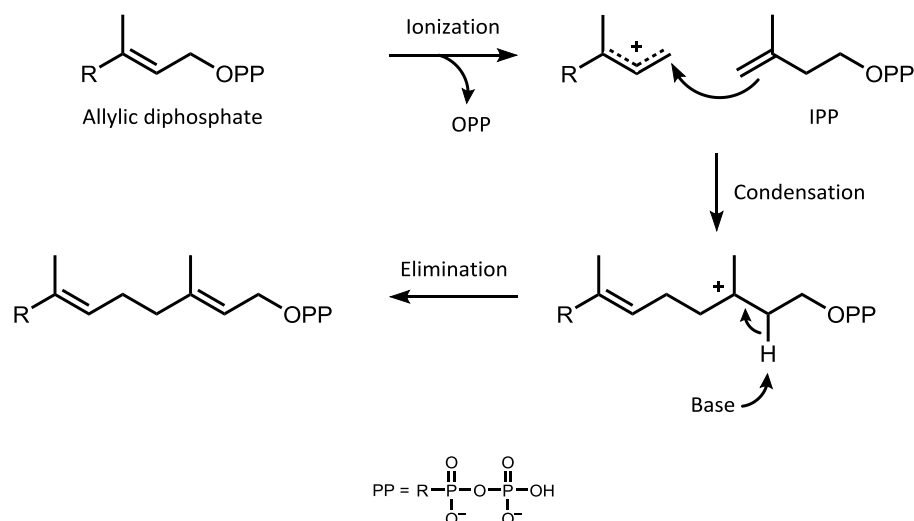


**Figure 4** Sequential ionization-condensation-elimination mechanism. Figure modified according to Lu et al. 2010<sup>[65]</sup>.

By using the alternative substrate 3-bromo-3-butenyl diphosphate (Br-BPP) in a TPT reaction (octaprenyl diphosphate synthase, OPPS) the condensation step is slowed down. The intermediate was trapped as farnesol, giving direct proof for the sequential ionization-condensation-elimination mechanism for *trans*-prenyltransferases.<sup>[66]</sup>

#### 1.4.2. *cis*-Prenyltransferases (CPTs)

The first CPT gene identified was encoding the undecaprenyl diphosphate synthase (UPPS) from *Micrococcus luteus* in 1998. Its amino acid sequence shows no sequence similarity to those of TPTs.<sup>[67]</sup> Since then, many *cis*-type prenyltransferases were identified in various organisms<sup>[2 and references therein]</sup>. CPTs exhibit five conserved regions but no aspartate-rich motifs like TPTs, although they require  $\text{Mg}^{2+}$  for catalytic activity<sup>[47]</sup>. Site-directed mutagenesis studies examined the conserved aspartate and glutamic acid of *E. coli* UPPS (EcUPPS) and revealed the importance in substrate binding and catalysis<sup>[47, 68]</sup>. In 2001, Fujihashi et al.

determined the first crystal structure of a CPT (UPPS from *M. luteus* B-P 26) which is completely different from that of TPTs<sup>[69]</sup> (Figure 5).

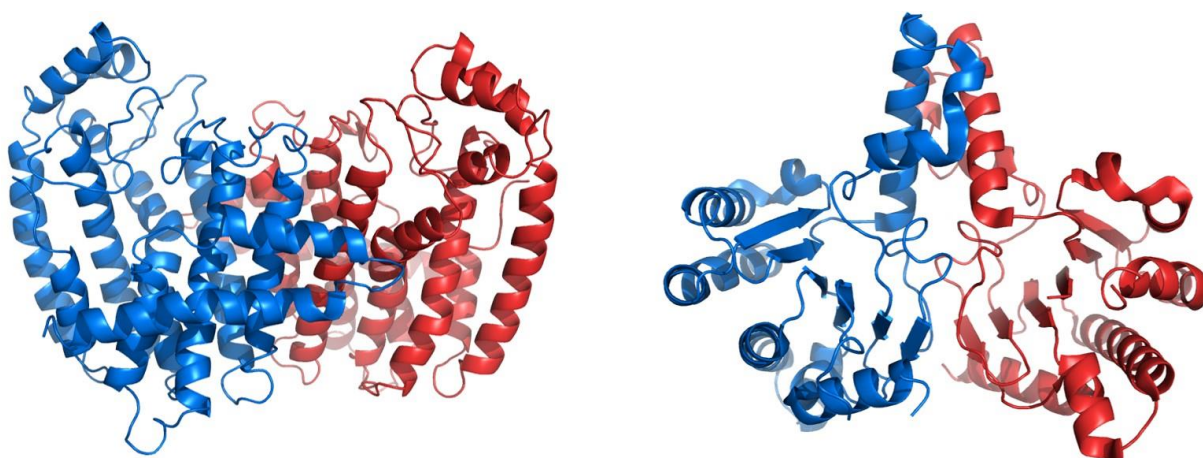


**Figure 5** Comparison of the crystal structures from a TPT (left, avian FPPS<sup>[58]</sup>, PDB code: 1FPS) and a CPT (right, *M. luteus* B-P 26 UPPS<sup>[69]</sup>, PDB code: 1F75). The structures were visualized using the software PyMOL 1.8<sup>[70]</sup>.

For the CPTs a concerted condensation-elimination mechanism has been suggested, where ionization of the allylic substrate and condensation of IPP occur simultaneously (Figure 6). In contrast to the TPT reaction (see above), no farnesyl carbocation was trapped by using the alternative substrate Br-BPP in a CPT reaction (UPPS), indicating a concerted mechanism. Furthermore, it could be shown that the rate of 2-fluoro-FPP condensing with IPP is similar to that of FPP, supporting the proposed concerted condensation-elimination mechanism for UPPS.<sup>[65, 66]</sup>

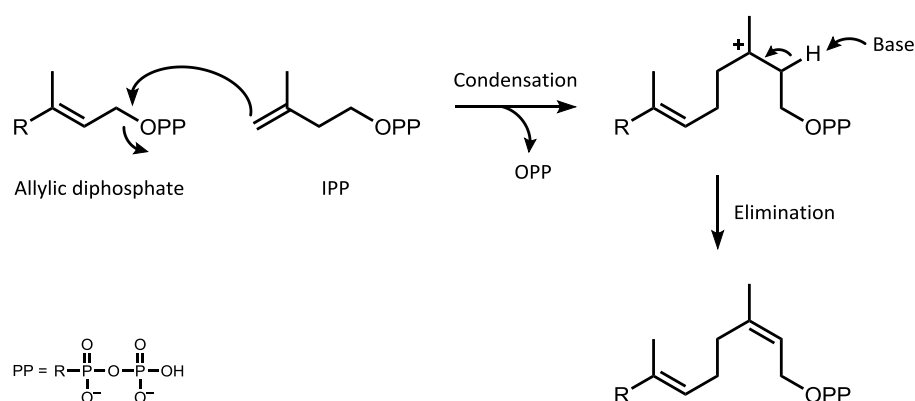


**Figure 6** Concerted condensation-elimination mechanism. Figure modified according to Teng & Liang 2012<sup>[71]</sup>.

According to the formed product chain length *cis*-prenyltransferases can be further subdivided into short- (up to C<sub>20</sub>), medium- (C<sub>25-55</sub>) and long- (C<sub>>55</sub>) chain CPTs<sup>[2]</sup>. In the following, medium- and long-chain CPTs are described in more detail.

#### 1.4.2.1. Medium-chain *cis*-prenyltransferases

A very well-studied example for medium-chain CPTs is the already mentioned UPPS from *E. coli* (EcUPPS, EC 2.5.1.31). It catalyzes condensation reactions of FPP with eight IPP units to generate a C<sub>55</sub> product. In 2001, its crystal structure was determined which shows a nearly similar structure to the enzyme from *M. luteus* (Figure 5). The three dimensional structure of the EcUPPS shows a hydrophobic tunnel which is considered to accommodate the elongated intermediates. On the top of the tunnel, there are several conserved hydrophilic amino acids. This region has been suggested as the FPP- and IPP-binding site based on site-directed mutagenesis studies.<sup>[72]</sup> It was also possible to crystalize the EcUPPS in complex with Mg<sup>2+</sup>, IPP and farnesyl thiopyrophosphate, a less reactive analogue of FPP. Comparison of the crystal structures of EcUPPS with and without substrates revealed a conformational change between the open (apoenzyme and product-bound) and closed (substrate-bound) forms (Figure 7).<sup>[73]</sup>

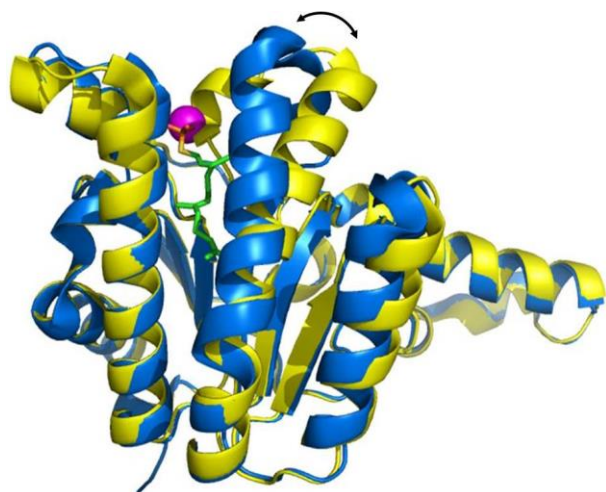


**Figure 7** Comparison of the crystal structures of the open (PDB code: 3QAS<sup>[74]</sup>, yellow) and the closed (PDB code: 1X06<sup>[73]</sup>, blue) form of the EcUPPS in complex with Mg<sup>2+</sup> (magenta sphere) and the substrate analogue farnesyl thiopyrophosphate (shown as sticks, carbon: green, sulfur: yellow, phosphate: orange, oxygen: red). It has to be noted that only one monomer of the dimeric enzyme is shown. The delocalization of the  $\alpha$ -helix due to substrate binding is highlighted by an arrow. The structures were visualized using the software PyMOL 1.8<sup>[70]</sup>.

During catalysis it is assumed that UPPS binds FPP first and then IPP as a Mg<sup>2+</sup> complex via chelation with Asp26. Mg<sup>2+</sup> is then transferred to the diphosphate of FPP to facilitate its dissociation and the simultaneous attack of IPP on FPP. Subsequent elimination of the H<sub>5</sub> proton leads to a new *cis*-double bond to neutralize the carbocation and form the C<sub>5</sub>-extended product for each cycle (see also Figure 6).<sup>[65]</sup> It is questionable which amino acid

acts as potential base to accept the H<sub>5</sub> proton. It was assumed that a catalytic diad, consisting of Asn74 and Glu73, is involved. By site-directed mutagenesis studies it could be confirmed that Asn74 acts as potential catalytic base as the alanine variant showed no activity and no product formation. It could also be shown that Glu73 acts as potential proton acceptor as the aspartate variant had increased activity compared to the alanine variant, indicating the important function of the carboxyl group. So it is assumed that Asn74 abstracts the H<sub>5</sub> proton which is then passed on to Glu73 (Figure 8).<sup>[3]</sup>

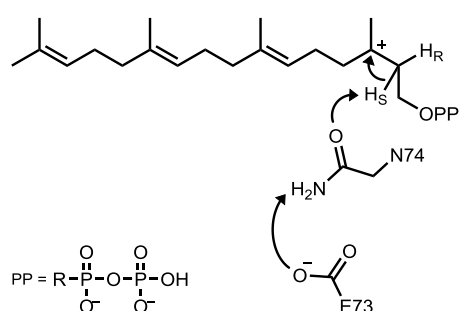


**Figure 8** Schematic presentation of the transition state during the enzymatic condensation of IPP with FPP including the proposed catalytic diad Asn74 and Glu73. Figure modified according to Keim 2014<sup>[3]</sup>.

Ko and coworkers reported that the bulky side chain of Leu137 (located at the bottom of the hydrophobic tunnel in EcUPPS) serves to block further elongation, as the substitution with alanine results in the synthesis of longer products. Another important amino acid for correct product chain-length formation is Ala69, located at a distance corresponding to 3 isoprene units away from FPP bound in EcUPPS. The substitution of Ala69 with leucine results in accumulation of a short-chain intermediate (C<sub>30</sub>).<sup>[72]</sup>

In 2009, Yamada et al. isolated a CPT from *Thermococcus kodakaraensis*, a hyperthermophilic archaeon<sup>[75]</sup>. It is particularly interesting to note that the enzyme is quite thermostable as it is not fully denatured even at 90°C<sup>[75]</sup>. It is described that it forms mainly the C<sub>60</sub>-C<sub>65</sub> products by what the enzyme is categorized as medium-chain CPT<sup>[75]</sup>. As the *cis*-prenyltransferase from *T. kodakaraensis* (ThkCPT, EC 2.5.1.87) is a main part of the presented thesis, further information are provided in a separate section (see 3.1.).

#### 1.4.2.2. Long-chain *cis*-prenyltransferases

The long-chain CPTs represent a focused topic in research as they are involved in the synthesis of natural rubber<sup>[76-79]</sup>. Rubber biosynthesis takes place in the latex of laticifers and is stored in rubber particles. Rubber particles contain a homogeneous hydrophobic rubber



core surrounded by an intact monolayer membrane which contains a mixture of lipids, proteins and other molecules with the hydrophilic portions of phospholipids and glycosylated particle-bound proteins facing the cytoplasm (Figure 9). The polymer is synthesized from hydrophilic substrates obtained from the cytoplasm, meaning one allylic diphosphate, which initiates the reaction, and sequential condensations of the homoallylic IPP. So, a high molecular weight (>1 million Da) product is formed which is channeled into the rubber particle interior.<sup>[77, 80, 81]</sup> Rubber elongation factor, small rubber particle protein, and CPT have been implicated in natural rubber biosynthesis<sup>[82-85]</sup>. CPTs are studied for a long time but it was only recently discovered that eukaryotes have evolved a unique protein complex, comprised of CPT and CPT-binding protein (CBP), to synthesize *cis*-polyisoprenoids (Figure 9).<sup>[81, 86, 87]</sup> It was shown that plants contain both the prokaryotic CPT in plastids (class I) and the eukaryotic CPT complexed with CBP in the endoplasmic reticulum (class II)<sup>[87]</sup>. The CBPs do not possess the conserved motifs for CPT catalysis but directly interact with catalytic CPTs. Furthermore, CPT alone appears to be unstable *in vivo* without forming a complex with CBP. In CPTs, no obvious membrane-bound domain is present. In contrast, all CBPs possess integrating membrane domains at their N-termini. The formation of a complex between CPTs and CBPs yields stability, protects the CPT from degradation and is required for enzymatic activity.<sup>[81, 86, 87]</sup> Very recently, Yamashita et al. established a novel system for cell-free, translation-coupled, hydrophobic protein introduction on detergent-washed rubber particles from *H. brasiliensis*, allowing *de novo* synthesis of natural rubber *in vitro* by the used recombinant CPT<sup>[88]</sup>. This was an important step for the further understanding of how natural rubber biosynthesis machinery works.

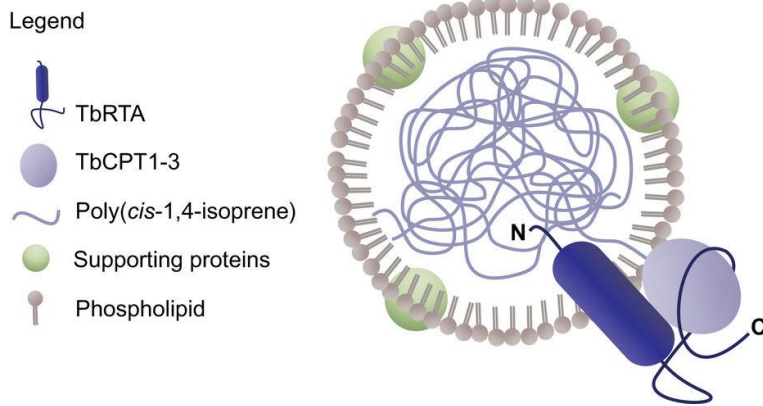


**Figure 9** Proposed model of long-chain rubber CPT and CBP complex on the surface of rubber particles.

Reprinted by permission from Springer Customer Service Centre GmbH: Springer Nature, Nature Plants, A rubber transferase activator is necessary for natural rubber biosynthesis in dandelion, Janina Epping et al. 2015<sup>[86]</sup> (<https://www.nature.com/articles/nplants201548?beta=true>).

TbRTA: *Taraxacum brevicorniculatum* rubber transferase activator (CBP), TbCPT1-3: *T. brevicorniculatum* *cis*-prenyltransferase 1-3.

In 2000, Oh et al. and Cunillera et al. reported about a dehydrololichyl diphosphate synthase from *Arabidopsis thaliana*<sup>[4, 54]</sup>. Even though it could not catalyze the formation of high molecular weight polyisoprene, this *cis*-prenyltransferase ranks among the long-chain CPTs as it forms polyprenyl diphosphates with predominant 120 carbon atoms. It shows high homology in several conserved regions to the CPTs from *M. luteus*, *E. coli* and yeast.<sup>[4]</sup> As the *cis*-prenyltransferase from *A. thaliana* (AtCPT, EC 2.5.1.87) is part of the presented thesis, further information are provided in a separate section (see 4.1.).

## 2. Materials and methods

### 2.1. Materials

#### 2.1.1. Chemicals

Used chemicals are listed in table 1. Unless stated otherwise, solvents were purified by distillation before use (purchased from Prolabo (VWR), Darmstadt).

**Table 1** Used chemicals.

Chemicals	Source
6x DNA loading dye	Thermo Fisher Scientific, Waltham, USA
1-Butanol	Merck, Darmstadt
$\alpha$ -Lactose	Sigma-Aldrich, St. Louis, USA
$\beta$ -Mercaptoethanol	Roth, Karlsruhe
Acetic acid	Roth, Karlsruhe
Acetonitrile	Merck, Darmstadt
Acrylamide	Merck, Darmstadt
Agar	Roth, Karlsruhe
Agarose	Roth, Karlsruhe
Ammonium bicarbonate	Sigma-Aldrich, St. Louis, USA
Ammonium sulfate	Roth, Karlsruhe
Ampicillin	Roth, Karlsruhe
Ammonium peroxodisulfate (APS)	Roth, Karlsruhe
Boric acid	Sigma-Aldrich, St. Louis, USA
Bromophenol blue	Roth, Karlsruhe
Chloramphenicol	Roth, Karlsruhe
CoCl <sub>2</sub>	Alfa Aesar, Heysham, UK
Coomassie Brilliant Blue G-250	Sigma-Aldrich, St. Louis, USA
CuCl <sub>2</sub>	Sigma-Aldrich, St. Louis, USA
Deoxynucleotide triphosphate (dNTP) mix (10 mM each dNTP)	Thermo Fisher Scientific, Waltham, USA
Disodium hydrogen phosphate	Sigma-Aldrich, St. Louis, USA
Dithiothreitol (DTT)	Sigma-Aldrich, St. Louis, USA
Ethylenediaminetetraacetic acid (EDTA) dihydrate	Roth, Karlsruhe

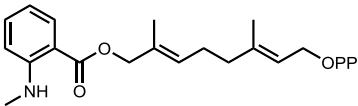
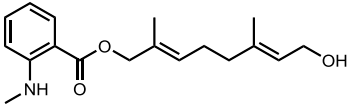
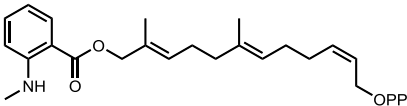
Ethanol	Merck, Darmstadt
Ethidium bromide	VWR, Radnor, USA
Farnesol	Sigma-Aldrich, St. Louis, USA
Formic acid	Roth, Karlsruhe
GeneRuler™ 1 kb DNA Ladder	Thermo Fisher Scientific, Waltham, USA
Glucose	Roth, Karlsruhe
Glycerin	Roth, Karlsruhe
Glycine	Roth, Karlsruhe
4-(2-Hydroxyethyl)-1-piperazineethanesulfonic acid (HEPES)	Roth, Karlsruhe
Hydrochloric acid	Roth, Karlsruhe
Imidazole	Roth, Karlsruhe
Iodoacetamide	Sigma-Aldrich, St. Louis, USA
Isopropyl $\beta$ -D-1-thiogalactopyranoside (IPTG)	Roth, Karlsruhe
FeCl <sub>3</sub>	Merck, Darmstadt
Isopropanol	Merck, Darmstadt
Kanamycin	Roth, Karlsruhe
Liquid nitrogen	Air Liquide, Paris, France
MgCl <sub>2</sub>	Sigma-Aldrich, St. Louis, USA
Magnesium sulfate, heptahydrate	Sigma-Aldrich, St. Louis, USA
MnCl <sub>2</sub>	Merck, Darmstadt
Monopotassium phosphate	Sigma-Aldrich, St. Louis, USA
<i>n</i> -Heptane	Merck, Darmstadt
<i>n</i> -Hexane (Rotisolv® HPLC)	Roth, Karlsruhe
NiCl <sub>2</sub>	Merck, Darmstadt
PageRuler™ prestained protein ladder	Thermo Fisher Scientific, Waltham, USA
Pierce® LTQ Velos ESI positive ion calibration solution	Thermo Fisher Scientific, Waltham, USA
Phenylmethane sulfonyl fluoride (PMSF)	Sigma-Aldrich, St. Louis, USA
Potassium chloride	Sigma-Aldrich, St. Louis, USA
Roti®-Quant (Bradford reagent)	Roth, Karlsruhe
Sodium dodecyl sulfate (SDS)	Roth, Karlsruhe
Sodium acetate, trihydrate	Merck, Darmstadt
Sodium chloride	Roth, Karlsruhe

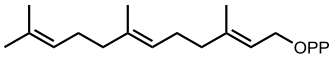
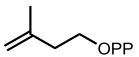
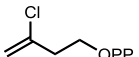
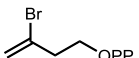
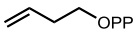
Sodium hydroxide	Roth, Karlsruhe
Sodium molybdate, dihydrate	Sigma-Aldrich, St. Louis, USA
Sodium selenite	Sigma-Aldrich, St. Louis, USA
Solanesol	Sigma-Aldrich, St. Louis, USA
Sucrose	Roth, Karlsruhe
Tetramethylethylenediamine (TEMED)	Roth, Karlsruhe
Trifluoroacetic acid	Thermo Fisher Scientific, Waltham, USA
Tris	Roth, Karlsruhe
Triton® X-100	Roth, Karlsruhe
Tryptone/Peptone	Roth, Karlsruhe
Urea	Sigma-Aldrich, St. Louis, USA
Yeast extract	Roth, Karlsruhe
ZnCl <sub>2</sub>	Merck, Darmstadt
Zinc sulfate, hexahydrate	Sigma-Aldrich, St. Louis, USA

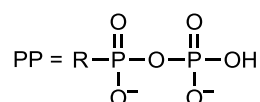
### 2.1.2. Prenyl diphosphates

All prenyl diphosphates (Table 2) were synthesized in-house by Dr. Roman Weber, Dr. Marco Dessoy, Dr. Tula Beck and Dr. Steve Ludwig. Structural integrity was verified by NMR spectroscopy.<sup>[89-91]</sup> For the preparation of stock solutions (5 mM for the allylic and 10 mM for the homoallylic substrates) the required amount was solved in 25 mM ammonium bicarbonate solution<sup>[92]</sup>.

**Table 2** Used prenyl diphosphates.

Structural formula	Substance name	Chemical name	In-house code
	MANT-O-GPP	(2 <i>E</i> ,6 <i>E</i> )-8- <i>O</i> -( <i>N</i> -Methylantranil)-3,7-dimethyl-2,6-octandien-1-diphosphate	DBT137
	MANT-O-Geraniol	(2 <i>E</i> ,6 <i>E</i> )-8- <i>O</i> -( <i>N</i> -Methylantranil)-3,7-dimethyl-2,6-octandien-1-ol	DBT134
	MANT-O-nor FPP	(2 <i>E</i> ,6 <i>E</i> ,10 <i>Z</i> )-12- <i>O</i> -( <i>N</i> -Methylantranil)-7,11-dimethyl-2,6,10-dodecatrien-1-diphosphate	LUS354

	FPP	Farnesyl diphosphate	LUS090 DDM227
	IPP	Isopentenyl diphosphate	DDM243 WER295
	Cl-BPP	3-Chloro-3-butenyl diphosphate	LUS100
	Br-BPP	3-Bromo-3-butenyl diphosphate	LUS075
	BPP	3-Butenyl diphosphate	LUS019



### 2.1.3. Solutions, culture media and buffers

For the preparation of culture media ultrapure water was used. The compositions of used solutions, culture media and buffers are listed in table 3. The culture media were autoclaved after preparation and supplemented with the relevant antibiotic directly before utilization (final concentration: 50 µg ml<sup>-1</sup> kanamycin, 100 µg ml<sup>-1</sup> ampicillin or 50 µg ml<sup>-1</sup> chloramphenicol). For auto-induction (AI) medium the individual components were first sterilized (autoclaved or sterile filtered) and then combined under sterile conditions. Kanamycin and ampicillin were prepared as 1000-fold stock solutions in water, sterile-filtered and kept at -20°C until usage. Chloramphenicol was prepared as 1000-fold stock solution in methanol, sterile-filtered and kept at -20°C until usage.

For cultivation of bacteria on plates the medium was supplemented with 1.5 % (w/v) agar. Transformation of bacterial cells was carried out in SOC (super optimal broth with catabolite repression) medium.

**Table 3** Compositions of used solutions, culture media and buffers.

<b>Designation</b>	<b>Composition</b>
20xNPS	0.5 M (NH <sub>4</sub> ) <sub>2</sub> SO <sub>4</sub> 1 M KH <sub>2</sub> PO <sub>4</sub> 1 M Na <sub>2</sub> HPO <sub>4</sub>
50x5052	25 % (w/v) Glycerin 2.5 % (w/v) Glucose 10 % (w/v) α-Lactose
AI medium	ZY medium containing: 1 mM MgSO <sub>4</sub> 1x5052 1x Trace metal mix 1xNPS Antibiotic
Assay buffer	50 mM HEPES/NaOH 100 mM NaCl 1 mM DTT 0.5 mM MgCl <sub>2</sub> 10 % (v/v) Glycerin 0.1 % (v/v) Triton® X 100 pH 8.0 (for ThkCPT)/pH 7.5 (for AtCPT)
Binding/wash buffer	50 mM Tris/HCl 0.5 M NaCl 10 % (v/v) Glycerin 20 mM Imidazole pH 8.5
Coomassie destaining solution	30 % (v/v) Methanol 10 % (v/v) Acetic acid
Coomassie staining solution	0.25 % (w/v) Coomassie Brilliant Blue G-250 50 % (v/v) Methanol 10 % (v/v) Acetic acid
Dialysis buffer AtCPT	100 mM Tris/HCl 1 mM MgCl <sub>2</sub> 1 mM DTT pH 8.5

Dialysis buffer ThkCPT	50 mM HEPES/NaOH 100 mM NaCl 1 mM DTT 10 mM EDTA 10 % (v/v) Glycerin pH 8.0
Elution buffer	50 mM Tris/HCl 0.5 M NaCl 10 % (v/v) Glycerin 300 mM Imidazole pH 8.5
Hydrolysis buffer	50 mM Sodium acetate/acetic acid 20 % (v/v) Isopropanol 0.1 % (v/v) Triton® X 100 pH 4.7
LB agar plate	1 % (w/v) Tryptone/Peptone 0.5 % (w/v) Yeast extract 1 % (w/v) NaCl 1.5 % (w/v) Agar Antibiotic pH 7.0 (adjusted with NaOH)
LB medium	1 % (w/v) Tryptone/Peptone 0.5 % (w/v) Yeast extract 1 % (w/v) NaCl pH 7.0 (adjusted with NaOH)
Lysis buffer	50 mM Tris/HCl 150 mM NaCl 1 mM EDTA dihydrate 1 mM DTT 0.1 % (v/v) Triton® X-100 pH 8.5
SDS-PAGE running buffer (10x)	1 % (w/v) SDS 250 mM Tris 2 M Glycine
SDS-PAGE sample buffer (5x)	10 % (w/v) SDS 10 mM β-Mercaptoethanol 20 % (v/v) Glycerin 0.2 mM Tris/HCl 0.05 % (w/v) Bromophenol blue



## Materials and methods

---

Sucrose buffer	25 % (w/v) Sucrose 10 mM EDTA 10 mM Triton X-100
SOC medium	2 % (w/v) Tryptone/Peptone 0.5 % (w/v) Yeast extract 20 mM Glucose 10 mM NaCl 2.5 mM KCl 10 mM MgCl <sub>2</sub> 10 mM MgSO <sub>4</sub> pH 7.0
TAE buffer (50x)	2 M Tris 0.1 M EDTA 1 M Acetic acid pH 8.3
Trace metal mix (1000x)	50 mM FeCl <sub>3</sub> in 50 mM HCl 20 mM NaCl 10 mM ZnSO <sub>4</sub> 2 mM CoCl <sub>2</sub> 2 mM CuCl <sub>2</sub> 2 mM NiCl <sub>2</sub> 2 mM Na <sub>2</sub> MoO <sub>4</sub> 2 mM Na <sub>2</sub> SeO <sub>3</sub> 2 mM H <sub>3</sub> BO <sub>3</sub>
Tris buffer	100 mM Tris/HCl 1 mM MgCl <sub>2</sub> 1 mM DTT pH 8.0
Tris buffer MTP	10 mM Tris/HCl 1 mM MgCl <sub>2</sub> 1 mM DTT 0.1 % (v/v) Triton® X-100 pH 8.0
TSE buffer	100 mM Tris/HCl 20 % (w/v) Sucrose 1 mM EDTA pH 7.5
ZY medium	10 g Tryptone/Peptone 5 g Yeast extract 925 ml H <sub>2</sub> O

## 2.1.4. Consumables

**Table 4** Used consumables.

Consumables	Description	Source
Capillary tubes	80 x 0.6 mm	Marienfeld-Superior, Lauda-Königshofen
Centrifugal tubes	15/50 ml Amicon® Ultra-15 centrifugal filter, Ultracel® regenerated cellulose membrane, MWCO: 10 kDa	Sarstedt, Nümbrecht Merck, Darmstadt
Cryogenic vials	1.5 ml	Sarstedt, Nümbrecht
Cultivating tubes	13 ml	Sarstedt, Nümbrecht
Desalting column	PD-10	GE Healthcare, Chalfont St. Giles, England
Deepwell plates	96-Well plates, 2 ml	VWR, Radnor, USA
Dialysis membrane	Spectra/Por® Biotech, regenerated Cellulose, MWCO: 8,000, nominal area: 16 mm, diameter: 10 mm, Volume/length: 0.79 ml/cm, total length: 15 m	Spectrum Laboratories, Los Angeles, USA
Glass vials	1.5 ml	Macherey-Nagel, Düren
HisTrap™ FF	crude, 1 ml, Ni-NTA	GE Healthcare, Chalfont St Giles, England
HPLC column	YMC-Pack ODS-AQ, 12 nm, 5 µm, 150 x 4.6 mm	YMC Europe, Dinslaken
Microtiter plates	96-Well plates (sterile)	VWR, Radnor, USA
Pipette tips	1-10 µl, 10-200 µl, 100-1000 µl	Sarstedt, Nümbrecht
Reaction tubes	1.5/2.0 ml	Sarstedt, Nümbrecht
SPE columns	Chromabond® HR-X, hydrophobic polystyrene-divinylbenzene resin, 1 ml/30 mg, 85 µm, RP SPE	Macherey-Nagel, Düren
Syringe filter	0.2 µm, Minisart NML plus (hydrophilic), sterile	Sigma-Aldrich, St. Louis, USA

TLC plates	Silica gel 60 RP-18 F <sub>254</sub> S	Merck, Darmstadt
UHPLC columns	EASY-Column, 2 cm, 100 µm, 5 µm, C18	Thermo Fisher Scientific, Waltham, USA
	EASY-Column, 10 cm, 75 µm, 3 µm, C18-A2	
UV cuvettes	1 ml	VWR, Radnor, USA

### 2.1.5. Instruments

**Table 5** Used devices.

Device	Description	Source
Autoclave	Steam sterilizer HV 110	HMC Europe, Tüßling
Automated liquid handling platform	Bravo	Agilent, Santa Clara, USA
Central robot unit	F5 Robot system	Thermo Fisher Scientific, Waltham, USA
Centrifuges	Allegra® X-30R	Beckman Coulter, Brea, USA
	Avanti® J-E	Beckman Coulter, Brea, USA
	Centrifuge 5424 (15,000 rpm)	Eppendorf, Hamburg
	Rotanta 460 Robotic	Hettich, Tuttlingen
	Mikro 185 (13,300 rpm)	Hettich, Tuttlingen
Clean bench	Universal 320 R	Hettich, Tuttlingen
	Safe 2020	Thermo Fisher Scientific, Waltham, USA
Colony picking system	QPix 420	Molecular Devices, Sunnyvale, USA
Electrophoresis chamber	Hoefler mini vertical gel electrophoresis (SDS-PAGE)	Serva Electrophoresis GmbH, Heidelberg
	Compact horizontal gel electrophoresis (DNA)	Analytik Jena AG, Jena

Gel documentation	Biodocanalyze	Biometra, Göttingen
HPLC	Agilent 1260 Infinity (quaternary pump, DAD & FLD detector, auto sampler, fraction collector, column oven)	Agilent, Santa Clara, USA
Incubator	Ecotron	Infors HT, Bottmingen, Switzerland
	Cytomat 2 C-LIN	Thermo Fisher Scientific, Waltham, USA
Mass spectrometer	Orbitrap Elite	Thermo Fisher Scientific, Waltham, USA
	Orbitrap Velos Pro	
pH electrode	pHenomenal® 110	VWR, Radnor, USA
pH meter	pHenomenal® pH 1000 L	VWR, Radnor, USA
Photometer	BioPhotometer plus	Eppendorf, Hamburg
Rotors	4-Place swing-out rotor	Hettich, Tuttlingen
	Fixed angle rotor 1689-A (14,000 rpm)	Hettich, Tuttlingen
	Fixed angle rotor C0650 (10,000 rpm)	Beckman Coulter, Brea, USA
	Fixed angle rotor F2402H (26,000 rpm)	Beckman Coulter, Brea, USA
	Fixed angle rotor JA-10 (10,000 rpm)	Beckman Coulter, Brea, USA
	Fixed angle rotor JLA-16.250 (16,000 rpm)	Beckman Coulter, Brea, USA
	Swing-out rotor SX 4400 (4700 rpm)	Beckman Coulter, Brea, USA
Shakers	Vortex-Genie 2	Scientific Industries, Bohemia, USA
	Polymax 1040	Heidolph, Schwabach
Spectrometer	Colibri (microvolume)	Titertek-Berthold, Pforzheim
Thermocycler	TProfessional TRIO Thermocycler®, Biometra	Analytik Jena AG, Jena
Thermoshaker	BioShake iQ	Analytik Jena AG, Jena

TLC development	TLC chamber	Camag, Muttenz, Switzerland
TLC documentation	Reprostar 3	Camag, Muttenz, Switzerland
TLC visualization	UV lamp	Camag, Muttenz, Switzerland
UHPLC	EASY-nLC™ 1200	Thermo Fisher Scientific, Waltham, USA
Ultrapure water unit	Milli-Q® Gradient A10	Merck Millipore, Darmstadt
Ultrasonic homogenizer	Sonopuls UW 3100	Bandelin electronic, Berlin
Ultrasonic probe	Sonopuls micro tip MS 73	Bandelin electronic, Berlin
Voltage source	Standard Power Pack P25	Biometra, Göttingen
Water bath	Lauda A100	Lauda, Lauda-Königshofen

### 2.1.6. Proteins

**Table 6** Used proteins. FDU: FastDigest unit.

Protein	Source
Acidic phosphatase from potato (3-10 U mg <sup>-1</sup> )	Merck, Darmstadt
Bovine serum albumin (BSA)	Roth, Karlsruhe
DNase I (≈ 3,000 U mg <sup>-1</sup> , bovine pancreas)	AppliChem, Darmstadt
Lysozyme (≈ 70,000 U mg <sup>-1</sup> , chicken egg white)	Sigma-Aldrich, St. Louis, USA
Fast Digest® DpnI (1 FDU μl <sup>-1</sup> )	Thermo Fisher Scientific, Waltham, USA
Pfu DNA Polymerase (2.5 U μl <sup>-1</sup> )	Thermo Fisher Scientific, Waltham, USA
Phusion DNA Polymerase (2 U μl <sup>-1</sup> )	Thermo Fisher Scientific, Waltham, USA
DreamTaq DNA Polymerase (5 U μl <sup>-1</sup> )	Thermo Fisher Scientific, Waltham, USA
T4 ligase (5 U μl <sup>-1</sup> )	Thermo Fisher Scientific, Waltham, USA
Trypsin	Thermo Fisher Scientific, Waltham, USA
Nco I (10 U μl <sup>-1</sup> )	Thermo Fisher Scientific, Waltham, USA
Hind III (10 U μl <sup>-1</sup> )	Thermo Fisher Scientific, Waltham, USA

### 2.1.7. Oligonucleotides

Oligonucleotides (Table 7) were purchased from Eurofins Genomics (Ebersberg). All were of HPSF (high purity salt free) purified grade, received lyophilized and dissolved in ultrapure water.

**Table 7** Used oligonucleotides for site-directed mutagenesis and sequencing. For  $T_m$  calculations the tool OligoCalc (<http://biotools.nubic.northwestern.edu/OligoCalc.html>, nearest neighbor) was used. fw: forward primer, re: reverse primer, ThkCPT: *Thermococcus kodakaraensis* cis-prenyltransferase,  $T_m$ : melting temperature, **bold**: mutagenesis positions, lower script letters: attachment sites for cloning.

Name	Sequence (5'-3')	$T_m$ (°C)
AtCPT_d33_fw	catgcatg <b>CCATGG</b> CGCTGCTTAAATTGATCGGGCTGATC	72.7
AtCPT_d33_re	catgcatg <b>AAGCTT</b> CACGCGACAACCAAAGCGACGTTC	71.1
ThkCPT_C- His_del_fw	CCGCGGATCCCTCGAGT <b>AG</b> CACCACCACCACCACT	71.2
ThkCPT_C- His_del_re	AGTGGTGGTGGTGGT <b>GCT</b> ACTCGAGGGATCCGCGG	71.2
ThkCPT_E68A_fw	CGGTTCGAAGAAACTGG <b>CGG</b> GAGATCCTTGAATGGTGCCGC	72.2
ThkCPT_E68A_re	GCGGCACCATTCAAGGATCTCC <b>GCC</b> AGTTTCTTCGAACCG	72.2
ThkCPT_I41A_fw	CCCGAAACATGTCGCCATT <b>GCC</b> ATGGATGGCAATCGTCGTTGG	72.6
ThkCPT_I41A_re	CCAACGACGATTGCCATCCATG <b>GCA</b> ATGGCGACATGTTTCGGG	72.6
ThkCPT_I41F_fw	CCCGAAACATGTCGCCATTTTCATGGATGGCAATCGTCGTTGG	71.0
ThkCPT_I41F_re	CCAACGACGATTGCCATCCATG <b>AAA</b> ATGGCGACATGTTTCGGG	71.0
ThkCPT_I41G_fw	CCCGAAACATGTCGCCATT <b>GG</b> CATGGATGGCAATCGTCGTTGG	72.6
ThkCPT_I41G_re	CCAACGACGATTGCCATCCATG <b>GCA</b> ATGGCGACATGTTTCGGG	72.6
ThkCPT_K109A_fw	CTGATGAATCTGTTTCGAGGA <b>AGC</b> GTTTAAAGAACTGGTCCAGG	69.5
ThkCPT_K109A_re	CCTGGACCAGTTCTTTAAAC <b>GCT</b> TCCTCGAACAGATTCATCAG	69.5
ThkCPT_L113A_fw	CGAGGAAAAGTTTAAAGA <b>AGC</b> GGTCCAGGATGAACGTGTGC	69.4
ThkCPT_L113A_re	GCACACGTTTCATCCTGGAC <b>CGCT</b> TCTTTAAACTTTTCCTCG	69.4
ThkCPT_L158A_fw	CGGAAATACAGCAACTACAAC <b>GCCA</b> ACATTGCGTTAGCCTATGG	70.9
ThkCPT_L158A_re	CCATAGGCTAACGCAATGTT <b>GCG</b> TTGTAGTTGCTGTATTTCCG	70.9
ThkCPT_Y156A_fw	GCGACACGGAAATACAGCAAC <b>GCCA</b> ACCTCAACATTGCGTTAGCC	72.9
ThkCPT_Y156A_re	GGCTAACGCAATGTTGAGGTT <b>GCG</b> TTGCTGTATTTCCGTGTCGC	72.9
ThkCPT_Y85W_fw	CCGCACCCTGACGGTAT <b>GGG</b> CCTTTAGTACCGAGAAC	69.4
ThkCPT_Y85W_re	GTTCTCGGTACTAAAG <b>GCC</b> CATACCGTCAGGGTGCGG	69.4
T7	TAATACGACTCACTATAGGG	46.4
T7 term	CTAGTTATTGCTCAGCGGT	50.7

### 2.1.8. Plasmids

**Table 8** Used plasmids.

Name	Source	Resistance gene
pET20b(+)-AtCPT	Received from Dr. Jeanette Ludwig (IPB Halle)	$\beta$ -Lactamase
pET28a(+)-ThkCPT	Synthesized by Eurofins Genomics (Ebersberg)	Aminoglycoside-3'-phosphotransferase
pTG10-GroESL (pGroESL) <sup>1</sup>	Received from Prof. Poulter, University of Utah, USA	Chloramphenicol acetyltransferase
pUC19	Thermo Fisher Scientific, Waltham, USA	$\beta$ -Lactamase

### 2.1.9. *E. coli* strains

**Table 9** Used *E. coli* strains.

Strain	Genotype, source
DH5 $\alpha$	F <sup>-</sup> $\Phi$ 80/ <i>lacZ</i> $\Delta$ M15 $\Delta$ ( <i>lacZYA-argF</i> ) U169 <i>recA1 endA1 hsdR17</i> ( <i>r<sub>k</sub><sup>-</sup>, m<sub>k</sub><sup>+</sup></i> ) <i>phoA supE44 <math>\lambda</math> thi<sup>-</sup>1 gyrA96 relA1</i> Invitrogen, Karlsruhe
BL21 (DE3)	F <sup>-</sup> <i>ompT hsdS<sub>B</sub></i> ( <i>r<sub>B</sub><sup>-</sup>, m<sub>B</sub><sup>-</sup></i> ) <i>gal dcm</i> (DE3) Invitrogen, Karlsruhe

Competent *E. coli* DH5 $\alpha$  and BL21 (DE3) cells were prepared according to Inoue<sup>[94]</sup>. Cell batches yielding 10<sup>6</sup>-10<sup>8</sup> transformants after transformation with the vector pUC19 (2  $\mu$ g) and subsequent transfer to LB ampicillin selection medium were used in further experiments.

<sup>1</sup> Plasmid pTG10 is a pACYC184 derived cloning vector and pGroESL is a pTG10 derivative encoding the *groE* operon under control of both its native and the IPTG-inducible *lac* promoters.<sup>[93]</sup>

## 2.1.10. Software

**Table 10** Used software.

<b>Provider</b>	<b>Purpose for use</b>
BoxShade	Alignment of multiple protein sequences
CAVER 3.01 <sup>[95]</sup>	Analysis of the hydrophobic tunnel of the ThkCPT homology model
ChemDraw Professional 15.0	Generation of structural formulas and calculation of exact masses
ChemSketch 14.0 (ACD/Labs)	Visualization of 3D structures of the used homoallylic substrates
DoubleDigest Calculator - Thermo Fisher Scientific	Determination of optimal reaction conditions for a double digest reaction
Eurofins Genomics	Synthesis of oligonucleotide Sequencing
ExPASy	Translation of nucleotide sequence to a protein sequence
ExPASy ProtParam tool	Computation of physical and chemical parameters for a protein sequence
Mascot software 2.4 (Matrix Science)	Peptide identification
MultiAlin	Alignment of multiple protein sequences
OligoCalc	Oligonucleotide properties calculator $T_m$ calculations
Proteome Discoverer 1.4 (Thermo Fisher Scientific)	Peptide identification
PyMOL 1.8	Generation of figures from protein crystal structures or homology models
Sequence Manipulation Suite (reverse complement)	Conversion of DNA sequence into its reverse-complement
Sequence Manipulation Suite (reverse translate)	Generation of a DNA sequence from a protein sequence
SigmaPlot 13.0	Plotting of primary data Figure generation



SwissProt protein database	Peptide identification
TAIR10 protein database	Peptide identification
T <sub>m</sub> calculator (NEB, Thermo Fisher Scientific)	Calculation of the annealing temperature
Xcalibur software 2.7 SP1	Mass spectrometric data evaluation

## 2.2. Microbiological methods

### 2.2.1. Cultivation of bacteria

Overnight cultures were prepared in culture tubes containing 5 ml of LB medium supplemented with the appropriate antibiotic. A single colony was used for inoculation. The cultures were incubated at 37°C overnight under shaking (220 rpm).

For long-term storage an overnight culture was centrifuged (5 min, 4700 rpm, Allegra® X-30R, swing-out rotor SX 4400, Beckman Coulter), the supernatant was discarded and the cell pellet was dissolved in 1 ml of LB medium supplemented with 20 % (v/v) glycerin. The cultures were then transferred to cryogenic vials, frozen in liquid nitrogen and stored at -80°C.

For short-term storage the bacterial strains were cultivated on LB agar plates supplemented with appropriate antibiotic. LB agar plates were sealed with parafilm and stored at 4°C for a maximum of 4 weeks.

The cultivation in a microtiter plate (MTP) was performed by using an automated integrated robotic platform (central F5 robot system, Thermo Fisher Scientific). The wells of a 96-well plate were filled with 200 µl of LB medium supplemented with the appropriate antibiotic. Bacteria grown on a LB agar plate were automatically picked (QPix 420, Molecular Devices) and transferred to the medium-filled wells of the MTP. The MTP was then incubated for 4 h at 37°C and 900 rpm with high humidity to prevent dehydration (Cytomat 2 C-LIN, Thermo Fisher Scientific). The obtained master plate was then stored at 4°C until further use.

## **2.3. Molecular biological methods**

### **2.3.1. Plasmid preparation from *E. coli***

The isolation of plasmid DNA from *E. coli* was carried out by using the Invisorb® Spin Plasmid Mini Two Kit (Stratec Molecular, Berlin) according to manufacturer's instructions<sup>[96]</sup>. Therefore, 5 ml of a pre-culture were prepared.

To obtain a higher amount of plasmid DNA a large-scale preparation was carried out by using the NucleoBond® Xtra Midi Kit (Macherey-Nagel, Düren) according to manufacturer's instructions<sup>[97]</sup> using 500 ml of an *E. coli* suspension.

### **2.3.2. Determination of DNA concentration**

The DNA concentration was determined photometrically at a wavelength of 260 nm by using the microvolume spectrometer Colibri (Titertek-Berthold, Pforzheim). An OD<sub>260</sub> of 1 corresponds to 50 µg ml<sup>-1</sup> double-stranded DNA. 2 µl of the plasmid DNA were applied and compared to pure water as blank.

### **2.3.3. Agarose gel electrophoresis**

Agarose gel electrophoresis is used for size-dependent separation of DNA fragments. Therefore, gels containing 1% (w/v) agarose were prepared in TAE buffer (1x) and supplemented with 0.5 µg ml<sup>-1</sup> ethidium bromide. DNA samples were mixed with DNA loading dye (Thermo Fisher Scientific, Darmstadt) and applied to the gel. Separation was carried out at 120 V in a horizontal electrophoresis device in TAE buffer (1x). To determine the DNA fragment size a molecular weight marker was used (GeneRuler™ 1 kb Plus DNA Ladder, Thermo Fisher Scientific, Darmstadt). Visualization was achieved by irradiation with UV light using a gel documentation device, based on the DNA-intercalating properties of ethidium bromide.

### **2.3.4. Sequencing of plasmid DNA**

Sequencing of plasmid DNA was carried out by Eurofins Genomics (Ebersberg) using the vector specific primers T7 and T7 term (Table 7, section 2.1.7.). The data were evaluated by using the software listed in table 10 (section 2.1.10.).

### 2.3.5. Transformation

For transformation chemically-competent *E. coli* cells were used (BL21 (DE3) or DH5 $\alpha$ ). An aliquot of 50  $\mu$ l (stored at -80°C) of the corresponding cells was thawed on ice. Afterwards, 50 ng of the plasmid DNA were added to the cells and the mix was incubated for 10 min on ice. Subsequently, a heat shock (30 s at 42°C, water bath) was applied to allow the plasmid DNA to enter the bacterial cells. After cooling on ice, 250  $\mu$ l of SOC medium were added and the sample was incubated under shaking (220 rpm) for 1 h at 37°C. For selection the cells were plated on a LB agar plate supplemented with the corresponding antibiotic and incubated overnight at 37°C.

### 2.3.6. Polymerase chain reaction (PCR)

#### 2.3.6.1. Site-directed mutagenesis

For site-directed mutagenesis of a gene (according to the QuikChange manual<sup>[98]</sup>) modified oligonucleotides were used (Table 7, section 2.1.7.). The complementary oligonucleotides were used in PCR reactions to amplify the entire plasmid. The reagents used for a reaction with a total volume of 20  $\mu$ l are listed in table 11. The experiments were carried out in a thermocycler. The PCR program used for the amplification of DNA is shown in table 12.

For the calculation of the annealing temperature tools from Thermo Fisher Scientific (<https://www.thermofisher.com/>) or NEB (<http://tmcalculator.neb.com/#/>) were used.

**Table 11** Components used in the site-directed mutagenesis PCR reactions. fw: forward, re: reverse.

Reagent	Amount per assay
10x Pfu buffer + MgSO <sub>4</sub>	1x
DNA template	20 ng
10 mM dNTPs	0.2 mM
10 pmol $\mu$ l <sup>-1</sup> Primer fw	50 ng
10 pmol $\mu$ l <sup>-1</sup> Primer re	50 ng
H <sub>2</sub> O	add to V <sub>total</sub> = 20 $\mu$ l
2.5 U $\mu$ l <sup>-1</sup> Pfu DNA polymerase	add 0.5 $\mu$ l

**Table 12** PCR program for site-directed mutagenesis. Annealing temperature did not exceed 72°C.

1	Initial denaturation	95°C	1 min	
2	Denaturation	95°C	30 s	} 18x
3	Annealing	$T_m - 5^\circ\text{C}$	1 min	
4	Extension	72°C	1 min/kb of plasmid length	
5	Hold	4°C	Pause	

After amplification the residual methylated template DNA was digested with 1  $\mu\text{l}$  of FastDigest DpnI (1 h, 37°C). Subsequently, 3-5  $\mu\text{l}$  of the sample were used for the transformation (section 2.3.5.) of chemically-competent *E. coli* cells.

### 2.3.6.2. Colony PCR

Colony PCR was used to check the success of a transformation. Therefore, an appropriate reaction mixture was prepared and the colony of interest was added by means of a tooth pick. The reagents used for a reaction with a total volume of 20  $\mu\text{l}$  are listed in table 13. As primer pair the oligonucleotides T7 and T7 term were used (Table 7, section 2.1.7.). As positive or negative control a sample supplemented with purified plasmid DNA containing the fragment of interest or 1  $\mu\text{l}$  of water, respectively, was prepared. The experiments were carried out in a thermocycler. The PCR program used for the amplification of DNA is shown in table 14.

**Table 13** Components used in the colony PCR reactions.

Reagent	Amount per assay
10x DreamTaq buffer	1x
10 mM dNTPs	0.2 mM
10 pmol $\mu\text{l}^{-1}$ T7 Primer	50 ng
10 pmol $\mu\text{l}^{-1}$ T7 term Primer	50 ng
H <sub>2</sub> O	add to $V_{\text{total}} = 20 \mu\text{l}$
Bacterial colony	add by using a tooth pick
5 U $\mu\text{l}^{-1}$ DreamTaq DNA polymerase	add 0.1 $\mu\text{l}$

**Table 14** Cycling program for colony PCR.

1	Initial denaturation	94°C	2 min	
2	Denaturation	94°C	1 min	} 25x
3	Annealing	55°C	1 min	
4	Extension	72°C	1 min	
5	Final extension	72°C	7 min	
6	Hold	4°C	Pause	

Afterwards the samples were checked for the presence of fragments by agarose gel electrophoresis (section 2.3.3.).

### 2.3.6.3. Truncation of AtCPT

The gene sequence from *Arabidopsis thaliana* cis-prenyltransferase (AT2G23410.1) codes for a N-terminal transmembrane region<sup>[4]</sup> (<http://www.uniprot.org/uniprot/O80458>). As the purification of such membrane-bound proteins proved to be challenging it was desired to truncate the gene sequence via PCR to obtain a recombinant protein. Therefore, corresponding primers were designed (Table 7, section 2.1.7.). The reagents used for a reaction with a total volume of 50 µl are listed in table 15. The experiments were carried out in a thermocycler. The PCR program used for the amplification of DNA is shown in table 16. Truncated AtCPT is referred to as AtCPT\_Δ33.

For the calculation of the annealing temperature tools from Thermo Fisher Scientific (<https://www.thermofisher.com/>) or NEB (<http://tmcalculator.neb.com/#/>) were used.

**Table 15** Components used in the PCR to truncate the AtCPT gene. fw: forward, re: reverse.

Reagent	Amount per assay
5x HF buffer	1x
DNA template	200 ng
10 mM dNTPs	0.2 mM
10 µM Primer fw	0.5 µM
10 µM Primer re	0.5 µM
H <sub>2</sub> O	add to V <sub>total</sub> = 50 µl
2.5 U µl <sup>-1</sup> Phusion DNA polymerase	add 0.5 µl at the end

**Table 16** PCR program used to truncate the AtCPT gene.

1	Initial denaturation	98°C	30 s	} 35x
2	Denaturation	98°C	10 s	
3	Annealing	66°C	30 s	
4	Extension	72°C	50 s	
5	Final extension	72°C	5 min	
6	Hold	4°C	Pause	

After checking the amplification by agarose gel electrophoresis (section 2.3.3.), the DNA fragment was purified by gel extraction using the NucleoSpin® Gel and PCR Clean-Up Kit from Macherey-Nagel (Düren) according to manufacturer's instructions<sup>[99]</sup>. To introduce the amplified DNA fragment into a vector, both were cut by corresponding restriction enzymes. The recommended buffer and enzyme ratio was chosen according to the DoubleDigest Calculator (<https://www.thermofisher.com/>). The reagents used for a reaction with a total volume of 10 µl are listed in table 17. For digestion of the truncated AtCPT fragment and the vector of interest, the restriction enzymes Nco I and Hind II were used in a ratio of 1:2. The sample was then incubated for 1 h at 37°C.

**Table 17** Components used in enzymatic restriction digestion.

Reagent	Amount per assay
10x Tango buffer	1x
DNA sample	50 ng
10 U µl <sup>-1</sup> Nco I	1 U
10 U µl <sup>-1</sup> Hind III	2 U
H <sub>2</sub> O	add to V <sub>total</sub> = 10 µl

After checking the amplification by agarose gel electrophoresis (section 2.3.3.), the DNA fragments were purified by gel extraction using the NucleoSpin® Gel and PCR Clean-Up Kit from Macherey-Nagel (Düren) according to manufacturer's instructions<sup>[99]</sup>. The concentration of insert and vector was determined (section 2.3.2.). The insert was used with a 2:1 molar ratio of insert to vector. The reagents used for a reaction with a total volume of 20 µl are listed in table 18. The sample was incubated for 30 min at room temperature.

**Table 18** Components used for the ligation of fragment and vector.

Reagent	Amount per assay
10x T4 ligase buffer	1x
Vector plasmid	100 ng
DNA insert	2:1 molar ratio of insert to vector
5 U $\mu\text{l}^{-1}$ T4 ligase	1 U
H <sub>2</sub> O	add to $V_{\text{total}} = 20 \mu\text{l}$

The sample was then used for transformation (section 2.3.5.) and grown colonies were checked for the presence of the insert by colony PCR (section 2.3.6.2.).

## 2.4. Protein biochemical methods

### 2.4.1. Recombinant protein production

Expression of recombinant proteins was carried out with transformed *E. coli* growing in LB medium. An overnight culture in 50 ml LB medium was prepared as described in section 2.2.1. in a sterile Erlenmeyer flask. The medium was supplemented with 50  $\mu\text{g ml}^{-1}$  kanamycin when cultivating for ThkCPT, or 100  $\mu\text{g ml}^{-1}$  ampicillin/50  $\mu\text{g ml}^{-1}$  chloramphenicol when cultivating for AtCPT and GroESL. The overnight culture was then added to 950 ml of LB medium supplemented with the appropriate antibiotic (1:20 dilution) and incubated at 37°C (ThkCPT) or 30°C (AtCPT) under shaking (220 rpm) until an OD<sub>600</sub> (optical density at 600 nm) of  $\approx 0.8$  was reached. A sample of 500  $\mu\text{l}$  was taken and pelletized (centrifugation at 15,000 rpm for 5 min; Centrifuge 5424, Eppendorf) for SDS-PAGE (section 2.4.10.). The induction of recombinant protein expression was carried out by adding 0.1 mM IPTG, from a 1 M stock, followed by incubation for 4 h at 37°C (ThkCPT) or 30°C (AtCPT) under shaking (220 rpm). Another sample of 500  $\mu\text{l}$  was taken and pelletized (centrifugation at 15,000 rpm for 5 min; Centrifuge 5424, Eppendorf) for SDS-PAGE (see section 2.4.10.). The cells were harvested by centrifugation for 20 min at 4°C and 10,000 rpm (Avanti® J-E, JA-10 fixed angle rotor, Beckmann Coulter). The supernatant was discarded, the cells were transferred into centrifugal tubes (50 ml) and the cell weight was determined. The cells were further processed or stored at -20°C until further usage.

#### **2.4.1.1. Recombinant protein production in microtiter plates (MTP)**

The following steps were performed by using an automated integrated robotic platform (central F5 robot system, Thermo Fisher Scientific). The wells of a 96-well plate were filled with 200  $\mu\text{l}$  of AI medium (Table 3, section 2.1.3.) supplemented with the appropriate antibiotic. Bacterial cultures were automatically picked (QPix 420 Colony Picking System, Molecular Devices) from a master plate (section 2.2.1.) and transferred to the wells of the MTP. The MTP was then incubated overnight at 37°C and 900 rpm with high humidity to prevent dehydration (Cytomat 2 C-LIN, Thermo Fisher Scientific). Afterwards, the cells were pelletized by centrifugation for 20 min at 4°C and 4,600 rpm (Rotanta 460 Robotic, 4-place swing-out rotor, Hettich). The supernatant was discarded automatically (Bravo automated liquid handling platform, Agilent) and the cells were stored at -80°C until further usage.

#### **2.4.2. Cell lysis by ultrasonic treatment**

For cell lysis by ultrasonic treatment the cell pellet was resuspended in 20 ml of lysis buffer (Table 3, section 2.1.3.). 1 mM PMSF (a serine protease inhibitor), 100  $\mu\text{g ml}^{-1}$  lysozyme and 125  $\mu\text{g ml}^{-1}$  DNase I were added. As the lysis buffer contains EDTA,  $\text{MgCl}_2$  had to be added to confer activity of added DNase I. The mixture was then incubated for 15 min at room temperature on a shaker (50 rpm). Cell disruption was carried out by ultrasonic treatment. The sample was sonificated three times with an amplitude of 70 % for 30 s (1 s on-off-pulse interval). During cell disruption the sample was cooled on ice. In case of the AtCPT 1 % (v/v) Triton X-100 was added and the sample was again incubated on ice for 30 min on a shaker (50 rpm) to aid solubilization of the protein<sup>[4]</sup>. Afterwards, the sample was centrifuged for 30 min at 4°C and 10,000 rpm (Avanti® J-E, JLA-16.250 fixed angle rotor, Beckmann Coulter). The protein containing supernatant was transferred to a separate centrifugal tube (50 ml) and used for further process.

#### **2.4.3. Cell lysis by osmotic shock**

For small amounts of cells the lysis was carried out in 1.5 ml reaction tubes by osmotic shock (only for ThkCPT). The cell pellet was first resuspended with 1 ml of sucrose buffer (Table 3, section 2.1.3.) and incubated for 10 min at 25°C and 400 rpm in a thermoshaker (BioShake iQ, Analytik Jena AG, Jena). After centrifugation (15,000 rpm for 10 min; Centrifuge 5424,



Eppendorf) the supernatant was discarded and the cell pellet was resuspended in 470  $\mu\text{l}$  of Tris buffer (Table 3, section 2.1.3.) supplemented with 100  $\mu\text{g ml}^{-1}$  lysozyme and 125  $\mu\text{g ml}^{-1}$  DNase I. The sample was incubated for 25 min at 25°C and 800 rpm in a thermoshaker (BioShake iQ, Analytik Jena AG, Jena). After centrifugation (15,000 rpm for 10 min; Centrifuge 5424, Eppendorf) the supernatant was transferred to a separate 1.5 ml reaction tube. As the ThkCPT is thermophilic and stable at higher temperatures the supernatant was precipitated by heat (20 min at 65°C, 400 rpm) in a thermoshaker (BioShake iQ, Analytik Jena AG, Jena). Precipitated proteins were separated by centrifugation (15,000 rpm for 10 min; Centrifuge 5424, Eppendorf) and the supernatant (= crude extract) was used for activity assays (section 2.5.1.3.).

#### **2.4.3.1. Cell lysis by osmotic shock in microtiter plates (MTP)**

The following steps were performed by using an automated integrated robotic platform (central F5 robot system, Thermo Fisher Scientific). After recombinant expression in a MTP (section 2.4.1.1.), the cell pellets were resuspended in 200  $\mu\text{l}$  of lysis buffer for MTPs (Table 3, section 2.1.3.) and incubated at 30°C and 900 rpm for 2 h at high humidity to prevent dehydration (Cytomat 2 C-LIN, Thermo Fisher Scientific). Afterwards, the cells were pelletized by centrifugation for 20 min at 4°C and 4,600 rpm (Rotanta 460 Robotic, 4-place swing-out rotor, Hettich). The supernatant (150  $\mu\text{l}$ ) was transferred automatically to a separate MTP (Bravo automated liquid handling platform, Agilent). The cleared lysate was then used for activity assays (section 2.5.1.4.).

#### **2.4.4. Protein purification via immobilized metal ion affinity chromatography (IMAC)**

Proteins containing an N- or C-terminal poly-histidine tag can bind specifically and non-covalent to bivalent cation-NTA matrices. In aqueous solutions NTA (nitrilotriacetic acid) forms complexes with metal ions, e.g.  $\text{Ni}^{2+}$  or  $\text{Co}^{2+}$ . The bivalent cation can be additionally complexed by the free electron pair of the nitrogen in the imidazole ring of the histidine (Figure 10). By increasing concentrations of imidazole the bound protein can be eluted from the resin. As imidazole is a substructural unit of histidine it replaces the protein and binds instead to the resin<sup>[100]</sup>.

The protein purification was carried out by using 1 ml HisTrap™ FF columns (Ni<sup>2+</sup>-NTA) according to manufacturer's instructions. After cell lysis by ultrasonic treatment (section 2.4.2.) the protein containing supernatant was applied to a 1 ml HisTrap™ FF column (GE Healthcare, England) with a flow rate of 0.8 ml min<sup>-1</sup> by using a peristaltic pump. The column was then washed with 10-15 ml of binding/wash buffer (Table 3, section 2.1.3.) to remove unbound proteins. Afterwards, the protein was eluted with 8 ml of elution buffer (Table 3, section 2.1.3.), a highly concentrated imidazole buffer. Fractions of 1 ml were collected and checked for protein by using diluted Bradford reagent (Roth, Karlsruhe) according to manufacturer's instructions. Protein-containing fractions were then used for buffer exchange via size-exclusion chromatography (section 2.4.6.) or dialysis (section 2.4.7.) and optionally for concentration via ultrafiltration (section 2.4.8.). The protein concentration was then determined (section 2.4.9.) and the obtained protein solution was shock frozen in aliquots (500 µl) in liquid nitrogen and stored at -20°C until further usage. Purification steps were controlled by SDS-PAGE (section 2.4.10.).

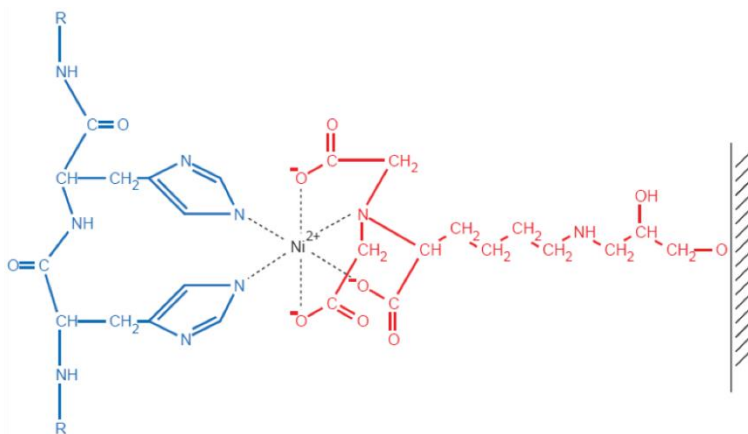


**Figure 10** Schematic representation of the poly-histidine (blue) binding to Ni<sup>2+</sup>-NTA (red). Figure taken from University of Oklahoma Libraries (OU Open Educational Resources)<sup>[101]</sup>.

#### 2.4.5. Protein purification via preparation of periplasmic extracts (AtCPT)

As the AtCPT contains a *pelB* signal sequence (Figure A1, appendix section 8.2.) the protein is assumed to be transported to the periplasm<sup>[102]</sup>. Therefore, a purification via preparation of periplasmic extracts was carried out adapted to an osmotic shock protocol from Neu and Heppel<sup>[103]</sup>.

The protein expression (section 2.4.1.) was carried out at 20°C overnight. After centrifugation for 20 min at 4°C and 5,000 rpm (Avanti® J-E, JA-10 fixed angle rotor, Beckmann Coulter) the cell pellet was resuspended in TSE buffer (4 ml g<sup>-1</sup> pellet; Table 3,

section 2.1.3.) supplemented with 1 mM PMSF and 100  $\mu\text{g ml}^{-1}$  lysozyme. The suspension was then incubated on ice for 1 h with shaking. Afterwards, the sample was centrifuged for 10 min at 4°C and 5,000 rpm (Avanti® J-E, JA-10 fixed angle rotor, Beckmann Coulter) and the supernatant was removed and stored at -20°C until further processing (= TSE supernatant). The remaining cell pellet was then resuspended in 30 ml of cold ultrapure water supplemented with 1 mM  $\text{MgCl}_2$  and 1 mM PMSF and incubated on ice for 15 min shaking. 125  $\mu\text{g ml}^{-1}$  DNase I were added and the sample was then centrifuged for 30 min at 4°C and 10,000 rpm (Avanti® J-E, JA-10 fixed angle rotor, Beckmann Coulter). The supernatant was removed and stored at -20°C until further processing (= H<sub>2</sub>O supernatant). The remaining cell pellet was then used for cell lysis by ultrasonic treatment as it is described in section 2.4.2. The supernatant (= lysate) was removed and stored at -20°C until further processing. The remaining cell pellet was resuspended in assay buffer (Table 3, section 2.1.3.) and stored at -20°C until further usage.

#### **2.4.6. Buffer exchange of protein samples via size-exclusion chromatography**

Size-exclusion chromatography (SEC) is used to separate substances according to their molecular size. As stationary phase cross-linked dextran (e.g. sephadex) or agarose can be used<sup>[104]</sup>. Small molecules are able to enter the pores of the material so that they flow more slowly through the stationary phase. In contrast, larger molecules pass through the material without entering the pores and are eluted earlier. For buffer exchange a PD-10 desalting column (GE Healthcare, England) was used according to manufacturer's instructions<sup>[105]</sup>. First, the column was equilibrated with 25 ml of assay buffer without Triton X-100 (Table 3, section 2.1.3.) and the flow-through was discarded. Afterwards, the sample was applied and eluted with 3.5 ml of the same buffer (Table 3, section 2.1.3.). For experiments in which the influence of bivalent cations was tested, an assay buffer without additional bivalent cations was used.

#### **2.4.7. Dialysis**

Dialysis is an osmotic process driven by concentration which is used for removing small molecules or ions (salts, sugars) by passage of a semipermeable membrane. For dialysis the sample was transferred into a dialysis membrane (Spectrum Laboratories, USA) which was

then sealed. The sample was dialyzed twice against 1 l of appropriate dialysis buffer (Table 3, section 2.1.3.). First, for 1 h at 4°C and then overnight at 4°C.

#### 2.4.8. Concentrating of protein samples

To concentrate protein samples, centrifugal tubes with a semipermeable membrane were used (Amicon® Ultra-15, see table 4 in section 2.1.4.). During centrifugation the membrane holds back bigger molecules, like proteins, whereas smaller molecules can pass through. The sample was applied to the membrane and centrifuged for 10 min at 4700 rpm and 4°C (Allegra® X-30R, swing-out rotor SX 4400, Beckman Coulter) until the desired volume of protein solution was obtained.

#### 2.4.9. Determination of the protein concentration

The protein concentration was determined according to Bradford<sup>[106, 107]</sup>. Therefore, Coomassie Brilliant Blue G-250 was used which binds to the proteins. By this, the dye is transferred from the cationic to the anionic state and absorption at 595 nm ( $E_{595}$ ) can be measured. Concentration determination was carried out by means of a calibration line which was prepared with bovine serum albumin (BSA) for concentrations ranging between 1  $\mu\text{g ml}^{-1}$  and 20  $\mu\text{g ml}^{-1}$ . The sample, with a total volume of 1 ml, was prepared in an UV cuvette. The required amount of protein solution was diluted with ultrapure water to a total volume of 800  $\mu\text{l}$ . Then 200  $\mu\text{l}$  of 5x concentrated Bradford reagent (Roti®-Quant) were added and the sample was incubated for 10 min at room temperature. The absorption at 595 nm was then measured and the concentration was calculated considering the dilution factor (Equation 1). As a blank, assay buffer (Table 3, section 2.1.3.) instead of protein solution was used.

$$c \left[ \frac{\mu\text{g}}{\text{ml}} \right] = \frac{E_{595}}{m_{\text{calibration line}}} \cdot DF$$

**Equation 1** Determination of the protein concentration on the basis of a BSA calibration line. DF: dilution factor.

### 2.4.10. Sodium dodecyl sulfate polyacrylamide gel electrophoresis (SDS-PAGE)

Separation of protein samples was carried out according to Laemmli<sup>[108]</sup> in a discontinuous system with stacking SDS-gel (5 % (w/v) crosslinking) and running SDS-gel (12 % (w/v) crosslinking). For the composition of the gels see table 19 below. The molecules are separated in an electric field according to their molecular mass. The protein samples were treated with 5x SDS-PAGE sample buffer (Table 3, section 2.1.3.) to cover their individual charge so that they have a consistent negative charge. The samples were then denatured for 10 min at 95°C and cooled on ice. The gel was covered with SDS-PAGE running buffer (Table 3, section 2.1.3.) and the samples as well as a size standard (PageRuler™ Prestained Protein Ladder, Thermo Fisher Scientific, Darmstadt) were applied. The samples were separated at a current of 15-20 mA. Visualization of the protein bands was carried out by using Coomassie staining<sup>[109]</sup>. After briefly rinsing the gel with distilled water it was heated in Coomassie staining solution (Table 3, section 2.1.3.) in a microwave (30 s, 360 W) and shaken for 5-10 min. For destaining the gel was heated in Coomassie destaining solution (Table 3, section 2.1.3.) in a microwave (30 s, 360 W) and shaken for 5-10 min. This was repeated until the staining background was marginal. Afterwards, the gel was documented (Biodocanalyze, Biometra, Göttingen).

**Table 19** Composition of the gels for SDS-PAGE (description for 2 gels).

Reagent	Running gel (12 %)	Stacking gel (5 %)
Acrylamide	12 % (w/v)	5 % (w/v)
Running gel buffer (Tris pH 8.8)	375 mM	-
Stacking gel buffer (Tris, pH 6.8)	-	125 mM
10 % SDS	0.1 % (v/v)	0.1 % (v/v)
10 % APS	0.1 % (v/v)	0.1 % (v/v)
TEMED	0.1 % (v/v)	0.1 % (v/v)

#### **2.4.11. In-solution tryptic digestion of protein samples**

To enable analysis of protein fragments from protein solutions via LC-MS, the samples have to be digested with trypsin. This was done in cooperation with Petra Majovsky and Dr. Wolfgang Hoehenwarter at the IPB Halle. For in-solution digestion, a sample (30  $\mu\text{l}$ ) with a concentration of 1  $\text{mg ml}^{-1}$  was used (protein was dissolved in 6 M urea in 50 mM Tris-HCl, pH 8.0). First, 0.5  $\mu\text{l}$  of the reducing agent (195 mM DTT in 100 mM Tris-HCl, pH 7.8) were added and incubated for 1 h at 22°C to break disulfide bonds. Afterwards 2  $\mu\text{l}$  of the alkylating agent (195 mM iodoacetamide in 100 mM Tris-HCl, pH 7.8) were added and incubated for 1 h at 22°C to block SH-groups of cysteine residues. Then, 2  $\mu\text{l}$  of the reducing agent were added to neutralize any remaining alkylating solution and the reaction was proceeded for 1 h at 22°C. A suitable amount of ammonium bicarbonate (pH 8.5) was added to provide alkaline environment, at which trypsin retains its activity, and to dilute remaining urea to 0.6 M. Trypsin solution ( $c = 0.2 \mu\text{g } \mu\text{l}^{-1}$ ) was added to achieve a protease:substrate ratio of 1:25. Digestion was carried out overnight at 37°C and 750 rpm. The next day, the reaction was stopped by adding a suitable amount of formic acid to acidify the medium. The sample was then desalted (section 2.4.13.).

#### **2.4.12. In-gel tryptic digestion of protein samples**

To enable direct LC-MS analysis of protein fragments in gels, the samples have to be digested with trypsin. This was done in cooperation with Petra Majovsky and Dr. Wolfgang Hoehenwarter at the IPB Halle. For in-gel digestion, the protein bands of interest were cut out from a gel after SDS-PAGE and transferred to 1.5 ml reaction tubes. The gel piece was washed with 100  $\mu\text{l}$  of LC grade water (shook for 10 min at 22°C), supernatant was discarded and procedure was repeated. Then, 100  $\mu\text{l}$  of destaining solution (30% (v/v) acetonitrile in 100 mM ammonium bicarbonate, pH 8.5) were added and incubated for 10 min at 22°C under shaking. The supernatant was discarded and the destaining step was repeated. The gel piece was again washed with 100  $\mu\text{l}$  of LC grade water (shook for 15 min at 22°C), supernatant was discarded and procedure was repeated. Afterwards, 100  $\mu\text{l}$  of acetonitrile were added and the sample was incubated for 15 min at 22°C under shaking. The supernatant was discarded and the gel piece was dried in a vacuum concentrator for 15 min. For the reduction of the disulfide bonds, 70  $\mu\text{l}$  of reduction solution (10 mM DTT in 100 mM ammonium bicarbonate, pH 8.5) were added to the gel piece and the sample was incubated

under shaking at 22°C for 5 min. The temperature was raised to 50°C and the sample was incubated under shaking for further 30 min. The supernatant was discarded, 100 µl of acetonitrile were added and the sample was incubated under shaking for 15 min at 22°C. The supernatant was discarded again and then 100 µl of alkylating solution (54 mM iodoacetamide in 100 mM ammonium bicarbonate, pH 8.5) were added to block SH-groups of cysteine residues. The sample was incubated under shaking at 22°C for 15 min in the dark and then the supernatant was discarded. Afterwards, 100 µl of destaining solution (30% (v/v) acetonitrile in 100 mM ammonium bicarbonate, pH 8.5) were added and the sample was incubated under shaking at 22°C for 10 min. The supernatant was discarded and the procedure was repeated with an incubation time of 15 min. After that, the supernatant was discarded and the gel piece was dried in a vacuum concentrator for 15 min. For the trypsin digestion 3 µl of the trypsin stock solution (200 ng µl<sup>-1</sup>) were diluted with 197 µl of digestion buffer (50 mM ammonium bicarbonate, pH 8.5, in 5 % (v/v) acetonitrile). Then, a sufficient amount of this solution was added to the sample until the gel piece was covered. The sample was then incubated under shaking at 37°C overnight. The next day, the same volume of extraction solution (0.4 % (v/v) trifluoroacetic acid in acetonitrile/LC grade H<sub>2</sub>O (35:65, v/v)) was added and the mixture was incubated under shaking for 40 min at 22°C. The supernatant was transferred to a separate 1.5 ml reaction tube. Again, extraction solution was added to the gel piece (same volume as before). The sample was incubated under shaking for 15 min at 22°C. The supernatant was taken off and combined with the supernatant saved before. After that, the sample was completely dried in a vacuum concentrator. For the following desalting step (section 2.4.13.), dried peptides were dissolved in 100 µl of 0.1 % (v/v) aqueous formic acid.

#### **2.4.13. Desalting of peptide fragments**

The desalting of peptide fragments was carried out in C18 STAGE-tips (stop-and-go-extraction). Therefore, a STAGE-tip was inserted into a 2 ml reaction tube and conditioned by applying 100 µl of 80 % (v/v) acetonitrile/0.1 % (v/v) formic acid. After centrifugation at 4000 rpm for 2 min, the flow-through was discarded and the STAGE-tip was equilibrated by applying 100 µl of 0.1 % (v/v) aqueous formic acid (centrifugation at 4000 rpm for 2 min). The flow-through was discarded and the equilibration step was repeated. Then, 100 µl of the protein digest were applied onto the STAGE-tip and the sample was centrifuged at 4000 rpm

for 2 min. The flow-through was discarded and the STAGE-tip was washed with 100  $\mu\text{l}$  of 0.1 % (v/v) aqueous formic acid (centrifugation at 4000 rpm for 2 min). Again, the flow-through was discarded and the wash step was repeated. Afterwards, the STAGE-tip was placed into a separate 2.0 ml reaction tube. Bound peptides were eluted by applying 50  $\mu\text{l}$  of 80 % (v/v) acetonitrile/0.1 % (v/v) formic acid followed by centrifugation at 4000 rpm for 1 min. The eluate was retained in the tube and the elution step was repeated. The whole eluate was then transferred to a separate 1.5 ml reaction tube and the peptides were dried in a vacuum concentrator. The obtained peptides were then analyzed by LC-MS (section 2.5.6.).

## 2.5. Analytical methods

### 2.5.1. Activity assay for *cis*-prenyltransferases

Enzymatic activity assays ( $V_{\text{total}}$ : 500  $\mu\text{l}$ ) were carried out in 1.5 ml reaction tubes. The assay buffer (Table 3, section 2.1.3.) was supplemented with 10  $\mu\text{M}$  enzyme, 50  $\mu\text{M}$  starter substrate and 500  $\mu\text{M}$  elongation substrate (given concentrations are final concentrations, obtained by adding appropriate volumes of stock solutions). Under standard conditions, the reaction mixture was then incubated at 65°C (ThkCPT) or 30°C (AtCPT) overnight. To accumulate short-chain products the incubation time was decreased (1 min for ThkCPT). The obtained polyprenyl diphosphates were then extracted with 500  $\mu\text{l}$  of 1-butanol (1-BuOH; vigorous mixing for 30 s and centrifugation at 15,000 rpm for 10 min for phase separation; Centrifuge 5424, Eppendorf) and the organic phase was transferred to a separate 1.5 ml glass vial. The solvent was then evaporated under a mild nitrogen stream. Hydrolysis of the polyprenyl diphosphates<sup>[65, 110]</sup> was carried out by adding 500  $\mu\text{l}$  of hydrolysis buffer (Table 3, section 2.1.3.) supplemented with 4.4 U ml<sup>-1</sup> acidic phosphatase from potato to the residue. After overnight incubation at 37°C, the sample was transferred to a 1.5 ml reaction tube and the polyprenols were then extracted with 500  $\mu\text{l}$  of *n*-hexane (vigorous mixing for 30 s and centrifugation at 15,000 rpm for 10 min for phase separation; Centrifuge 5424, Eppendorf). The organic phase was transferred to a separate 1.5 ml glass vial and the mixing/centrifugation step was repeated. The solvent was then evaporated under a mild nitrogen stream and the sample was dissolved in 100  $\mu\text{l}$  of methanol (MeOH; for TLC, section



2.5.2.) or 150  $\mu\text{l}$  of MeOH (for HPLC, section 2.5.3.). For HPLC analysis the sample was diluted 1:3.

#### **2.5.1.1. ThkCPT activity assay in a biphasic system**

The enzymatic reaction was carried out as described above (section 2.5.1.). The aqueous reaction mixture ( $V_{\text{total}}$ : 500  $\mu\text{l}$ ) was overlaid with 500  $\mu\text{l}$  of 1-BuOH. 10  $\mu\text{M}$  of the enzyme were added to the aqueous phase when the two phases had been formed. Afterwards the mixture was incubated at 65°C overnight. The organic phase was then transferred to a separate 1.5 ml glass vial and the polyprenyl diphosphates from the aqueous phase were then extracted with 500  $\mu\text{l}$  of 1-BuOH as described above. The 1-BuOH phase obtained from this extraction step was not combined with the 1-BuOH phase that covered the aqueous phase before. Both were then prepared and analyzed separately. The samples were processed as described above (hydrolysis of polyprenyl diphosphates, extraction) and used for analysis.

#### **2.5.1.2. ThkCPT activity assay with alternative bivalent cations**

The bivalent cations ( $\text{Mn}^{2+}$ ,  $\text{Co}^{2+}$ ,  $\text{Ni}^{2+}$ ,  $\text{Zn}^{2+}$ ,  $\text{Cu}^{2+}$  and  $\text{Mg}^{2+}$  as a control) were added separately to the magnesium-free assay buffer (Table 3, section 2.1.3.) with a final concentration of 0.5 mM. The different solutions were then used for activity assays that were carried out as described above (section 2.5.1.).

#### **2.5.1.3. ThkCPT activity assay with crude extracts**

As the ThkCPT has its temperature optimum at 65°C it is also possible to perform the activity assay with crude extracts. Here, the cell lysis was carried out by using osmotic shock (section 2.4.3.). The samples (470  $\mu\text{l}$ ) from cell lysis were supplemented with 0.1 % (v/v) Triton X-100, 50  $\mu\text{M}$  starter substrate and 500  $\mu\text{M}$  elongation substrate (final concentration each). The activity assay was then carried out as described in section 2.5.1. and the sample was then used for analysis.

#### **2.5.1.4. Activity assay in microtiter plates (MTP)**

The following steps were performed by using an automated integrated robotic platform (central F5 robot system, Thermo Fisher Scientific). For activity assays in MTPs, the substrates (50  $\mu\text{M}$  starter substrate and 500  $\mu\text{M}$  elongation substrate) were directly added to 150  $\mu\text{l}$  of the cleared lysate (see section 2.4.3.1.). The reaction mixture was then incubated overnight at 65°C and 900 rpm with high humidity to prevent dehydration (Cytomat 2 C-LIN, Thermo Fisher Scientific). Afterwards, the polyprenyl diphosphates were extracted with 150  $\mu\text{l}$  of 1-BuOH (centrifugation at 4,600 rpm for 10 min for phase separation after shaking; Rotanta 460 Robotic, 4-place swing-out rotor, Hettich) and the organic phases were transferred to a separate MTP. The solvent was then evaporated. Hydrolysis of the polyprenyl diphosphates<sup>[65, 110]</sup> was carried out by adding 150  $\mu\text{l}$  of hydrolysis buffer (Table 3, section 2.1.3.) supplemented with 4.4 U ml<sup>-1</sup> acidic phosphatase from potato and overnight incubation at 37°C. The samples were transferred to a deep well plate and the products were extracted with 1 ml of *n*-heptane (centrifugation at 4,600 rpm for 10 min for phase separation after shaking; Rotanta 460 Robotic, 4-place swing-out rotor, Hettich). The organic phases were transferred to a separate MTP and the solvent was evaporated. The residue was dissolved in 20  $\mu\text{l}$  of *n*-heptane.

#### **2.5.2. Thin layer chromatography (TLC) for chain length determination**

Thin layer chromatography (TLC) was carried out to quickly analyze product formation. With this method, the corresponding product alcohols (prepared as described in section 2.5.1.) were evaluated. As solid phase silica gel 60 RP-18 F<sub>254</sub>S (Merck, Darmstadt) was used. A mixture of acetone/H<sub>2</sub>O (19:1, v/v) served as mobile phase. Detection of polyprenols was carried out by using iodine fume. Short-chain polyprenols show a higher R<sub>f</sub> value while long-chain polyprenols show a lower R<sub>f</sub> value. As standards farnesol (C<sub>15</sub>H<sub>26</sub>O) and solanesol (C<sub>45</sub>H<sub>74</sub>O) were used.

#### **2.5.3. High performance liquid chromatography (HPLC) analytics**

High performance liquid chromatography (HPLC) analytics were used to determine the chain length of the generated polyprenols (see section 2.5.1.). Analysis<sup>[111]</sup> was carried out on a device from Agilent 1260 Infinity (quaternary pump, DAD & FLD detector, auto sampler,

fraction collector, column oven). As stationary phase a YMC-Pack ODS-AQ column (12 nm, 5  $\mu\text{m}$ , 150 x 4.6 mm; YMC Europe, Dinslaken) was used. Unless stated otherwise, 5  $\mu\text{l}$  of a sample were applied and the flow rate was set to 0.8 ml  $\text{min}^{-1}$ . The mobile phase consisted of solvent (SV) A (MeOH/H<sub>2</sub>O/isopropanol 12:1:8 (v/v/v)) and SV B (*n*-hexane/isopropanol 7:3 (v/v)). UV-Vis detection was carried out at 350 nm (DAD) and additionally an UV spectrum was recorded in the range of 190 - 400 nm. Unless stated otherwise, the following gradient was used:

0 % SV B  $\xrightarrow{20 \text{ min}}$  45 % SV B  $\xrightarrow{5 \text{ min}}$  70 % SV B  $\xrightarrow{1 \text{ min}}$  100 % SV B

### 2.5.3.1. HPLC analysis of polyprenols with MANT-O-GPP as starter substrate

An alternative fluorescent starter substrate enables a highly sensitive and selective detection of the enzymatically formed products by HPLC. Here, (2*E*,6*E*)-8-*O*-(*N*-methylantranyl)-3,7-dimethyl-2,6-octandien-1-diphosphate (MANT-O-GPP) was used<sup>[112]</sup> (Table 2, section 2.1.2.). HPLC analysis was carried out as described above. The detection of the fluorescent labeled products was carried out at 426 nm after excitation at 359 nm.

The corresponding product alcohol MANT-O-Geraniol [(2*E*,6*E*)-8-*O*-(*N*-Methylantranyl)-3,7-dimethyl-2,6-octandien-1-ol; see Table 2, section 2.1.2.] was used as standard for calibration (0.098  $\mu\text{M}$  to 50  $\mu\text{M}$ ). Each sample (5  $\mu\text{l}$ ) was analyzed via HPLC as described above, in triplicate. The gradient was adapted (0 to 45 % SV B for 5 min and 45 to 0 % SV B for 1 min). The evaluation was done with SigmaPlot by regression of the linear measuring range (0.098-18  $\mu\text{M}$  MANT-O-Geraniol, Equation 2).

$$y = 90.97 \cdot x - 21.85$$

$$R^2 = 0.9976$$

**Equation 2** MANT-O-Geraniol calibration line. *y*: Area of the compound peak, *x*: concentration of MANT-O-Geraniol in  $\mu\text{M}$ . The equation is given in the form  $y = bx + a$ . Additionally, the coefficient of determination  $R^2$  is given.

The limit of detection ( $x_{\text{LOD}}$ ) was determined according to Molt & Telgheder (University Duisburg-Essen)<sup>[113]</sup>, see equation 3. For a detailed calculation, see appendix (section 7.1.).

$$x_{LOD} = \frac{s_{y,x} \cdot t_{f,\alpha}}{b} \sqrt{\frac{1}{n} + \frac{1}{m} + \frac{\bar{x}^2}{Q_{xx}}}$$

**Equation 3** Determination of the limit of detection  $x_{LOD}$ .

$x_{LOD}$	limit of detection
$s_{y,x}$	residual standard deviation
$t_{f,\alpha}$	$t$ -distribution (value taken from a $t$ -distribution table referred to the number of degrees of freedom ( $f = n-2$ ) and the significance level ( $\alpha = 0.05$ ))
$b$	slope of calibration line
$n$	number of calibration samples
$m$	number of replicates
$\bar{x}$	mean of content of calibration samples (center of calibration line)
$Q_{xx}$	ordinary least squares of $x$ values of the calibration

Additionally, Molt & Telgheder (University Duisburg-Essen) described, if the true content of an analysis sample would be identical with the limit of detection, one would verify the analyte only in 50 % of all cases<sup>[113]</sup>. To increase the sensitivity in a manner so that the analyte can be verified in 95 % of all cases, the decision limit is set to the twofold limit of detection (method detection limit, Equation 4)<sup>[113]</sup>.

$$x_{MDL} = 2 \cdot x_{LOD}$$

**Equation 4** Determination of the method detection limit  $x_{MDL}$ .

### 2.5.3.2. Fractionation of products

For subsequent analyses by mass spectrometry (MS) the obtained products formed with MANT-O-GPP as starter substrate were fractionated by HPLC. Therefore, highly concentrated samples were used which were generated by performing individual activity assays (section 2.5.1.). The samples were combined and the solvent was evaporated under a mild nitrogen stream. Afterwards, the samples were dissolved in 150-200  $\mu$ l of MeOH. Analysis was carried out as described above (section 2.5.3.1.). As the obtained MANT-O-GPP derivatives can be detected due to their UV-Vis activity (DAD 350 nm), the samples were fractionated peak-based according to their DAD signals with a threshold of 10. The sample volume applied to the column ranged between 50 and 100  $\mu$ l. Fractions containing an individual product were

combined and the solvent was evaporated under a mild nitrogen stream. The samples were then dissolved in 150  $\mu\text{l}$  of MeOH each and used for further analyses (sections 2.5.4. and 2.5.5.).

#### **2.5.4. Sample preparation via solid phase extraction (SPE)**

For subsequent MS analyses (section 2.5.5.) sample preparation was carried out by solid phase extraction (SPE). The compounds in a mixture can be separated by SPE according to their physical or chemical properties. The analytes of interest are enriched on the solid phase and the solvent passes the sorbent. Impurities can be removed by washing the sample with suitable solvents. The analytes of interest can then be eluted by using appropriate solvent conditions.

For the samples containing polyprenols, Chromabond® HR-X columns (Macherey-Nagel, Düren) were used. The cartridge was first equilibrated with 1 ml of MeOH and then the sample was applied. Several wash steps were carried out, each with a volume of 400  $\mu\text{l}$  of H<sub>2</sub>O, MeOH/H<sub>2</sub>O (30:70, v/v), MeOH/H<sub>2</sub>O (50:50, v/v), MeOH/H<sub>2</sub>O (70:30, v/v) and MeOH. To elute the products the solvents from HPLC analytics [SV A (MeOH/H<sub>2</sub>O/isopropanol 12:1:8 (v/v/v)) and SV B (*n*-hexane/isopropanol 7:3 (v/v))] were used. All fractions were collected separately and the solvent was evaporated under a mild nitrogen stream. The samples were dissolved in 50  $\mu\text{l}$  of MeOH and used for HPLC analyses (see section 2.5.3.1.) to identify which fractions contained the products.

#### **2.5.5. HR-ESI-MS analysis**

The positive ion high resolution ESI mass spectra were obtained from an Orbitrap Elite mass spectrometer (Thermo Fisher Scientific) equipped with an HESI electrospray ion source (spray voltage 4.0 kV, capillary temperature 275°C, source heater temperature 40°C, FTMS resolution 60,000). Nitrogen was used as sheath gas. The sample solutions were introduced continuously via a 500  $\mu\text{l}$  Hamilton syringe pump with a flow rate of 5  $\mu\text{l min}^{-1}$ . The instrument was externally calibrated by the Pierce® LTQ Velos ESI positive ion calibration solution (product number 88323) from Thermofisher Scientific, Rockford, USA). The data were evaluated by the Xcalibur software 2.7 SP1.

### **2.5.6. Analysis of peptide fragments via LC-ESI-MS (AtCPT)**

The analysis of peptide fragments was carried out in cooperation with Petra Majovsky and Dr. Wolfgang Hoehenwarter at the IPB Halle. First, the samples were prepared by tryptic digestion (sections 2.4.11. and 2.4.12.) followed by desalting (section 2.4.13.). The peptides were injected into an EASY-nLC II UHPLC system (Thermo Fisher Scientific) coupled to an Orbitrap Velos Pro mass spectrometer (Thermo Fisher Scientific). Peptides were separated using reverse phase chemistry employing a C18 column (EASY-Column, 10 cm, 75  $\mu\text{m}$ , 3  $\mu\text{m}$ , C18-A2, Thermo Fisher Scientific) in-line with a precolumn (EASY-Column, 2 cm, 100  $\mu\text{m}$ , 5  $\mu\text{m}$ , C18, Thermo Fisher Scientific). Gradients of 60 min for gel samples, 90 min for solution samples from 5 to 40 % (v/v) acetonitrile in 0.1 % (v/v) aqueous formic acid at a flow rate of 300  $\text{nl min}^{-1}$  were used. ESI-MS measurements were performed with a data dependent acquisition (DDA) scan strategy where one full MS scan with a resolution of 30,000 in the Orbitrap mass analyser (spray voltage 1.9 kV, capillary temperature 275°C) was followed by up to 20 dependent MS/MS scans in the linear ion trap (LTQ). The maximum injection time (MaxIT) and acquired gain control (AGC) target values were 500 ms and  $1 \cdot 10^6$ , respectively, in the Orbitrap mass analyser and 200 ms and  $1 \cdot 10^4$  in the LTQ. Dynamic exclusion was enabled with an exclusion width of 10 ppm, a repeat count of 1 and an exclusion duration of 40 s. Mass spectra were internally calibrated on-the-fly with the lock mass 445.120024.

Peptides were identified by searching MS/MS spectra with the Mascot software v2.4 (Matrix Science) on an in-house Mascot server coupled to Proteome Discoverer v1.4 (Thermo Fisher Scientific). A peptide mass error of 7 ppm and a fragment ion mass error of 0.8 Da were tolerated. Carbamidomethylation of cysteine was set as a fixed and oxidation of methionine as a variable modification and 2 missed cleavages were tolerated in concatenated searches of the SwissProt and TAIR10 protein databases. For in-gel digested samples from gel bands the peptide identification error rate was controlled using the Mascot significance threshold of 0.05. For in-solution digested samples of his-tag purified recombinant proteins the error rate was controlled using the target-decoy database false discovery rate (FDR) with a threshold of 0.01.

### 3. *Thermococcus kodakaraensis* CPT

#### 3.1. General information

The *cis*-prenyltransferase from *Thermococcus kodakaraensis* (ThkCPT) is a thermostable enzyme as it is not fully denatured even at 90°C<sup>[75]</sup>. It catalyzes the consecutive *cis*-condensation of IPP to allylic diphosphate, whereby it utilizes both GPP as well as FPP to form mainly C<sub>60</sub>-C<sub>65</sub> products<sup>[75]</sup>. It has been reported that the ThkCPT is able to form even longer products up to C<sub>90</sub><sup>[75]</sup>. The best enzymatic activity was achieved at 60-70°C<sup>[75]</sup>. The single protein band (SDS-PAGE) has a molecular mass of 30 kDa (264 amino acids). It was shown that its native form shows a molecular mass of 120 kDa, indicating that it forms a tetramer unlike other described CPTs.<sup>[75]</sup> Yamada and coworkers created three alanine variants at positions in vicinity of a vent-like architecture leading to the hydrophobic cleft (for product accommodation) since the extension of the product length was desired<sup>[75]</sup>. They could show that the product distribution of all variants was shifted to longer chain lengths, resulting in main products exhibiting 65-70 carbon atoms. One variant also showed changes in the product formation as it formed chains with more than 70 carbon atoms. The use of a dual-liquid phase reaction system also had an impact on the product distribution.<sup>[75]</sup> It was shown before that the ThkCPT is able to convert artificial substrates<sup>[3]</sup>. It accepts the fluorescent starter substrate MANT-O-GPP<sup>[112]</sup> [(2*E*,6*E*)-8-*O*-(*N*-Methylantranyl)-3,7-dimethyl-2,6-octandien-1-diphosphate] which enables a highly sensitive and selective detection of the enzymatically formed products by HPLC<sup>[3, 112]</sup> (section 2.5.3.1.). The non-natural elongation substrates 3-butenyl diphosphate (BPP), 3-chloro-3-butenyl diphosphate (Cl-BPP) and 3-bromo-3-butenyl diphosphate (Br-BPP) are poorly converted compared to the native substrate IPP<sup>[3]</sup>.

#### 3.2. Results and discussion

##### 3.2.1. Removal of C-terminal poly-histidine tag in ThkCPT

The ThkCPT gene was synthetically produced by Eurofins Genomics (Ebersberg) in the expression vector pET28a(+) which contains both N- and C-terminal poly-histidine tags. Although, the expression of the gene was very efficient the C-terminal tag should be removed as it is not necessary for purification to have two His<sub>6</sub> tags.

A stop codon was introduced in front of the C-terminal tag by site-directed mutagenesis (section 2.3.6.1.) to remove the C-terminal tag. For this, the oligonucleotides ThkCPT\_C-His\_del\_fw and ThkCPT\_C-His\_del\_re, listed in table 7 (section 2.1.7.), were used. After transformation (section 2.3.5.) six colonies were picked, cultivated on a LB agar plate (section 2.2.1.) and used for colony PCR to check the success of a transformation (section 2.3.6.2.). The correct amino acid sequence was confirmed by sequencing (section 2.3.4.) of isolated plasmid DNA (section 2.3.1.) and is shown in figure A1 in the appendix (section 7.2.). This variant was used for all further experiments.

### **3.2.2. Production and purification of recombinant ThkCPT protein**

Recombinant expression of the ThkCPT gene was carried out in the expression strain *E. coli* BL21 (DE3) (section 2.4.1.). The expression vector pET28a(+) has resistance to kanamycin and exhibits a T7 expression system which enables an IPTG-induced protein production. The cell pellet was then lysed by ultrasonic treatment (section 2.4.2.) and the protein was purified via Ni<sup>2+</sup>-mediated IMAC (section 2.4.4.). The purification steps were controlled by SDS-PAGE (section 2.4.10.) as shown in figure 11. The recombinant ThkCPT has a molecular weight of approximately 34 kDa (indicated by arrows in figure 11). The induction of protein biosynthesis is clearly visible (lane 2). Some of the enzyme remains in the insoluble fraction (lane 3) but a major part can be found in the soluble fraction (lane 4). As a small amount of imidazole (20 mM) is present in the washing buffer (Table 3, section 2.1.3.), according to a standard protocol, it might be that some of the protein is already eluted and can be therefore found in the flow-through (lane 5). As the ThkCPT binds via the His<sub>6</sub> tag to the Ni<sup>2+</sup>-NTA matrix, unbound proteins, e.g. from the expression host, could be washed out (lane 6). Afterwards, ThkCPT was eluted by imidazole containing buffer (lane 7). Buffer exchange and desalting was carried out via SEC (section 2.4.6., lane 8 in figure 11). The yield was in average amount of 14 mg per liter of liquid culture.



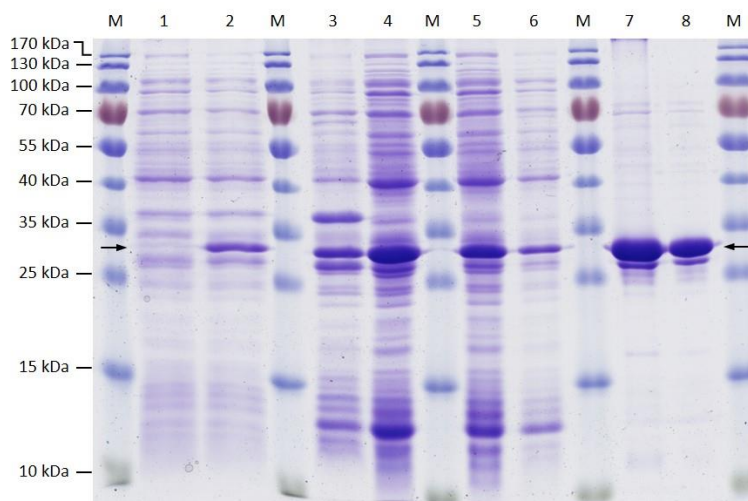


**Figure 11** SDS-PAGE gel with Coomassie staining of the purification steps of ThkCPT. The ThkCPT band is marked with arrows. M: PageRuler™ prestained protein ladder, 1: before IPTG induction, 2: after IPTG induction, 3: insoluble protein fraction, 4: soluble protein fraction, 5: column flow-through, 6: wash fraction (unbound proteins), 7: eluted protein fraction, 8: desalted protein fraction.

### 3.2.3. MANT-O-GPP as fluorescence marker for HPLC analyses

The fluorescent FPP analog (*2E,6E*)-8-*O*-(*N*-Methylantranyl)-3,7-dimethyl-2,6-octandien-1-diphosphate (MANT-O-GPP) was already successfully applied as starter substrate for different CPTs<sup>[3, 112]</sup> and as sensitive marker for product formation analyzed by HPLC<sup>[3]</sup>. Synthesis of MANT-O-GPP was done by Dr. Tula Beck at the IPB according to the published procedure from Teng et al.<sup>[112]</sup>.

#### 3.2.3.1. Emission spectrum of MANT-O-GPP

To achieve optimal detection of the fluorescence signal, the excitation wavelength of the hydrolysis product of the fluorescent substrate (MANT-O-Geraniol) in MeOH was determined with regard to the HPLC system (Agilent 1260 Infinity). Figure 12 shows that the excitation maximum for the fluorophore is at a wavelength of 359 nm. By using 359 nm as excitation wavelength the emission maximum was determined which is at a wavelength of 426 nm (Figure 12).

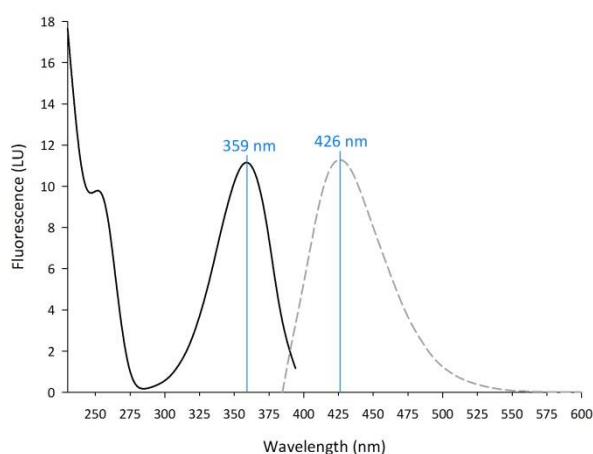


**Figure 12** Excitation (black line) and emission (dashed black line) spectra of MANT-O-Geraniol in MeOH. The maxima are highlighted by blue lines (359 nm for excitation, 426 nm for emission). LU: luminescence units.

### 3.2.3.2. HPLC analysis with MANT-O-GPP

To obtain analyses in a linear range of detection, a calibration line was prepared. Therefore, a quantification of the hydrolysis product of the fluorescent substrate, MANT-O-Geraniol, was performed. A dilution series in MeOH was analyzed via HPLC (section 2.5.3.1.; Figure 13). The linear range of detection, in which a quantification is possible with the used setup, is between 0.098 and 18  $\mu\text{M}$  MANT-O-Geraniol. The substance peak in this range shows an intensity of 1.4 - 233.6 luminescence units (LU). With the labeled substrate it is possible to detect even low concentrations of product very sensitively and selectively. The method detection limit for MANT-O-Geraniol was  $x_{\text{MDL}} = 1.35 \mu\text{M}$  (sections 2.5.3.1. and 7.1. in the appendix). Furthermore, assay components like Triton X-100 do not disturb the detection, as already stated by Keim in 2014<sup>[3]</sup>.

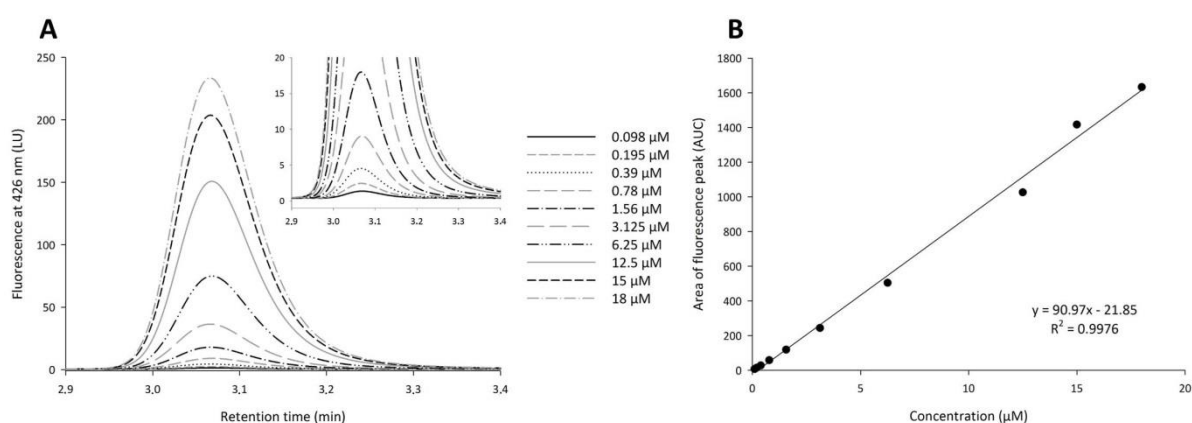


**Figure 13** HPLC analysis of MANT-O-Geraniol using stocks with different concentrations. (A) Chromatograms representing the injection of different amounts (0.098-18  $\mu\text{M}$ ) of MANT-O-Geraniol. LU: luminescence units. (B) Calibration line obtained from the resulting areas of the fluorescence peaks. The linear regression was done by using SigmaPlot 13.0, the corresponding equation and the root mean square deviation are given.  $y$ : area of fluorescence peak (AUC),  $x$ : concentration of MANT-O-Geraniol ( $\mu\text{M}$ ).

### 3.2.4. Natural and artificial substrates

#### 3.2.4.1. Current issue

The chemical modification of the alkyl chain of the natural elongation substrate IPP often leads to a reduced enzymatic activity of prenyl transferases. The conversion of artificial homoallylic substrates by CPTs has been investigated in the past by different working groups. It was shown that the substitution of the methyl group at position C3 by an ethyl group leads to a decreased substrate conversion as the *M. luteus* UPPS and HexPPS were

able to condense only two of these elongation units to FPP<sup>[114, 115]</sup>. The conversion of such elongation substrates by medium-chain CPTs becomes difficult with increasing length of the C3 alkyl substituent<sup>[114, 116]</sup>. Substitution of the C3 methyl group by hydrogen or halogens (Cl, Br) was also investigated in the past. When using 3-butenyl diphosphate (BPP) as elongation substrate only one condensation to the allylic substrate has been observed so far<sup>[3, 114-116]</sup>. Substrates like chlorinated IPP or DMAPP were successfully applied as alternative substrates for avian FPPS giving linear monochlorinated geranyl and farnesyl analogues<sup>[117]</sup>. By using 3-chloro-3-butenyl diphosphate (Cl-BPP) in a condensation reaction catalyzed by *E. coli* UPPS two elongation steps could be observed<sup>[3]</sup>. As mentioned before Br-BPP was used to study the reaction mechanisms of *E. coli* OPPS and UPPS<sup>[66]</sup>. It could be demonstrated that both, OPPS<sup>[66]</sup> as well as UPPS<sup>[3, 66]</sup> are able to catalyze two condensations of Br-BPP to the allylic starter substrate. Studies on structurally non-related terpene synthases proved Br-BPP to have inhibitory properties<sup>[118]</sup>.

Such artificial polymers would be attractive for industrial application as several synthetic rubbers contain structurally modified polyisoprenes. A common synthetic rubber is for example polychloroprene<sup>[119]</sup> (DuPont's trade name: neoprene®). In industry polychloroprene is produced by 1,4-polymerization of its monomer chloroprene (2-chloro-1,3-butadiene)<sup>[119, 120]</sup> whereby the monomer is obtained from 1,3-butadiene and chlorine<sup>[121]</sup>. Polychloroprene is a resilient, non-plastic and elastic mass that appears to be more dense and resistant (against water, heat, ozone) compared to natural rubber<sup>[119]</sup>. Another important synthetic product is the polybutadiene rubber which is based on the polymerization of 1,3-butadiene<sup>[122]</sup>. It exhibits a high resistance to abrasion and is mainly used for the production of tires (over 70% of the polymer produced)<sup>[122, 123]</sup>. At the expense of the environment such synthetic polymers are all manufactured from mineral oil. Thus, a more natural synthesis would be a great advance for rubber manufacture.

#### **3.2.4.2. Substrate conversion**

To ensure a highly sensitive and selective detection of the enzymatically formed products the alternative fluorescent starter substrate MANT-O-GPP [(2*E*,6*E*)-8-*O*-(*N*-Methylanthranlyl)-3,7-dimethyl-2,6-octandien-1-diphosphate]<sup>[112]</sup> was used in this study. Concerning chain length it has been shown that the formed products are comparable to those formed with the natural starter substrate FPP<sup>[3]</sup>. For the UPPS from *E. coli* (EcUPPS) the  $K_m$  value for the

alternative starter substrate has been determined to be  $1.5 \mu\text{M}$ <sup>[112]</sup> and  $5.6 \mu\text{M}$ <sup>[3]</sup>, respectively, which is 3- to 4-fold larger than the  $K_m$  value of FPP<sup>[3, 112]</sup>. Due to steric effects in occupation of the larger MANT-O-GPP its relative catalytic efficiency is about 20 times lower compared to FPP in the EcUPPS reaction<sup>[3]</sup>. For the artificial homoallylic substrates BPP, Cl-BPP and Br-BPP the catalytic constants have been determined for ThkCPT conversions with FPP as starter substrate. Compared to IPP the non-natural substrates are converted much slower as the turnover rate ( $k_{\text{cat}}$ ) is around 140-fold lower. The determined  $K_m$  values are slightly higher ( $21.2 \mu\text{M}$  for Cl-BPP,  $54.0 \mu\text{M}$  for Br-BPP) compared to IPP ( $14.8 \mu\text{M}$ ). It was not possible to determine the catalytic parameters for BPP due to a very low reaction rate. Though it was shown that this substrate was converted.<sup>[3]</sup>

In this study, the allylic MANT-O-GPP and a homoallylic elongation substrate were converted by ThkCPT and fluorescently labeled polyprenyl diphosphates with distinct chain lengths were formed (section 2.5.1.). By means of an acidic phosphatase from potato the polyprenyl diphosphates were hydrolyzed and the corresponding product alcohols were obtained. The reaction scheme for substrate conversion and subsequent hydrolysis is shown in figure 14.

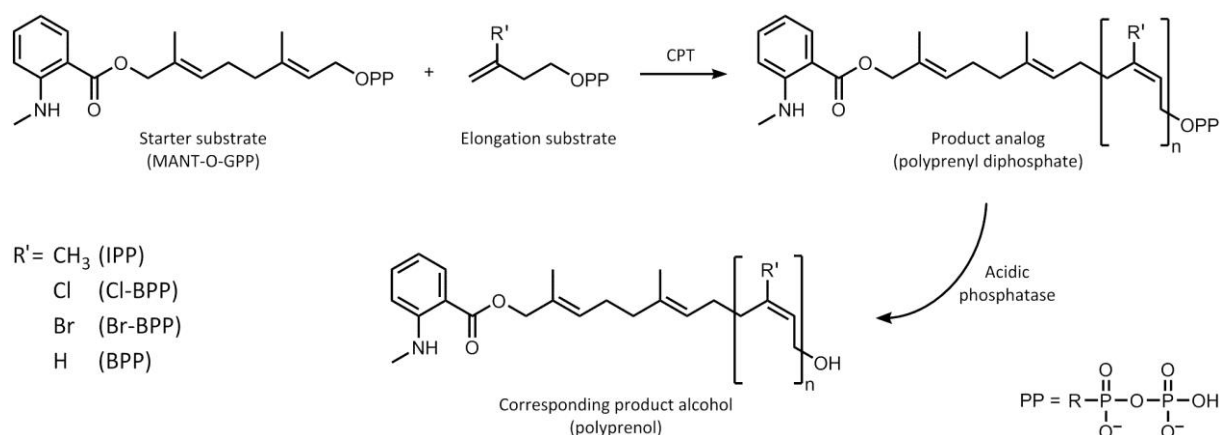


**Figure 14** Reaction scheme of the enzymatic conversion of MANT-O-GPP and different elongation substrates (as stated in the picture), leading to fluorescent labeled polyprenols with distinct chain lengths.

The polyprenols were analyzed via fluorescence-based HPLC (section 2.5.3.1.). When using the fluorescent starter substrate MANT-O-GPP a satisfying separation of the products and a very sensitive detection were achieved. In figure 15 the HPLC chromatograms of substrate conversion catalyzed by ThkCPT are shown. The natural substrate IPP is attached up to 13 times to the starter substrate, which corresponds to the formation of a  $\text{C}_{80}$  product analog. However, the  $\text{C}_{65}$  product analog constitutes the main product (Figure 15A). Previously it was

shown that ThkCPT is able to produce polyprenyl diphosphates having up to 90 carbon atoms, although mainly C<sub>60</sub>-C<sub>65</sub> products were formed<sup>[75]</sup>. In contrast, the artificial substrates give lower oligomers compared to IPP (Figure 15). The halogenated substrates Br-BPP and Cl-BPP are attached up to 8 times generating C<sub>55</sub> product analogs (Figure 15C and D). It has been already shown that ThkCPT is able to elongate the starter substrate by 8 units of Cl-BPP<sup>[3]</sup>. For Br-BPP a condensation up to 5 units has been demonstrated so far<sup>[3]</sup>. Strikingly, with BPP as elongation substrate mainly one elongated product can be seen, but there are also small peaks of longer products visible (Figure 15B). This is the first time that more than one attachment could be shown for this non-natural elongation substrate.

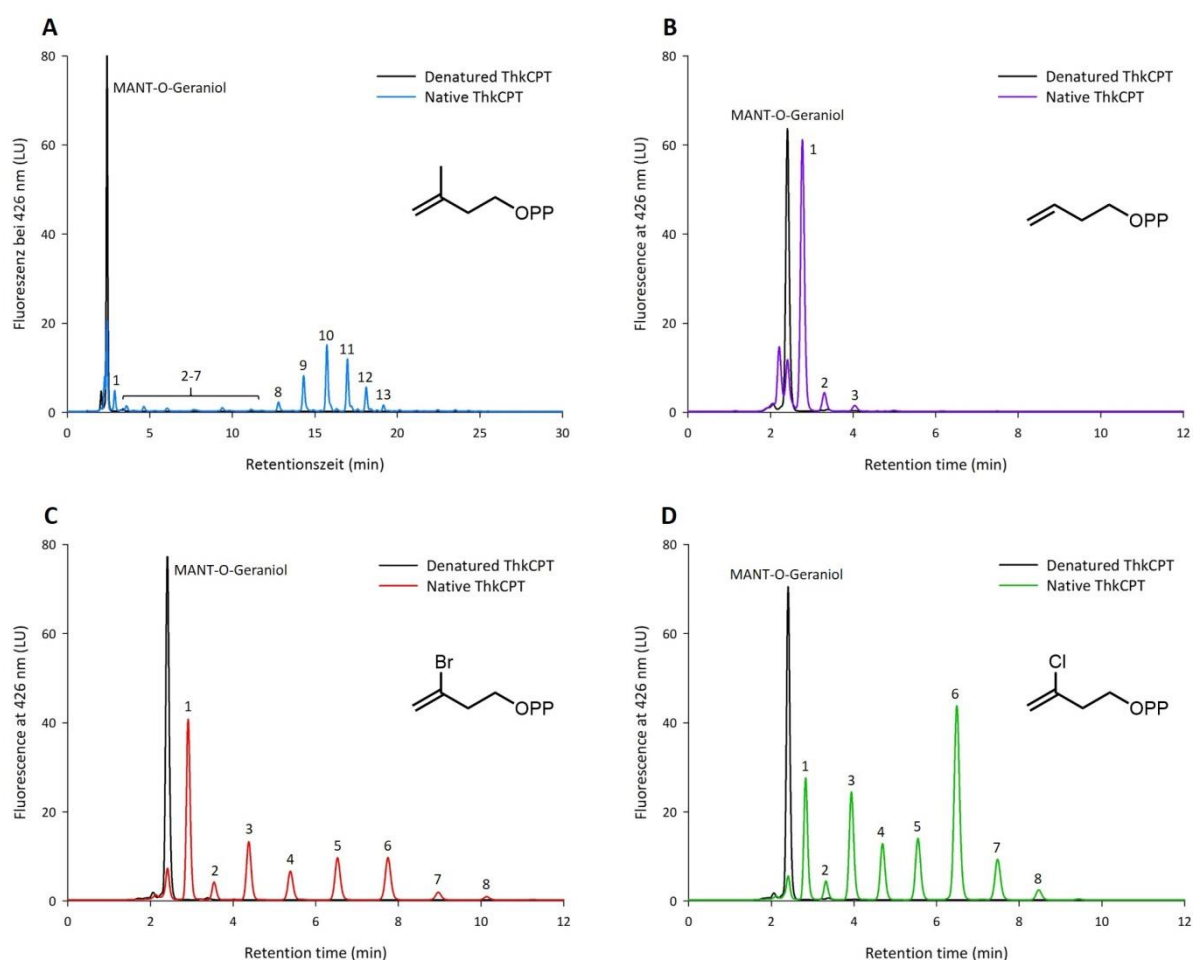


**Figure 15** HPLC chromatograms of the products of a ThkCPT reaction with MANT-O-GPP and (A) IPP, (B) BPP, (C) Br-BPP or (D) Cl-BPP as elongation substrates. Reactions were performed at 65°C reaction temperature followed by diphosphate hydrolysis. For the blank samples reactions with denatured enzyme were carried out. After excitation at 359 nm the emission was measured at 426 nm via fluorescence. It has to be noted that in this case a flow rate of 1.0 ml min<sup>-1</sup> (instead of 0.8 ml min<sup>-1</sup>) was used. Due to that the product peaks are shifted to an earlier retention time compared to the chromatograms recorded with the lower flow rate. LU: luminescence units. Numbers indicate the catalyzed elongation steps.

While a Gaussian product distribution profile can be seen with IPP as substrate, this is not observed with the halogenated substrates (Figure 15). It is assumed that the orientation of the formed products is somehow changed in the enzyme when using the artificial substrates. As a result, some of the generated intermediates possibly do not fit optimally into the active site, leading to a changed distribution profile compared to the natural substrate.

Furthermore, the differences in conversion are possibly based on the structures of the substrates and/or their electron density. Compared to the methyl group at the C3 position of IPP the halogen substituents solely differ slightly in size. In contrast, the proton present in BPP is much less voluminous (Figure 16). For this reason, BPP might be incorrectly bound in the active site of the enzyme and catalysis is therefore affected.

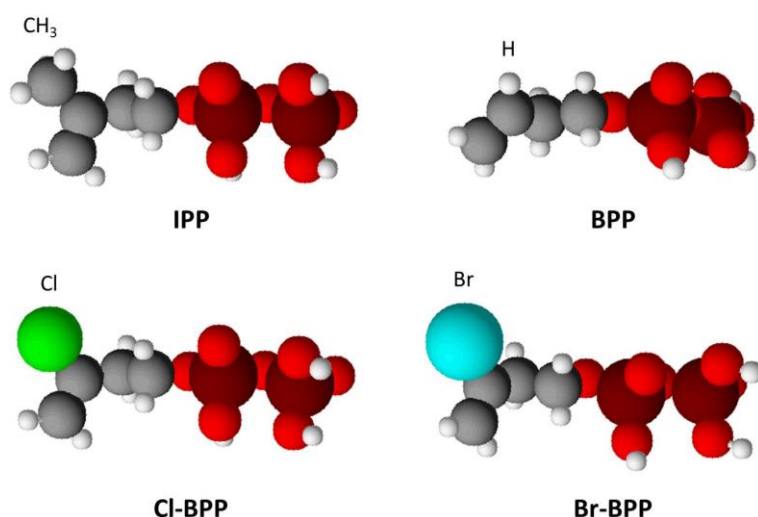


**Figure 16** Comparison of the used homoallylic substrates which are shown in ball & stick presentation. The size of the C3 substituents can be easily compared. It can be seen that the halogens chlorine (green) and bromine (cyan) are nearly equally voluminous as the methyl group of IPP whereas the proton of BPP is much less bulky. Grey: carbon, white: hydrogen, dark red: phosphorus, red: oxygen, green: chlorine, cyan: bromine. The figure was prepared by using ChemSketch (ACD/Labs).

Another aspect could be the inductive and the mesomeric effects (I and M effects) of the substituents which influence the electron density distribution. Atoms which are electron-withdrawing have a -I effect/-M effect and the ones that are electron-releasing possess a +I effect/+M effect. Alkyl groups, such as  $\text{CH}_3$ , exercise a slight +I effect but no M effect whereas halogens show a slight +M effect that is overcompensated by a -I effect. The larger the electronegativity of a heteroatom is, the stronger its -I effect is ( $\text{Cl} > \text{Br}$ ). Protons do neither exhibit an inductive nor a mesomeric effect.<sup>[124]</sup> The change in the electron density distribution for the alternative substrates BPP, Cl-BPP and Br-BPP might be the reason that their reaction kinetics are much slower compared to IPP. The +I effect of its methyl group supports the stabilization of the intermediate cation that is formed during the reaction

(Figure 6, section 1.4.2.) whereas this is not given with the alternative substrates (no or -I effect).

To gain access to the industrially interesting structurally modified polyisoprenes, such as polybutadiene or polychloroprene, further reactions were carried out with BPP or Cl-BPP as homoallylic substrates (compared to the natural substrate IPP). Thereby, the formed chain-length should be improved by the adjustment of the assay conditions (section 3.2.5.1.) or the generation of enzyme variants (section 3.2.5.3.). Furthermore, it was examined if the assay for the determination of the formed products could be optimized with regard to a faster screening system (section 3.2.6.).

### **3.2.5. Modulation of the product chain-length**

#### **3.2.5.1. Adjustment of assay conditions**

##### *i) Enzyme-to-substrate-ratio/use of detergents*

Within this study it was investigated if the product chain length formed by ThkCPT could be influenced and altered by medium engineering. In 2000, Pan et al. described the occurrence of different product distributions when using different ratios of EcUPPS to substrate or FPP to IPP<sup>[125]</sup>. This could be also confirmed for ThkCPT in activity assays (data not shown). Furthermore, it was shown that the use of a non-ionic detergent (Triton X-100) has an influence on the product chain length<sup>[125, 126]</sup>. Troutman and coworkers later analyzed the effect of different surfactants on the products formed by *Bacteroides fragilis* UPPS in more detail<sup>[127]</sup>. They found that there appears to be a correlation between the size of the surfactant and the size of the products formed in its presence. It was also demonstrated that the relative sizes of the formed products decreased with increasing surfactant concentration.<sup>[127]</sup> For ThkCPT it could be demonstrated that Triton X-100 supports the product formation as lower product amounts were observed without the use of this non-ionic detergent (Figure 17).

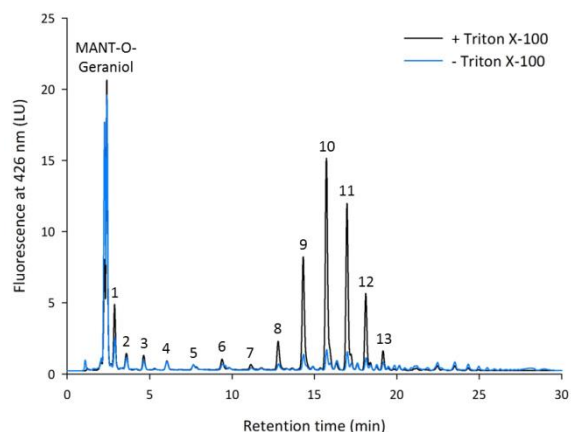


**Figure 17** HPLC chromatograms of the products of a ThkCPT reaction with MANT-O-GPP and IPP with (black) or without (blue) Triton X-100. Reactions were performed at 65°C reaction temperature followed by diphosphate hydrolysis. After excitation at 359 nm the emission was measured at 426 nm via fluorescence. It has to be noted that in this case a flow rate of 1.0 ml min<sup>-1</sup> (instead of 0.8 ml min<sup>-1</sup>) was used. Due to that the product peaks are shifted to an earlier retention time compared to the chromatograms recorded with the lower flow rate. LU: luminescence units. Numbers indicate the catalyzed elongation steps.

Due to the differences in the turnover rate ( $k_{cat}$ ) between IPP and the artificial substrates the impact of the incubation time was examined with MANT-O-GPP and IPP or CI-BPP as substrates. The substrate conversion was carried out as described in section 2.5.1. Different incubation times were chosen (1 min, 5 min, 10 min, overnight). The obtained products were hydrolyzed by means of an acidic phosphatase from potato and the corresponding product alcohols were analyzed via fluorescence-based HPLC (section 2.5.3.1.).

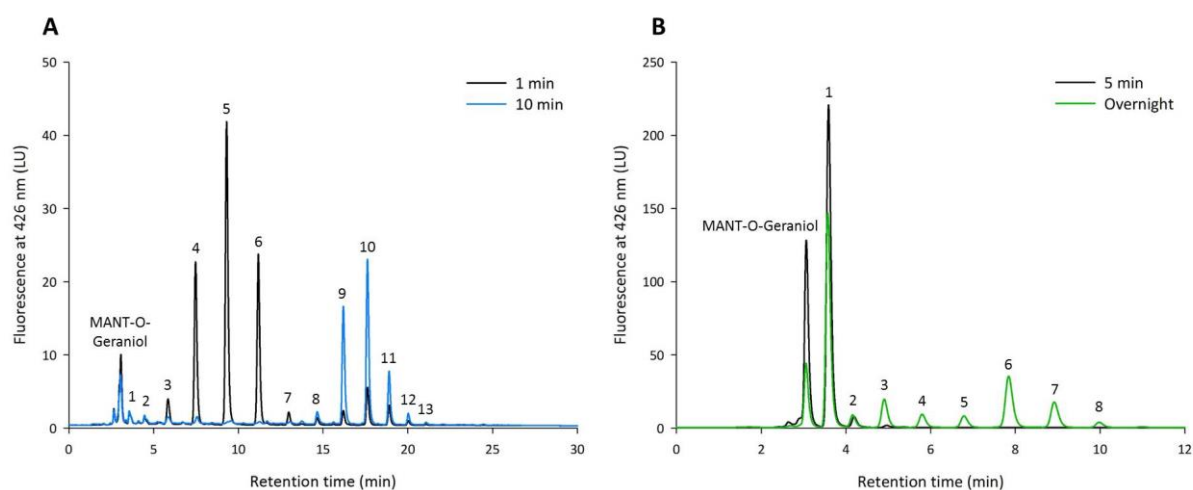


**Figure 18** HPLC chromatograms of the products of a ThkCPT reaction at different incubation times with MANT-O-GPP and (A) IPP or (B) CI-BPP as elongation substrates. Reactions were performed at 65°C reaction temperature followed by diphosphate hydrolysis. After excitation at 359 nm the emission was measured at 426 nm via fluorescence. LU: luminescence units. Numbers indicate the catalyzed elongation steps.

For IPP it can be clearly seen that the reaction proceeds rapidly as the long-chain products can be observed after 10 min incubation time (Figure 18A). Within 1 min the short-chain intermediates (4-6 elongations) are formed which are then rapidly converted to the long-chain products (9-11 attachments). In comparison, the enzymatic reaction with CI-BPP is



much slower as an overnight incubation is necessary to obtain long-chain products (Figure 18B). With a shorter incubation time (5 min) only one attachment of Cl-BPP to MANT-O-GPP can be seen. This is a further confirmation of the decreased reaction kinetics for artificial substrates.

The results obtained by medium engineering are summarized in table 20 at the end of the section.

*ii) Application of a biphasic system*

As thermostable enzymes show tolerance to various denaturants, e.g. organic solvents,<sup>[75]</sup> ThkCPT was applied to a biphasic system (section 2.5.1.1.) with MANT-O-GPP and IPP or Cl-BPP as substrates. As a control the reaction was also carried out in an aqueous system under standard conditions (section 2.5.1.). The obtained products (from the aqueous or the organic phases) were hydrolyzed and analyzed via fluorescence-based HPLC (section 2.5.3.1.).

As it can be seen in figure 19A for IPP the organic solvent of the biphasic system mainly contains short-chain products (1-7 elongations). Due to solubility it can be expected that the majority of the long-chain products (8-12 elongations) also diffuses into the organic phase. In contrast, they are mostly present in the aqueous phase. It could be possible that the mobility of those products is restricted in the aqueous buffer system so that they diffuse rather slowly to the organic solvent. In comparison, products with the same chain length were detected in both solvent systems, differing only concerning the product distribution.

In 2009, Yamada and coworkers also applied the ThkCPT to such a biphasic system with GPP and [4-<sup>14</sup>C]IPP as substrates<sup>[75]</sup>. In these experiments, different organic solvents (1-BuOH, 1-pentanol or 1-octanol) were tested. With 1-pentanol or 1-octanol as organic solvent, the main products showed 55-60 and 30-40 carbon atoms, respectively<sup>[75]</sup>. When 1-BuOH was used, products containing 60-65 carbon atoms were mainly formed but also short-chain intermediates could be observed<sup>[75]</sup>. In their experiment they carried out the reaction with magnetic stirring, so they could recover more than 90 % of the products from the 1-butanol phase<sup>[75]</sup>. Possibly the mobility of the products was thereby increased since diffusional limitation can be overcome by rapid agitation<sup>[128, 129]</sup>. This would explain why the amount of recovered long-chain products in the organic solvent in this study was lower compared to the previously published results.

When CI-BPP was used as the homoallylic substrate in the biphasic system, it can be observed that mainly one attachment is catalyzed by ThkCPT (Figure 19B). The organic phase rarely contains long products (only 2-3 attachments in small amounts) whereas the aqueous phase comprises also some long-chain products with a distribution pattern comparable to the reaction in the purely aqueous system. Here it is also possible that the mobility of the products is restricted and that additional stirring would improve the recovery from the organic phase. It should be also taken into account that the reaction with the artificial substrates is slower compared to the reaction with IPP as described above. This might be another reason that mainly one elongated product is formed.

The results obtained by medium engineering are summarized in table 20 at the end of the section.

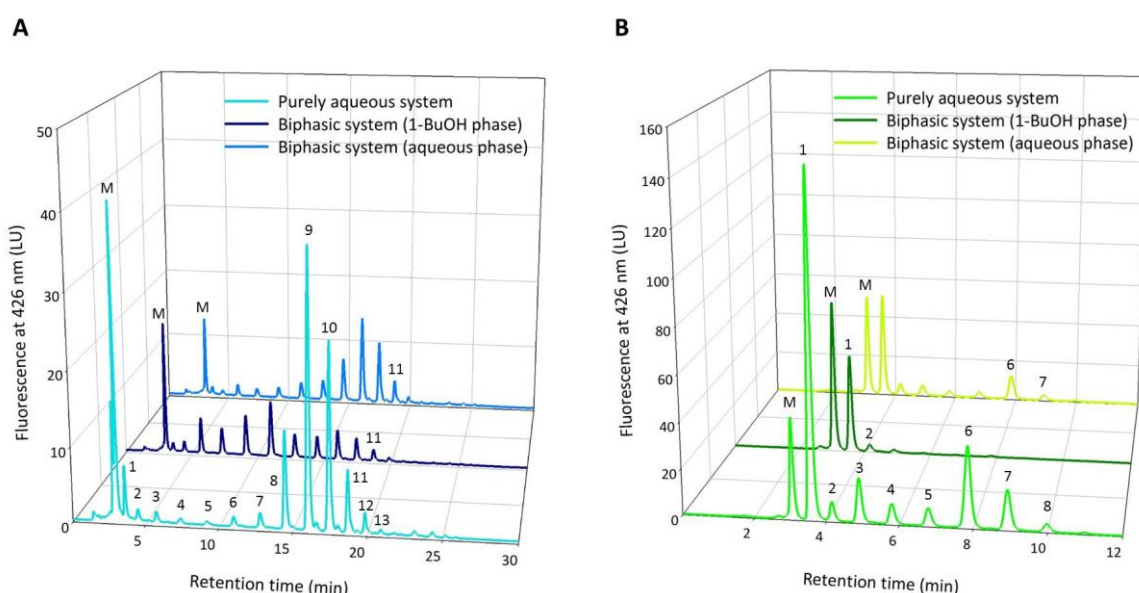


**Figure 19** HPLC chromatograms of the products of a ThkCPT reaction in a purely aqueous system or in a biphasic system with MANT-O-GPP and (A) IPP or (B) CI-BPP as elongation substrates. Reactions were performed at 65°C reaction temperature followed by diphosphate hydrolysis. After excitation at 359 nm the emission was measured at 426 nm via fluorescence. LU: luminescence units, M: MANT-O-Geraniol. Numbers indicate the catalyzed elongation steps.

### iii) Replacement of the bivalent cation

Cis-Prenyltransferases are magnesium-dependent enzymes<sup>[47]</sup>. As shown for other enzymes that are dependent on bivalent cations, e.g. caffeoyl-coenzyme A-dependent O-methyltransferases, the substitution of  $Mg^{2+}$  can have an influence on the turnover rate or substrate preferences<sup>[130]</sup>. Thus, it has been investigated if such an influence can also be seen for ThkCPT by replacing the bivalent cation. Therefore, the protein sample was dialyzed

against EDTA-containing buffer (section 2.4.7.) to remove the magnesium. Afterwards, the buffer was exchanged via size-exclusion chromatography (section 2.4.6.) so that the protein was present in the required assay buffer but did not contain additional bivalent cations. No additional experiment was performed to verify the presence of magnesium ions bound to the enzyme. Residual  $\text{Mg}^{2+}$  is expected to exit the active site after one turnover, bound to the diphosphate group that is split off during chain elongation<sup>[65, 66]</sup> (for the suggested mechanism see figure 6, section 1.4.2.). The substrate conversion was carried out as described in section 2.5.1.2. with MANT-O-GPP and IPP or Cl-BPP as substrates.

As it is known that  $\text{Mn}^{2+}$  ions often can replace  $\text{Mg}^{2+}$  in enzymatic reactions,  $\text{MnCl}_2$  was chosen as substitute. In order to examine, if other transition metals also have an influence,  $\text{Co}^{2+}$ ,  $\text{Ni}^{2+}$ ,  $\text{Zn}^{2+}$  and  $\text{Cu}^{2+}$  were added as chlorides. Although it was assumed that the salts of the heavy metals (Ni(II), Co(II) and Cu(II)) would be precipitated upon the enzymatic assay (pH 8), no optical precipitation could be observed. The used ions have approximately the same ionic radii compared to  $\text{Mg}^{2+}$  (Table A4 in the appendix, section 7.3.). Additionally, control reactions with  $\text{Mg}^{2+}$  and without the addition of any bivalent cation were performed. The obtained products were hydrolyzed and analyzed via fluorescence-based HPLC (section 2.5.3.1.).

Figure 20 shows the results of the assays using IPP as homoallylic elongation substrate. Even though no bivalent cation is added, the ThkCPT is able to catalyze up to 7 elongation steps with mainly 6 and 7 attached IPP units (Figure 20A, blue). This indicates that there are still  $\text{Mg}^{2+}$  ions bound to the enzyme during dialysis, as it seems to be impossible to completely remove them. This would explain the residual activity. By adding an excess of  $\text{MgCl}_2$  again, up to 11 IPP units are added to MANT-O-GPP, whereby products with 8-10 attachments constitute the major part (Figure 20A, yellow). The products formed after removal of  $\text{MgCl}_2$  followed by adding magnesium once again contain less IPP units compared to the products formed under standard conditions (see Figure 19). With  $\text{MnCl}_2$  the product distribution is comparable to that with  $\text{MgCl}_2$  (Figure 20A, red). Additionally, a small amount of long-chain products is formed (15-17 elongations). However, the product peaks nearly all possess shoulders which could correspond to rearranged intermediates. When  $\text{NiCl}_2$  is used instead of  $\text{MgCl}_2$ , the enzyme catalyzes up to 10 elongation steps, with mainly 8-9 IPP attachments (Figure 20A, green).  $\text{Mg}^{2+}$ ,  $\text{Mn}^{2+}$  and  $\text{Ni}^{2+}$  ions prefer an octahedral geometry in simple coordination compounds, i.e. coordination number 6<sup>[131, 132]</sup>. Therefore, it seems likely that

these ions can coordinate the phosphate from the substrates in a similar manner. As  $Mg^{2+}$  and  $Mn^{2+}$  both prefer oxygen donor atoms, e.g. phosphate ligands<sup>[131, 132]</sup>, the nearly equal product distribution can be achieved. In contrast,  $Ni^{2+}$  rather prefers sulfur or nitrogen donor atoms<sup>[131, 132]</sup> what could be a reason why predominantly products containing less IPP units are formed (8-9 elongations).

By the addition of  $ZnCl_2$  to the enzymatic reaction up to 11 attachments of IPP to MANT-O-GPP can be observed with a main product possessing 8 IPP units (Figure 20B, dark orange). Furthermore, a small amount of long-chain products can be seen (13-15 elongations).  $Zn^{2+}$  prefers a tetrahedral geometry in simple coordination compounds, i.e. coordination number 4<sup>[131, 132]</sup>. But  $Zn^{2+}$  ions are also able to form an octahedral geometry<sup>[131]</sup> which would be similar to  $Mg^{2+}$  ions. In contrast to  $Mg^{2+}$ ,  $Zn^{2+}$  prefers sulfur or nitrogen donor atoms but is also able to form a complex with oxygens from carboxylates<sup>[131]</sup>. Thus, the slightly shifted product distribution could be explained.  $Cu^{2+}$  and  $Co^{2+}$  treatment also results in a slightly shifted product distribution, showing main products with 7-8 and 8-9 IPP attachments, respectively (Figure 20B, purple and magenta). Again, a small amount of long-chain products can be seen (14 elongations).  $Cu^{2+}$  prefers a tetragonal geometry in simple coordination compounds, i.e. coordination number 6<sup>[131, 132]</sup>. This spatial arrangement is nearly similar to the octahedral coordination that  $Mg^{2+}$  ions show. But it could be possible that the overall coordination in the active site of the enzyme during catalysis is not optimal. Usually,  $Co^{2+}$  prefers nitrogen or sulfur donor atoms<sup>[131]</sup> but is also able to complex oxygen donor atoms from carboxylates in tetragonal geometry<sup>[132]</sup>.  $Co^{2+}$  shows again an octahedral geometry, similar to  $Mg^{2+}$  ions<sup>[131, 132]</sup>. Like  $Cu^{2+}$ ,  $Co^{2+}$  prefers nitrogen or sulfur donor atoms<sup>[131]</sup> but is also able to form a complex with oxygen donor atoms from carboxylates<sup>[132]</sup>. The considered characteristics of the used bivalent cations and the mainly formed product chain lengths are also summarized in table A4 (appendix section 7.3.).

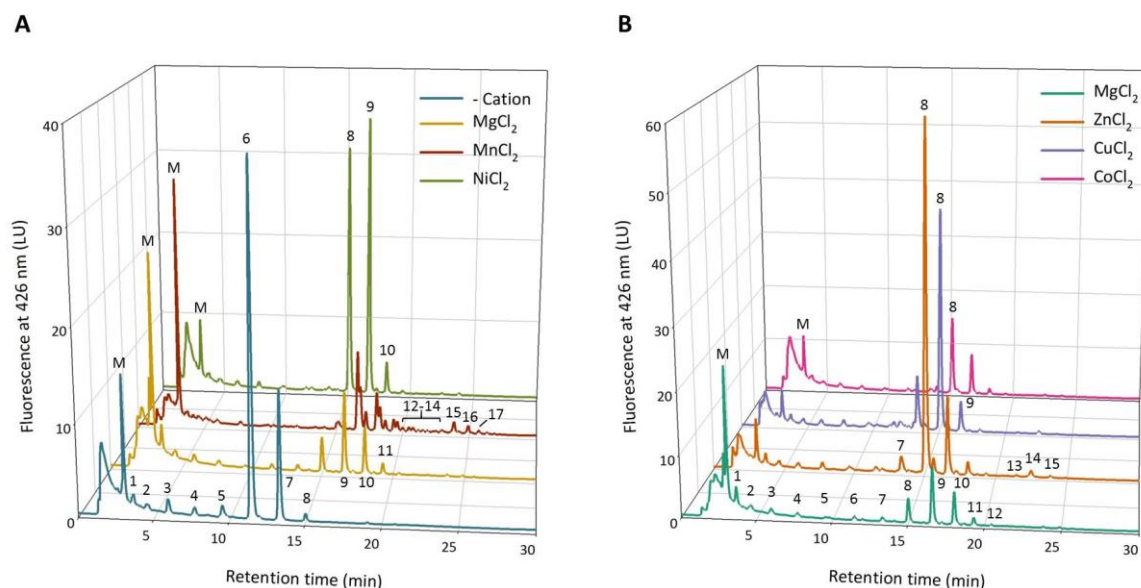


**Figure 20** HPLC chromatograms of the products of a ThkCPT reaction with MANT-O-GPP and IPP using different bivalent cations. Reactions were performed at 65°C reaction temperature followed by diphosphate hydrolysis. **(A)** Comparison of the products formed without addition of bivalent cation (blue) or with addition of MgCl<sub>2</sub> (yellow), MnCl<sub>2</sub> (red) or NiCl<sub>2</sub> (green). **(B)** Comparison of the products formed with addition of MgCl<sub>2</sub> (petrol green), ZnCl<sub>2</sub> (dark orange), CuCl<sub>2</sub> (purple) or CoCl<sub>2</sub> (magenta). After excitation at 359 nm the emission was measured at 426 nm via fluorescence. Prior to the corresponding alcohol of the remaining starter substrate (MANT-O-Geraniol) some impurities are still present. LU: luminescence units, M: MANT-O-Geraniol. Numbers indicate the catalyzed elongation steps.

When Cl-BPP was used as homoallylic substrate the addition of a bivalent cation is absolutely necessary. As shown in figure 21A (blue) only one attachment of Cl-BPP to MANT-O-GPP is catalyzed by ThkCPT when no additional bivalent cation is used. Furthermore, a quite high amount of starter substrate is not converted compared to the catalysis with added Mg<sup>2+</sup>. It is very likely that the remaining activity results from residual magnesium ions, as already discussed above. In addition, the conversion of alternative homoallylic substrates is slowed down compared to the reaction with IPP (see section 3.2.4.2.). By adding an excess of MgCl<sub>2</sub> again, up to 8 Cl-BPP units are added to MANT-O-GPP, whereby products with 6-7 attachments constitute the major part (Figure 21A, yellow). This is conform to the conversion with Cl-BPP under standard conditions (see Figure 19). By the addition of Mn<sup>2+</sup> or Ni<sup>2+</sup> ions products with a chain length of up to 9 attachments of Cl-BPP can be observed (Figure 21A, red and green), yielding mainly shorter products for Mn<sup>2+</sup> (1, 3-6 elongations) and slightly longer products for Ni<sup>2+</sup> (6-7 elongations), respectively. The product distribution is comparable to this in presence of MgCl<sub>2</sub>, due to octahedral geometry of Mn<sup>2+</sup> and Ni<sup>2+</sup> as described above. With zinc as bivalent cation, up to 6 Cl-BPP units are attached to the starter

substrate, with 1 or 3 times elongated compounds as most abundant products (Figure 21B, dark orange). And when using  $\text{Cu}^{2+}$  ions, only 3 elongation steps can be observed, generating mainly the 1-fold condensed product (Figure 21B, purple). The substrate conversion appears to be hindered with the alternative bivalent cations. This might be based on the different coordination geometry as described above. But the lower conversion rate of the alternative substrate itself might be the reason of the decreased product formation. For  $\text{Co}^{2+}$  the product distribution is slightly shifted compared to  $\text{Mg}^{2+}$  (Figure 21B, magenta), yielding mainly 3-5 elongation steps. As described above,  $\text{Co}^{2+}$  ions exhibit the same geometry as magnesium ions. Here, the slower substrate conversion with Cl-BPP ( $k_{\text{cat}}$  is around 140-fold lower compared to IPP<sup>[3]</sup>) could be also a reason for the occurrence of mainly short-chain products. The considered characteristics of the used bivalent cations and the mainly formed product chain lengths are also summarized in table A4 (appendix section 7.3.).

In summary, the enzyme remains active when substituting magnesium by other bivalent cations, but the product distribution in the catalyzed reactions is influenced. With IPP as homoallylic substrate, the short-chain products also occur as intermediates (compared to the catalysis under standard conditions) but long-chain products are mainly formed (7-11 elongations). Even longer products could be detected in small amounts. The exchange of the bivalent cation has a greater influence on the conversion with Cl-BPP as homoallylic substrate. Here, the product distribution is shifted to more short-chain products (except for  $\text{Mn}^{2+}$  and  $\text{Ni}^{2+}$ ).

The results obtained by medium engineering are summarized in table 20 at the end of the section.

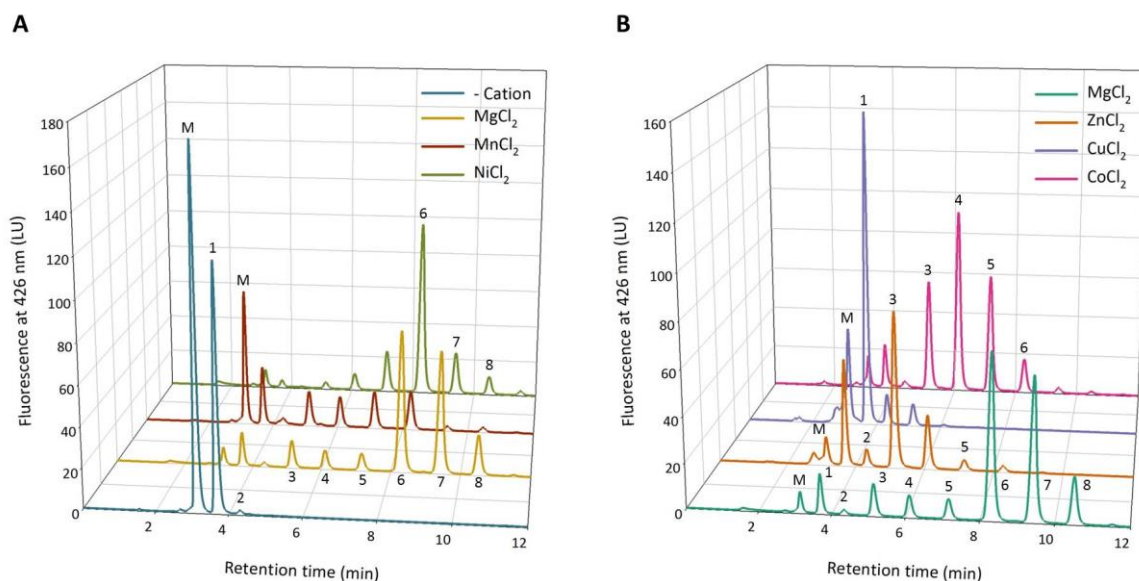


**Figure 21** HPLC chromatograms of the products of a ThkCPT reaction with MANT-O-GPP and Cl-BPP using different bivalent cations. Reactions were performed at 65°C reaction temperature followed by diphosphate hydrolysis. **(A)** Comparison of the products formed without addition of bivalent cation (blue) or with addition of MgCl<sub>2</sub> (yellow), MnCl<sub>2</sub> (red) or NiCl<sub>2</sub> (green). **(B)** Comparison of the products formed with addition of MgCl<sub>2</sub> (petrol green), ZnCl<sub>2</sub> (dark orange), CuCl<sub>2</sub> (purple) or CoCl<sub>2</sub> (magenta). After excitation at 359 nm the emission was measured at 426 nm via fluorescence. Prior to the corresponding alcohol of the remaining starter substrate (MANT-O-Geraniol) some impurities are still present. LU: luminescence units, M: MANT-O-Geraniol. Numbers indicate the catalyzed elongation steps.

For the *E. coli* UPPS it has been shown that the Mg<sup>2+</sup> is coordinated by the diphosphate moiety of either IPP or FsPP (an inactive FPP analog), the carboxylate of Asp26, and three water molecules<sup>[73]</sup>. When comparing a generated homology model of the ThkCPT (see section 3.2.5.3.) with the crystal structure of EcUPPS it appears that Asp43 might be the corresponding Mg<sup>2+</sup>-coordinating amino acid in ThkCPT. When using other bivalent cations that exhibit a different geometry than Mg<sup>2+</sup>, the potential change in coordination by the appropriate amino acid in the active site of the ThkCPT during catalysis might also influence the product distribution. In addition, it may change the coordination of the diphosphate moiety. Furthermore, the reaction kinetics could be influenced due to an incorrect coordination or because of the slow conversion rate for Cl-BPP. These aspects will be a part of future analyses.

Table 20 below summarizes the results obtained by medium engineering.

**Table 20** Summary of the results obtained by medium engineering.

<b>Medium engineering</b>	<b>IPP as substrate</b>	<b>Cl-BPP as substrate</b>
<b>Enzyme-to-substrate-ratio</b>	Different product distribution observed (data not shown)	-
<b>Use of a detergent</b>	Triton X-100 supports the product formation	-
<b>Incubation time</b>	Short-chain products are formed within 1 min (4-6 elongations), longer products can be observed within 10 min (9-11 elongations)	Only 1 elongation can be observed within 5 min, up to 8 elongations can be observed after overnight incubation
<b>Biphasic system</b>		
Aqueous phase	Mainly contains long-chain products (8-12 elongations)	Up to 7 elongations are observed in low amounts
Organic phase	Mainly contains short-chain products (1-7 elongations)	Mainly 1 elongation is observed, 2-3 condensations in very low amounts
<b>Bivalent cation</b>		
No additional cation	Up to 8 elongations, main products with 6-7 IPP units	Up to 2 elongations, main product with 1 Cl-BPP unit
Mg <sup>2+</sup>	Up to 11 elongations, main products with 8-10 IPP units	Up to 8 elongations, main products with 6-7 Cl-BPP units
Mn <sup>2+</sup>	Up to 17 elongations, main products with 8-10 IPP units	Up to 9 elongations, main products with 1/3-6 Cl-BPP units
Ni <sup>2+</sup>	Up to 10 elongations, main products with 8-9 IPP units	Up to 9 elongations, main products with 6-7 Cl-BPP units
Zn <sup>2+</sup>	Up to 15 elongations, main products with 8-9 IPP units	Up to 6 elongations, main products with 1-3 Cl-BPP units
Cu <sup>2+</sup>	Up to 14 elongations, main products with 7-8 IPP units	Up to 3 elongations, main product with 1 Cl-BPP unit
Co <sup>2+</sup>	Up to 9 elongations, main products with 8-9 IPP units	Up to 8 elongations, main products with 3-5 Cl-BPP units

### 3.2.5.2. Challenges in the elongation of prenyl diphosphates with BPP

As the conversion with the alternative substrate 3-butenyl diphosphate (BPP) has been proven to be difficult, the reaction was further investigated. It is considered that, due to the decreased size of the C3 substituent, the BPP cannot be bound correctly in the active site of



the enzyme. Another reason for the decrease in product length might be that the formed product (with 1 attachment of BPP to MANT-O-GPP) cannot be oriented correctly in the active site of the enzyme, due to the decreased size of the substituent at the C3 position, what could affect further catalysis (Figure 22).

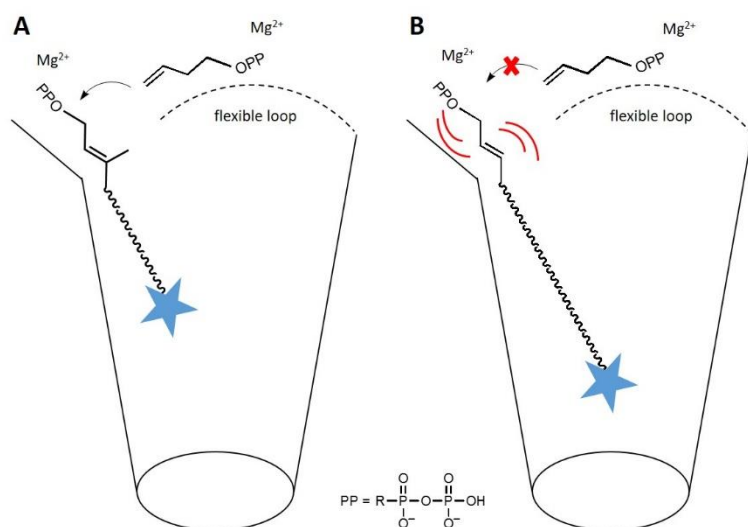


**Figure 22** Model of the active site during catalysis showing (A) the first attachment of BPP to MANT-O-GPP and (B) the problematic further addition of BPP units to the first formed product which contains a less voluminous substituent at the C3 position. Blue star: fluorescence label of MANT-O-GPP, red curves: possible flexibility of the first product. Figure was modified according to Liang et al. 2002<sup>[47]</sup>.

To examine if the latter reason is responsible for the observed effects, MANT-O-nor FPP [(2E,6E,10Z)-12-O-(N-Methylanthranlyl)-7,11-dimethyl-2,6,10-dodecatrien-1-diphosphate], an allylic substrate with one already attached BPP unit, was used for substrate conversion (section 2.5.1. and Figure 23). As a control reaction the assay was also carried out with IPP as homoallylic substrate. The obtained products were hydrolyzed and analyzed via fluorescence-based HPLC (section 2.5.3.1.).

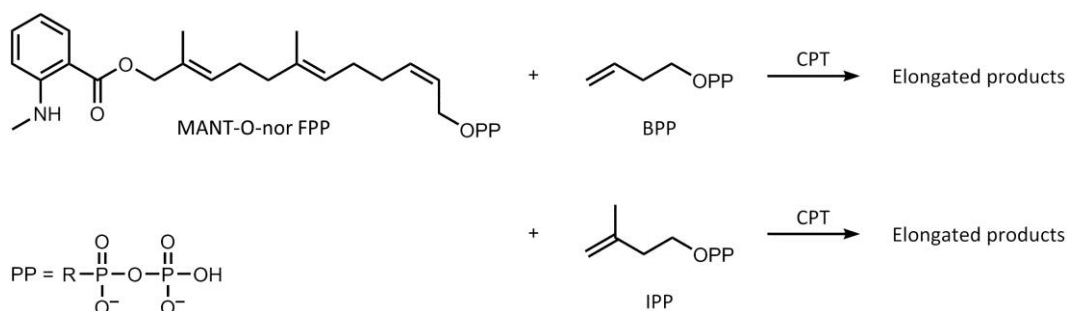


**Figure 23** Conversion of the alternative allylic substrate MANT-O-nor FPP with BPP or IPP.

The conversion of MANT-O-nor FPP with BPP leads to mainly one more attachment of the homoallylic substrate to the alternative starter substrate (Figure 24, red). Though, an

overnight incubation is needed to observe product formation. A high amount of residual starter substrate was observed, which is appropriate to the main product formed during the conversion of MANT-O-GPP and BPP (see Figure 15, section 3.2.4.2.). When IPP is used for substrate conversion with MANT-O-nor FPP, products with chain lengths comparable to the reaction with MANT-O-GPP are formed (Figure 24, for comparison see Figure 15 in section 3.2.4.2.). As with MANT-O-GPP, short-chain intermediates (1-7 elongations) are already formed after 1 min (Figure 24, yellow). The long-chain products are then formed during a longer incubation (overnight) with up to 11 attachments of IPP (Figure 24, blue). An elongation of an allylic substrate lacking the methyl group at the C3 position has not been reported yet. In 2001, Nagaki and coworkers described that nor FPP was not accepted as an allylic substrate in reactions catalyzed by the *M. luteus* HexPPS or the *Bacillus subtilis* HepPPS<sup>[115]</sup>. Furthermore, no product formation was possible with nor FPP or Z-nor GGPP as substrates in the reaction of *M. luteus* UPPS<sup>[133]</sup>.

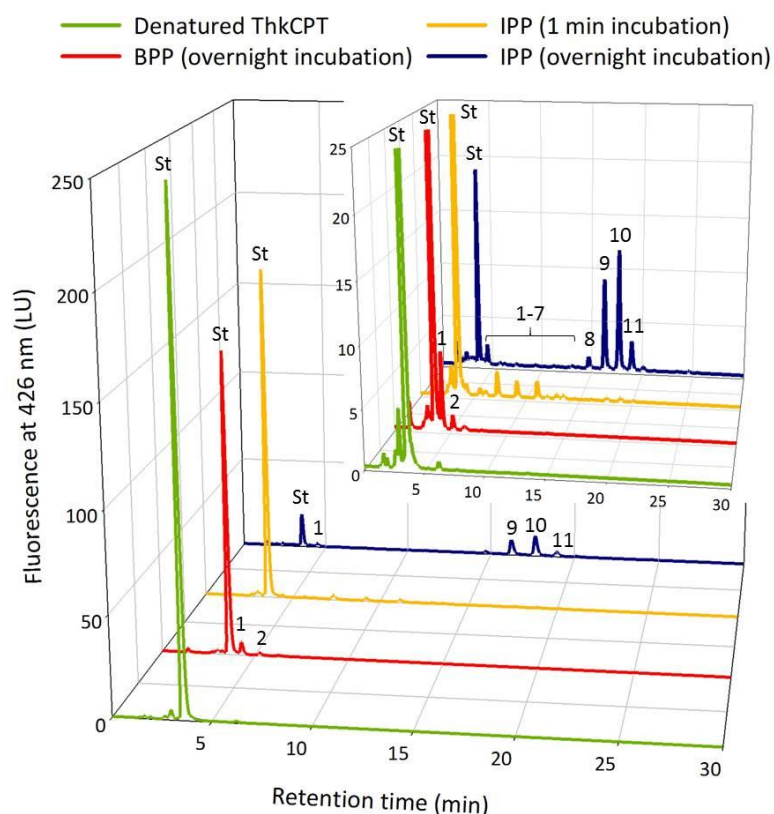


**Figure 24** HPLC chromatograms of the products of a ThkCPT reaction with MANT-O-nor FPP and BPP (red) or IPP (yellow and blue) as elongation substrates. Reactions were performed at 65°C reaction temperature followed by diphosphate hydrolysis. For the blank sample (green) reactions with denatured enzyme were carried out. After excitation at 359 nm the emission was measured at 426 nm via fluorescence. LU: luminescence units, St: starter substrate (corresponding alcohol). Numbers indicate the catalyzed elongation steps.

The successful product formation with MANT-O-nor FPP and IPP indicates that the substituent at the C3 position is important for elongation, besides its importance in the stabilization of the intermediate cation (as discussed in section 3.2.4.2.). When an IPP unit is attached to MANT-O-nor FPP, a methyl group is present at the C3 position of the product and catalysis continues. This step might be the rate-limiting one during this reaction. In contrast, no further substrate conversion can be observed with BPP. This supports the suggestion that the decreased size of the substituent at the C3 position complicates a correct orientation of the product formed from MANT-O-GPP and BPP in the active site of the enzyme. To confirm this assumption, further experiments have to be carried out in the future. The orientation of the allylic substrates in the active site could be investigated by X-ray crystallography. Such insights would be useful to better understand the differences in substrate conversion.

### 3.2.5.3. Generation of variants

In cooperation with Dr. Wolfgang Brandt (IPB Halle) a homology model of the ThkCPT (Figure 25) was generated by using the Phyre2 web portal<sup>[134]</sup>. Seven templates (PDB codes: 4H8E, 5HXP, 3ZDD, 2VG2, 5HC7, 2VFW and 4Q9M) were selected to model the protein based on heuristics to maximize confidence, percentage identity and alignment coverage. Thus, 88% of the residues were modelled at >90% confidence. According to this model, possible positions for mutations were chosen to enhance substrate conversion.

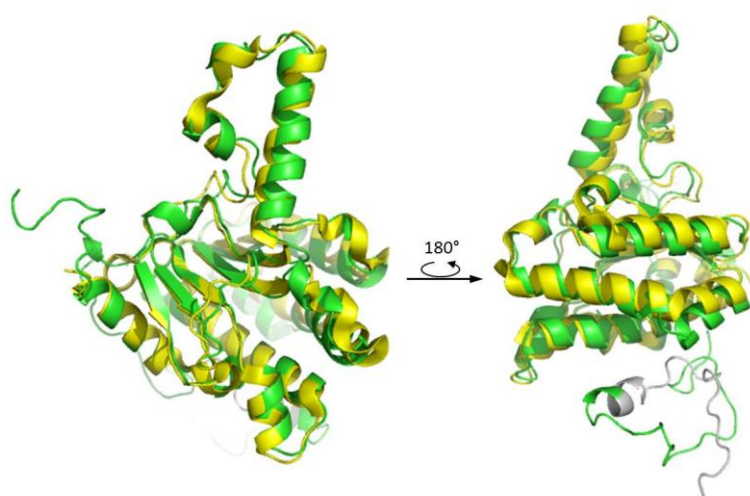


**Figure 25** Comparison of the homology model of ThkCPT (green) and the crystal structure of EcUPPS (PDB code: 1X06<sup>[73]</sup>, yellow). The N-terminal tag including the His<sub>6</sub> sequence of the ThkCPT is shown in grey. It has to be noted that only one monomer is shown for each enzyme. The structures were visualized using the software PyMOL 1.8<sup>[70]</sup>.

*i) Mutations in the active site to facilitate BPP conversion*

On the basis of the generated homology model (Figure 25), the active site of ThkCPT was analyzed. To support the orientation of BPP and the elongated product, amino acids surrounding the assumed binding site of the substrates were taken into consideration. As the C3 substituent of the elongation substrate is decreased in size, the most proximate isoleucine (I41) residue was exchanged against a more spacious phenylalanine leading to the variant I41F. On the other hand, the residue was exchanged against a less voluminous alanine/glycine to examine its involvement in substrate stabilization generating the variants I41A and I41G. Additionally, a spatially adjacent tyrosine (Y85) residue was enlarged to possibly support substrate binding yielding the variants I41A/Y85W and I41G/Y85W.

To obtain the variants, site-directed mutagenesis (section 2.3.6.1.) with the corresponding primers listed in table 7 (section 2.1.7.) was carried out. The mutations were verified by sequencing (section 2.3.4., sequences are shown in figure A1 in the appendix, section 7.2.). Production of the ThkCPT variants was carried out in the expression strain *E. coli* BL21 (DE3) (section 2.4.1.). Cell lysis was done by using osmotic shock (section 2.4.3.) and the activity assay was carried out with the crude extracts (section 2.5.1.3.) with MANT-O-GPP and BPP or IPP as substrates. The obtained products were hydrolyzed and analyzed via fluorescence-based HPLC (section 2.5.3.1.).

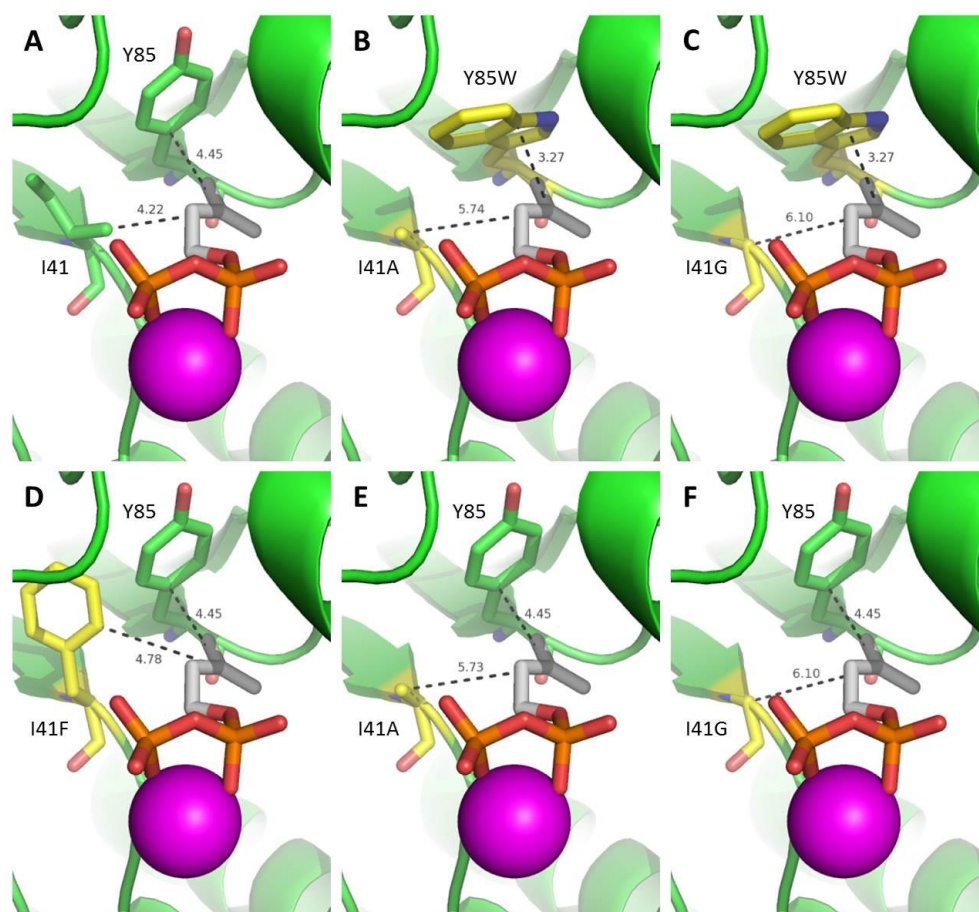


**Figure 26** Active sites in the homology models (green) of ThkCPT variants achieved by site-directed mutagenesis in complex with  $Mg^{2+}$  (magenta sphere) and IPP (shown as sticks, carbon: grey, phosphate: orange, oxygen: red). (A) WT, (B) I41A/Y85W, (C) I41G/Y85W, (D) I41F, (E) I41A, (F) I41G. Unmodified amino acids are shown in green, modified amino acids are shown in yellow (oxygen: red, nitrogen: blue). Additionally, the distances between the C3 atom of IPP and the amino acid residues are given (in Å) and the involved residues are labeled. The structures were visualized using the software PyMOL 1.8<sup>[70]</sup>.

The five obtained variants (Figure 26) were all active in the conversion of MANT-O-GPP and IPP. The activity was comparable to the wild type, with slightly shorter product chain lengths achieved (up to 11 elongations, Figure 27A and B). The altered size of the isoleucine residue of the variants seems to have no severe effect on the substrate conversion with IPP. For the double mutants the product distribution is shifted to marginally shorter products compared to the single mutants. Variant I41G/Y85W catalyzes mainly 7-8 elongations (Figure 27B, blue) and variant I41A/Y85W primarily forms products containing 8-9 IPP units (Figure 27B, yellow). The conversion of IPP is only marginally affected in the variants although the expansion of I41 theoretically decreases space in the active site for occupation of the homoallylic substrate. The expansion of Y85 leads to a bulkier residue but due to the simultaneous reduction of I41 the IPP unit seems to be arranged correctly.

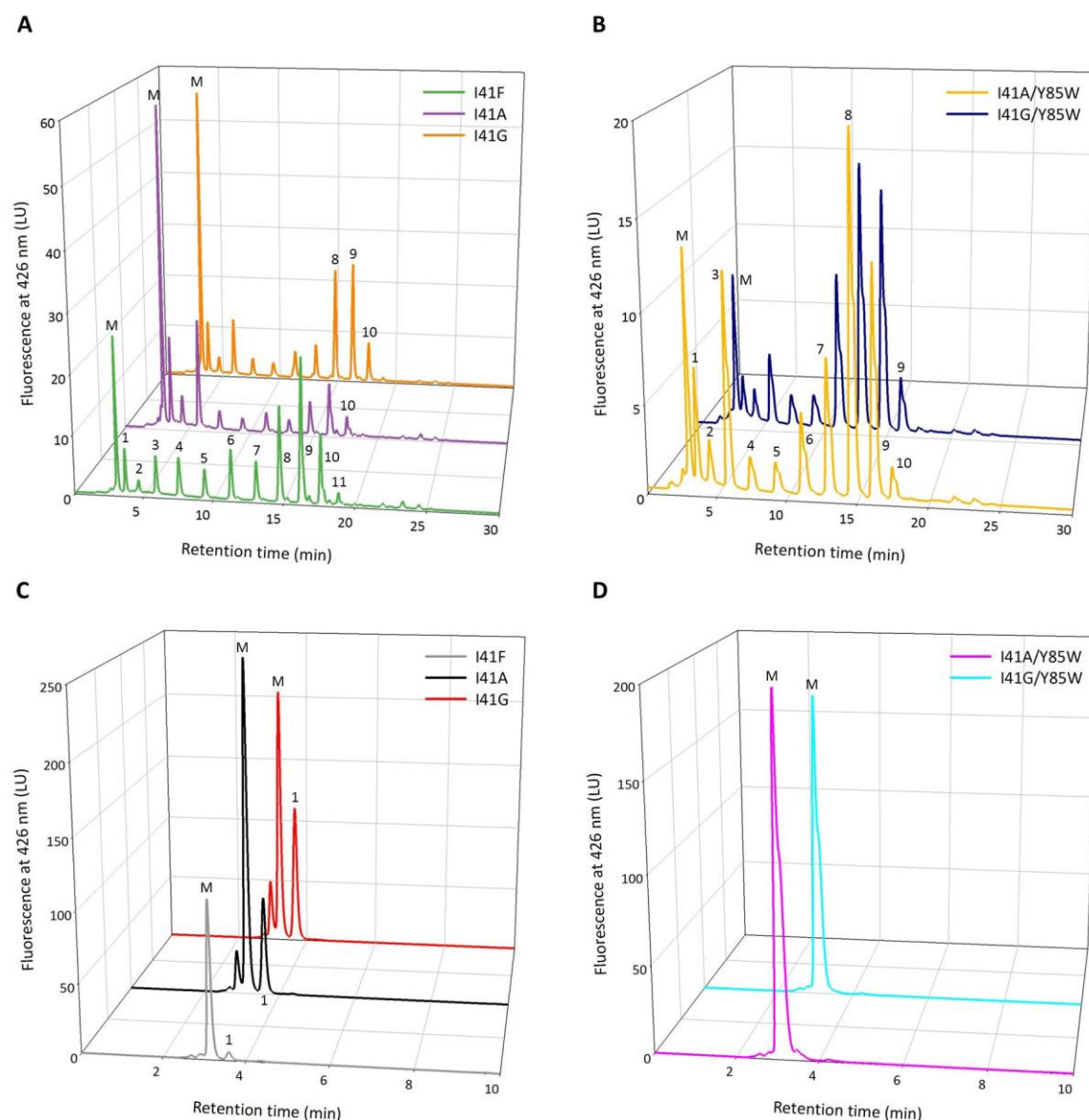


**Figure 27** HPLC chromatograms of the products of the reaction with MANT-O-GPP and IPP or BPP catalyzed by different ThkCPT variants. Reactions were performed at 65°C reaction temperature followed by diphosphate hydrolysis. **(A)** Products formed with IPP as elongation substrate by the variants I41F (green), I41A (purple) and I41G (orange). **(B)** Products formed with IPP as elongation substrate by the variants I41A/Y85W (yellow) and I41G/Y85W (blue). **(C)** Products formed with BPP as elongation substrate by the variants I41F (grey), I41A (black) and I41G (red). **(D)** Products formed with BPP as elongation substrate by the variants I41A/Y85W (magenta) and I41G/Y85W (cyan). After excitation at 359 nm the emission was measured at 426 nm via fluorescence. LU: luminescence units, M: MANT-O-Geraniol. Numbers indicate the catalyzed elongation steps.

Originally, the variants were generated to improve the conversion of BPP, but none of them showed enhanced product formation. When exchanging isoleucine by a more spacious residue (I41F) the MANT-O-GPP is barely elongated (Figure 27C, grey). In case of replacing isoleucine by a less voluminous residue (I41A, I41G), MANT-O-GPP is elongated with one BPP unit (Figure 27C, black and red). By simultaneously substituting tyrosine, no product formation can be observed with BPP (Figure 27D, magenta and cyan). The mutation does not



lead to a stabilization of the homoallylic substrate but to a hindrance of product formation. Thus, the question remains open if the conversion of BPP by ThkCPT can be improved by mutagenesis. It seems not easy to stabilize the binding of BPP and the reaction product lacking the methyl group at the C3 position.

The results obtained by genetic engineering are summarized in table 21 at the end of the section.

*ii) Mutations of the hydrophobic tunnel to further increase chain length in product formation*

During catalysis the formed *cis*-polyprenyl chain is accommodated in a hydrophobic tunnel. Yamada and coworkers could show for ThkCPT that the substitution of Glu68, Lys109 or Leu113 with alanine has an influence on the product chain length, with K109A being the most effective variant for product length extension<sup>[75]</sup>. Those variants were also examined during this study. Furthermore, the homology model of ThkCPT was compared to the crystal structure of *E. coli* UPPS. In EcUPPS, Leu137 is at most probably responsible for blocking further product elongation. It has been shown that substitution of Leu137 with alanine results in the synthesis of longer polyprenyl products<sup>[72]</sup>. Thus, Tyr156 and Leu158 were identified in ThkCPT as structural homologs of Leu137 from EcUPPS. A single alanine-substitution should be introduced into these positions to investigate if the product chain length could be altered. In cooperation with the group of Prof. Bornscheuer (University of Greifswald) the hydrophobic tunnel in the homology model of ThkCPT was analyzed using the software CAVER 3.01<sup>[95]</sup>. The analyses were done by Hubert Kasproski (University of Greifswald).

In the obtained models the tunnel in variant L158A is only slightly expanded (Figure 28B) so that this variant is probably not able to accommodate longer products compared to the wild type (Figure 28A). The exchange of Tyr156 seems to have a great influence on the topology of the tunnel (Figure 28C) compared to the wild type (Figure 28A). Thus, this variant might shows an improved chain elongation.

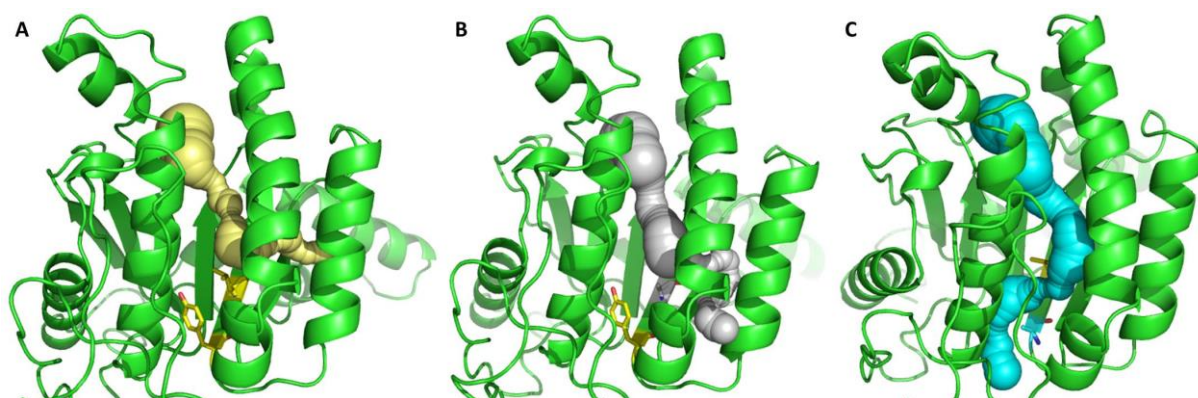


**Figure 28** Comparison of the structures of the hydrophobic tunnels in the homology models of ThkCPT variants. The protein backbone is shown as green cartoon. (A) WT enzyme with the tunnel shown in yellow. The amino acids Y156 and L158 are highlighted as yellow sticks (red: oxygen, blue: nitrogen). (B) Variant L158A with the tunnel shown in grey. The WT amino acid Y156 is shown as yellow sticks and the exchanged amino acid L158A is shown as grey sticks (red: oxygen, blue: nitrogen). (C) Variant Y156A with the tunnel shown in cyan. The WT amino acid L158 is shown as yellow sticks and the exchanged amino acid Y156A is shown as cyan sticks (red: oxygen, blue: nitrogen).

The variants were obtained as described above. In variant L158A an additional mutation was observed in all clones (L113A). Cell lysis was done by using osmotic shock (section 2.4.3.) and the activity assay was carried out with the crude extracts (section 2.5.1.3.) with MANT-O-GPP and IPP or Cl-BPP as substrates. The obtained products were hydrolyzed and analyzed via fluorescence-based HPLC (section 2.5.3.1.).

For the variants that were generated considering literature<sup>[75]</sup> the formation of long-chain products can be observed with IPP as homoallylic substrate (Figure 29A). Variant E68A catalyzes up to 17 elongations (Figure 29A, green), generating mainly 10 IPP attachments and variant L113A forms products with up to 19 elongations (Figure 29A, orange), yielding predominantly 12 IPP attachments. Variant K109A seems to realize even more extensions (Figure 29A, purple) which is in accordance with published results<sup>[75]</sup>. However, the amount of long-chain products (>12 attachments) is extremely low. For the conversion with Cl-BPP no long products could be detected with the variants from literature. In contrast, shorter products were formed (maximal 7 elongations, Figure 29C). In contrast to the wild type, variant E68A forms primarily products with 4 and 5 attached Cl-BPP units (Figure 29C, grey). Variant K109A catalyzes up to 7 elongations, yielding mainly 6 attachments of Cl-BPP to MANT-O-GPP (Figure 29C, black) and L113A primarily generates products with 5 and 6 attached Cl-BPP units (Figure 29C, red). Therefore, these exchanges do not seem to support the formation of long-chain products with artificial homoallylic substrates. It seems that the



size of the hydrophobic tunnel is not the only critical parameter influencing elongation. The decreased turnover rate of artificial substrates is also a limiting factor.

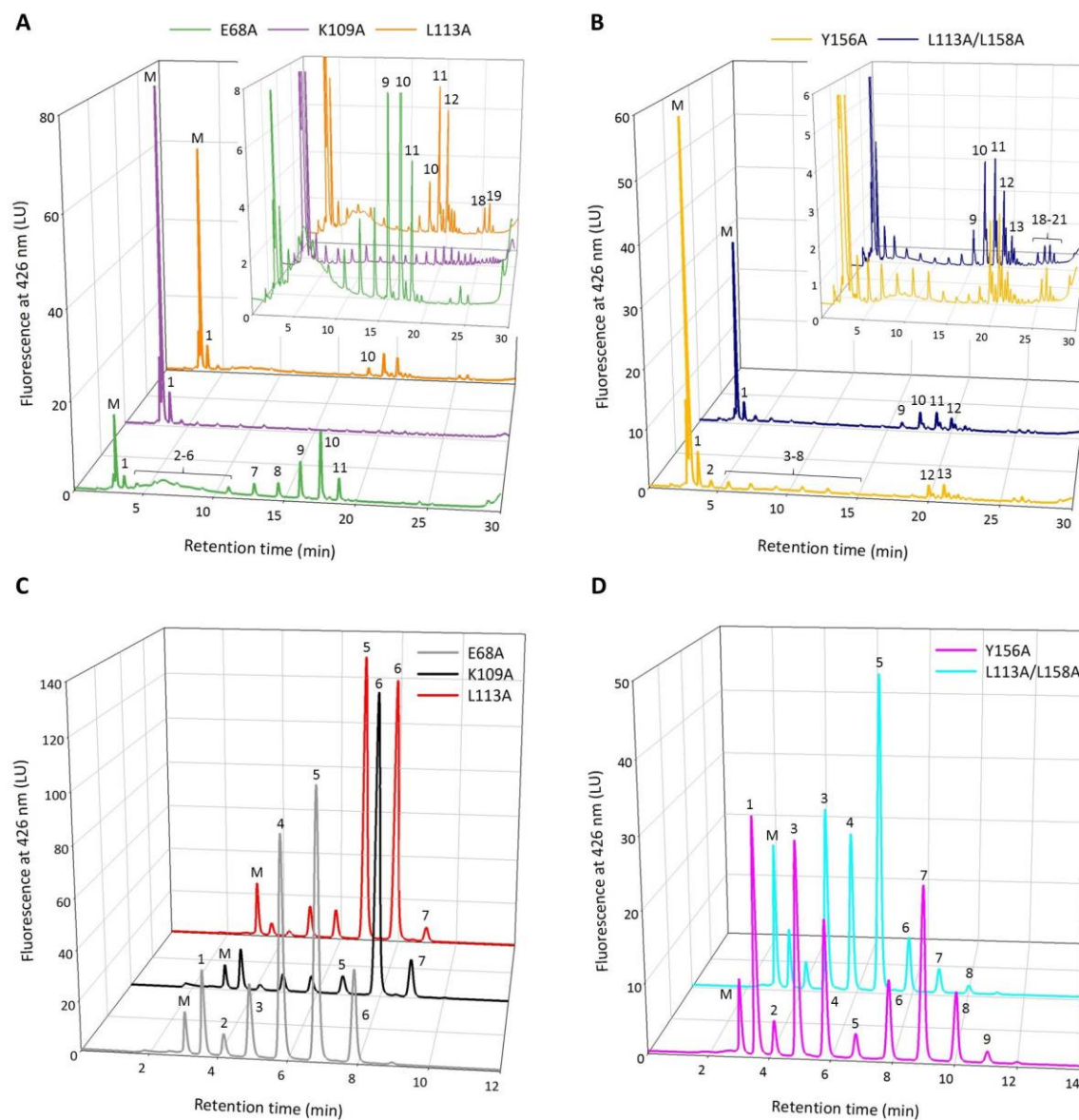


**Figure 29** HPLC chromatograms of the products of the reaction with MANT-O-GPP and IPP or CI-BPP catalyzed by different ThkCPT variants. Reactions were performed at 65°C reaction temperature followed by diphosphate hydrolysis. **(A)** Products formed with IPP as elongation substrate by the variants E68A (green), K109A (purple) and L113A (orange). **(B)** Products formed with IPP as elongation substrate by the variants Y156A (yellow) and L113A/L158A (blue). **(C)** Products formed with CI-BPP as elongation substrate by the variants E68A (grey), K109A (black) and L113A (red). **(D)** Products formed with CI-BPP as elongation substrate by the variants Y156A (magenta) and L113A/L158A (cyan). After excitation at 359 nm the emission was measured at 426 nm via fluorescence. LU: luminescence units, M: MANT-O-Geraniol. Numbers indicate the catalyzed elongation steps.

The variants generated based on our own homology model also form long-chain products with IPP as elongation substrate (Figure 29B). The double mutant L113A/L158A catalyzes mainly 10-12 attachments of IPP to MANT-O-GPP (Figure 29B, blue). Though, it cannot be

clearly determined if the formed long products (18-20 elongations) originate from the mutation L113A (the corresponding single variant also generates longer products, Figure 29A, orange) or from the introduction of the second exchange L158A. Unfortunately, it was not possible to obtain a pET28a(+)-ThkCPT construct harboring only the mutation L158A, so that the origin of the changed product distribution could not be clearly verified. For the reaction with Cl-BPP, the double mutant generates mostly 3- to 5-fold elongated products (Figure 29D, cyan) which is slightly different from the single variant L113A (Figure 29C, red). Additionally, L113A/L158A catalyzes up to 8 Cl-BPP attachments to MANT-O-GPP, which is one more compared to the single mutant. The main products of ThkCPT Y156A reflect 1 and 13 IPP attachments (Figure 29B, yellow), but this variant is able to catalyze up to 21 elongation steps. It appears that this amino acid exchange influences the topology of the hydrophobic tunnel in favor of longer product chains as it was indicated by the tunnel analyses (Figure 28). This apparent extension though has no great influence on the product chain length in the conversions with Cl-BPP (Figure 29D, magenta) as only the product distribution is slightly changed compared to the wild type (see Figure 15, section 3.2.4.2.). ThkCPT-Y156A is able to form a 9-fold elongated product but realizes mainly 1, 3 and 7 Cl-BPP attachments. This affirms that not only the nature of the hydrophobic tunnel is a limiting factor for long-chain product formation but also the lowered conversion rate of artificial substrates.

The amount of long products in the reaction with IPP is rather low. That arises potentially from a lowered affinity the longer the nascent products become and form a correlating lower rate constant for the attachment of another IPP unit<sup>[47, 71]</sup>. As judged from pre-steady-state kinetic studies, the rate constant of UPPS for a condensation of an additional IPP unit with an intermediate containing 55 carbon atoms to produce a product containing 60 carbon atoms is fivefold lower than that for condensation of IPP with more short-chain prenyl diphosphates<sup>[47, 71]</sup>. It is likely that this effect is further enhanced by even longer products, which complicates their formation.

Table 21 below summarizes the results obtained by genetic engineering.

**Table 21** Summary of the results obtained by genetic engineering.

<b>Genetic engineering</b>	<b>IPP as substrate</b>	<b>CI-BPP as substrate</b>	<b>BPP as substrate</b>
<b>Variants concerning the active site</b>			
I41F	Up to 11 elongation steps, main products with 8-10 IPP units	-	Only 1 elongation
I41A	Up to 11 elongation steps, main products with 8-10 IPP units	-	Only 1 elongation
I41G	Up to 11 elongation steps, main products with 8-10 IPP units	-	Only 1 elongation
I41A/Y85W	Up to 10 elongation steps, main products with 8-9 IPP units	-	No elongation
I41G/Y85W	Up to 10 elongation steps, main products with 7-8 IPP units	-	No elongation
<b>Variants concerning the hydrophobic tunnel</b>			
E68A	Up to 17 elongation steps, main product with 10 IPP units	Up to 6 elongation steps, main products with 4-5 CI-BPP units	-
K109A	More than 18 elongation steps, but in an extremely low amount	Up to 7 elongation steps, main product with 6 CI-BPP units	-
L113A	Up to 19 elongation steps, main product with 12 IPP units	Up to 7 elongation steps, main products with 5-6 CI-BPP units	-
Y156A	Up to 21 elongation steps, main products with 1/12-13 IPP units	Up to 9 elongation steps, main products with 1/3/7 CI-BPP units	-
L113A/L158A	Up to 21 elongation steps, main products with 10-12 IPP units	Up to 8 elongation steps, main products with 3-5 CI-BPP units	-

### 3.2.6. Adaption of the assay to high-throughput conditions

The substrate conversion of ThkCPT, followed by hydrolysis of the polyprenyl diphosphates and the HPLC-based analysis of the corresponding alcohols, is a time-consuming process. In order to develop a faster assay which could be developed into a high-throughput screening (HTS) platform for e.g. enzymatic libraries in a microtiter plate (MTP) format, it was tested if this procedure could be automated. This was done at the University of Greifswald in cooperation with the group of Prof. Bornscheuer. Cells expressing wild type ThkCPT or harboring an empty vector control were cultivated in a MTP as described in section 2.2.1. Afterwards, the cell lysis was carried out by osmotic shock (section 2.4.3.1.) and an activity assay was performed with the crude cell extracts using FPP and IPP as substrates (section 2.5.1.4.). A schematic representation of the general workflow for the developed method is shown in figure 30. The reaction scheme for the substrate conversion is shown in figure 37 (section 4.2.4.). In contrast to the assays previously performed, the formed products were then analyzed by TLC (section 2.5.2.).

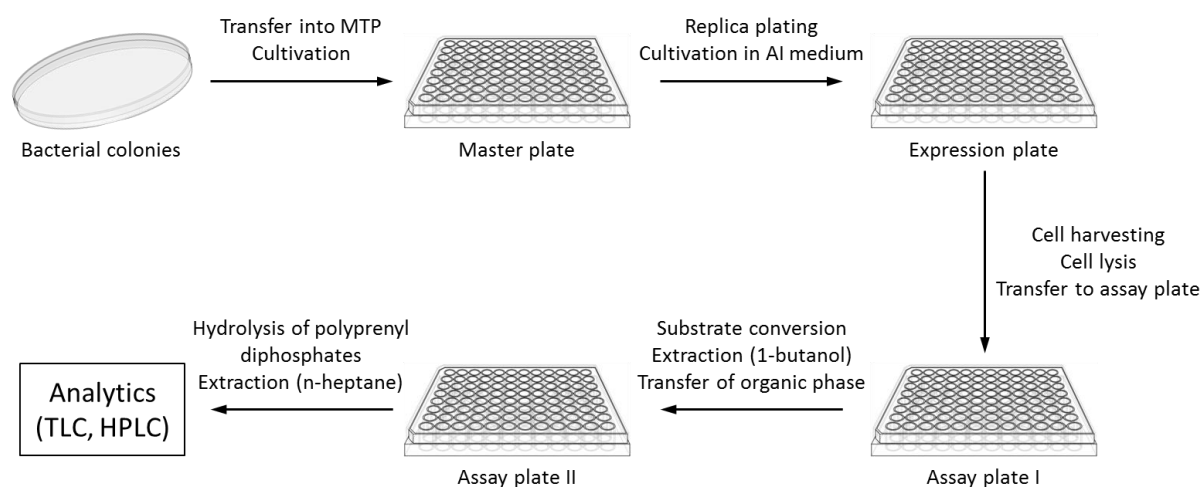


**Figure 30** Schematic representation of the HTS procedure including enzyme production and substrate conversion in microtiter plates. Figure was adapted from Böttcher & Bornscheuer 2006<sup>[135]</sup>. Clipart images were taken from <http://www.clker.com/> (petri dish) and <http://www.bidproposalexample.com/96-well-plate-template/> (MTP).

The possibility to express ThkCPT in the AI medium, which was also used in the MTP assay, was confirmed in previous shake flask experiments (data not shown). Proper cell lysis by osmotic shock was checked by SDS-PAGE (section 2.4.10.) as shown in figure 31. The band representing successfully produced His<sub>6</sub>-tagged ThkCPT (34 kDa) is indicated by an arrow.

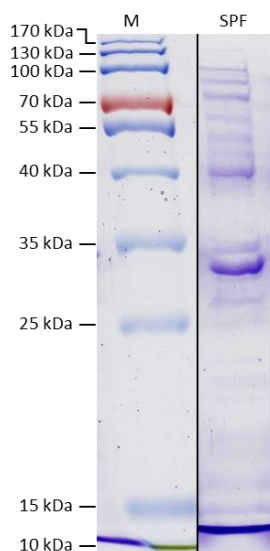


**Figure 31** SDS-PAGE gel with Coomassie staining indicating ThkCPT production in AI medium in MTPs. The ThkCPT band is marked with an arrow. M: PageRuler™ prestained protein ladder, SPF: soluble protein fraction. The figure was assembled from different parts of the same gel.

The feasibility of the activity assay with crude extracts could be shown in a previous section (3.2.5.3.) and was therefore also applied to enzyme preparations produced in MTP format. However, no product formation could be detected (Figure 32). One explanation could be that the amount of produced enzyme was too low. The concentration of ThkCPT might affect substrate conversion. Consequently, the elongated products are possibly formed in a very low amount.

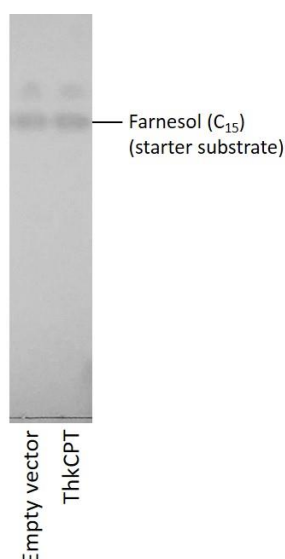


**Figure 32** TLC analysis of the products formed by ThkCPT expressed in MTPs with FPP and IPP as substrates. Reactions were performed at 65°C reaction temperature followed by diphosphate hydrolysis. TLC material: RP-18, solvent system: acetone/H<sub>2</sub>O (19:1, v/v), detection reagent: iodine fume.

Another critical step in small-scale MTP reactions is the proper product extraction. Due to its relatively high boiling point 1-BuOH (which was used in the regular assay conditions) evaporates slowly, resulting in a time-consuming solvent removal step. A direct hydrolysis of the diphosphates after substrate conversion by the ThkCPT is possible but leads to some impurities (data not shown). For this step, other alcoholic organic solvents could be tested. Yamada and coworkers<sup>[75]</sup> used e.g. 1-pentanol and 1-octanol, though they have higher boiling points compared to 1-BuOH which would not accelerate solvent evaporation.

On the other hand, extraction of the product alcohols by the more volatile solvent *n*-hexane proved to be difficult in such a small scale as the solvent evaporates too fast during the phase separation step. Thus, *n*-heptane as another nonpolar solvent with higher boiling point was used in further extraction steps. It can be seen in figure 32 that farnesol, the corresponding product alcohol of the starter substrate, can be detected with this optimized extraction protocol. That confirms effective extraction of the product alcohols with the

alternative organic solvent *n*-heptane. However, during phase separation a gel-like interphase forms, caused by addition of the detergent Triton X-100. Therefore, the extraction of the product alcohols in plates with another geometry, i.e. in deep well plates, turned out to be useful.

In conclusion, ThkCPT protein production in AI medium and the cell lysis by osmotic shock are possible in MTP format. However, the enzymatic activity seems to be influenced by the small scale as no product formation could be detected by TLC analyses. An extension of the time for expression might lead to increased protein production and consequently to enhanced substrate conversion. Furthermore, it could be shown that *n*-heptane can be used as an alternative solvent for the extraction of the product alcohols instead of *n*-hexane.

The analytics of the *cis*-polyprenols formed in the ThkCPT reaction in MTP format remains a critical point. The product analysis by TLC is a fast method but in contrast, the detection of the fluorescently labeled products by HPLC was shown to be very sensitive and therefore would be more suitable for the low product amounts expected in MTP format. Potentially, the formed polyprenols could also be evaluated by the application of a HPLC-MS system<sup>[111]</sup>. Advantageously, such an analysis via HPLC(-MS) can be done automated but requires additional time for analysis. Another possibility could be the direct detection of the formed polyprenyl diphosphates. Though, this might be rather difficult due to their amphiphilic character. In subsequent studies, already known methods to separate chemically similar compounds (e.g. phospholipids) by HPLC<sup>[136, 137]</sup> would have to be adjusted to the products formed in a CPT reaction. To facilitate product detection, radiolabeled substrates, which have been successfully employed in other working groups<sup>[4, 54, 66, 72, 126]</sup>, might be used.

### 3.2.7. HR-ESI-MS analysis of reaction products

The analytics concerning *cis*-polyprenols ought to be optimized. To clearly identify the enzymatically formed products, high resolution mass spectrometric approaches have been aspired. However, it has been shown that polyprenols can only be evaluated by application of a HPLC-MS system, since the signals of interest are not intense enough to be analyzed after direct injection<sup>[111]</sup>. To obtain intense signals, highly concentrated samples were used for fractionation via semi-preparative HPLC in previous experiments (section 2.5.3.2.). MANT-O-GPP and IPP or CI-BPP were used as substrates that led to 13 and 8 collectable

products, respectively. The fractions containing chlorinated products could be directly identified in HR-ESI-MS measurements (section 2.5.5.) without further preparation (all spectra are shown in the appendix, section 7.6.). This might be possible due to their more polar character compared to the products formed with IPP. The long-chain products formed during IPP conversion have a nonpolar character and could not be directly identified by HR-ESI-MS approaches. Due to this and a low tendency to form detectable ions in MS it turned out to be difficult to detect the products formed with IPP. To enrich the compounds of interest and to remove disturbing components, the IPP product fractions were prepared by solid phase extraction (SPE, section 2.5.4.). The obtained samples were verified via HPLC (section 2.5.3.1.) and the products were identified in the SPE fractions eluted with HPLC solvent B (Figures A2 and A3 in the appendix, section 7.5.). The product containing fractions were analyzed via HR-ESI-MS as described in section 2.5.5. (all spectra are shown in the appendix, section 7.6.). All formed products could be identified with only small deviation from the calculated mass-to-charge ratios (Tables 20 and 21). In addition, for some compounds also the ammonium and/or sodium adducts were identified.

**Table 22** HR-ESI-MS analysis of the product alcohols (ThkCPT reaction with MANT-O-GPP and the homoallylic substrate IPP at 65°C reaction temperature after diphosphate hydrolysis) in the positive ion mode. Calc.: calculated,  $m/z$ : mass-to-charge ratio, ppm: parts per million.

Product peak (corresponds to IPP units added)	Retention time (min)	Molecular formula	$m/z$ [M+H] <sup>+</sup>	Calc.	Error (ppm)
1	3.888	C <sub>23</sub> H <sub>33</sub> O <sub>3</sub> N	372.2521	372.2533	-3.3119
2	4.568	C <sub>28</sub> H <sub>41</sub> O <sub>3</sub> N	440.3151	440.3159	-1.8001
3	5.890	C <sub>33</sub> H <sub>49</sub> O <sub>3</sub> N	508.3781	508.3785	-0.8470
4	7.538	C <sub>38</sub> H <sub>57</sub> O <sub>3</sub> N	576.4410	576.4411	-0.1407
5	9.386	C <sub>43</sub> H <sub>65</sub> O <sub>3</sub> N	644.5031	644.5037	-0.9678
6	11.245	C <sub>48</sub> H <sub>73</sub> O <sub>3</sub> N	712.5663	712.5663	0.0129
7	13.126	C <sub>53</sub> H <sub>81</sub> O <sub>3</sub> N	780.6284	780.6289	-0.6283
8	14.975	C <sub>58</sub> H <sub>89</sub> O <sub>3</sub> N	848.6918	848.6915	0.3596
9	16.697	C <sub>63</sub> H <sub>97</sub> O <sub>3</sub> N	916.7553	916.7541	1.2506
10	18.206	C <sub>68</sub> H <sub>105</sub> O <sub>3</sub> N	984.8459	984.8167	-0.8218
11	19.385	C <sub>73</sub> H <sub>113</sub> O <sub>3</sub> N	1052.8804	1052.8793	0.9956
12	20.444	C <sub>78</sub> H <sub>121</sub> O <sub>3</sub> N	1120.9414	1120.9419	-0.4955
13	21.429	C <sub>83</sub> H <sub>129</sub> O <sub>3</sub> N	1189.0041	1189.0045	-0.3647

**Table 23** HR-ESI-MS analysis of the product alcohols (ThkCPT reaction with MANT-O-GPP and the homoallylic substrate Cl-BPP at 65°C reaction temperature after diphosphate hydrolysis) in the positive ion mode. Calc.: calculated,  $m/z$ : mass-to-charge ratio, ppm: parts per million.

Product peak (corresponds to Cl-BPP units added)	Retention time (min)	Molecular formula	$m/z$ [M+H] <sup>+</sup>	Calc.	Error (ppm)
1	2,892	C <sub>22</sub> H <sub>30</sub> O <sub>3</sub> NCl	392.1988	392.1987	0.1516
2	3,308	C <sub>26</sub> H <sub>35</sub> O <sub>3</sub> NCl <sub>2</sub>	480.2063	480.2067	-0.8025
3	4,013	C <sub>30</sub> H <sub>40</sub> O <sub>3</sub> NCl <sub>3</sub>	568.2147	568.2147	0.0716
4	4,784	C <sub>34</sub> H <sub>45</sub> O <sub>3</sub> NCl <sub>4</sub>	656.2219	656.2226	-1.0436
5	5,669	C <sub>38</sub> H <sub>50</sub> O <sub>3</sub> NCl <sub>5</sub>	744.2315	744.2306	1.2385
6	6,657	C <sub>42</sub> H <sub>55</sub> O <sub>3</sub> NCl <sub>6</sub>	832.2375	832.2386	-1.2858
7	7,729	C <sub>46</sub> H <sub>60</sub> O <sub>3</sub> NCl <sub>7</sub>	920.2464	920.2466	-0.1359
8	8,875	C <sub>50</sub> H <sub>65</sub> O <sub>3</sub> NCl <sub>8</sub>	1008.2541	1008.2545	-0.4008

### 3.3. Conclusions

In this chapter the enzymatic synthesis of natural and artificial polyprenyl diphosphates by the *cis*-prenyltransferase from *T. kodakaraensis* was investigated. As described before<sup>[3]</sup>, the fluorescent FPP analog MANT-O-GPP constitutes an alternative starter substrate for ThkCPT which enables a highly sensitive and selective detection of the corresponding product alcohols via HPLC. In this study, ThkCPT proved to be able to convert halogenated substrates (Cl-BPP, Br-BPP) as well as the natural substrate IPP. The reaction with BPP as homoallylic substrate still remains difficult as the condensation of more than one unit occurs only to a lesser extent. However, this was the first time that more than one attachment could be shown for BPP as elongation substrate.

By using another fluorescent alternative starter substrate (MANT-O-nor FPP), which is similar to MANT-O-GPP but has one additional BPP unit, it could be shown that the substituent at the C3 position in the substrates is important for further conversion. In contrast to the conversion with BPP, long-chain products can be generated when IPP is used as elongation substrate, indicating the significance of the C3-substituent. Mutagenesis studies concerning the active site of ThkCPT did not lead to an improved substrate conversion with BPP. Thus, the conversion of BPP by ThkCPT might only be improved by mutagenesis if its precise reaction mechanism is elucidated.



The modulation of the assay conditions demonstrated that the product distribution can be influenced by the incubation time (short-chain intermediates are formed very quickly and long-chain products require more time) and the used solvent system (differing allocation in the biphasic system). It was also shown that  $Mg^{2+}$  can be substituted by other bivalent cations. With IPP, some more elongation steps were observed in small amounts, whereas with Cl-BPP as elongation substrate, only the product distribution had changed. With this knowledge, the short-chain intermediates can be accumulated and maybe used as starting materials in chemical syntheses and pharmaceutical research.

Mutagenesis studies concerning the hydrophobic tunnel that accommodates the formed polyprenyl chains revealed that one variant (Y156A) was able to generate small amounts of products containing up to 21 IPP units. In contrast, the product formation with Cl-BPP could not be improved. This shows that the extension of the hydrophobic tunnel only is not sufficient to obtain longer products with non-natural substrates. To improve the conversion of artificial substrates, the catalytic mechanism has to be elucidated in more detail. It seems likely that the halogenated substrates are accommodated in a different way compared to the natural substrate IPP and that the elongation therefore stops earlier. Another important fact is the lowered conversion rate of the halogenated substrates. Furthermore, the affinity of the formed products to the enzyme lowers, the longer they become<sup>[47, 71]</sup>, what could be another reason that the formation of long-chain (artificial) products is limited.

To the best of my knowledge this is the first time that the products formed with MANT-O-GPP and IPP or Cl-BPP were identified by high resolution mass spectrometry. One could also try to identify the products directly via LC/MS measurements. Though, the analytics have to be adapted as the used solvent system does not provide sufficient ionization of the products in the mass spectrometric analysis<sup>[3]</sup>. As highly concentrated samples can also be detected via UV-Vis, a fluorescence detector would not be necessary in this case. Then, also samples derived from conversions of the natural allylic substrate FPP could be analyzed using this methodology.

In this study it could be shown that the ThkCPT can be also cultivated in microtiter plate format as the protein production in AI medium and the cell lysis by osmotic shock are feasible. However, the enzymatic activity might be influenced by the small scale since no product formation could be detected after activity assays. Though, it could be shown that

*n*-heptane can be used as an alternative solvent for the extraction of the product alcohols (e.g. farnesol) instead of *n*-hexane.

The ThkCPT was chosen deliberately as it catalyzes the consecutive addition of homoallylic substrates onto an allylic substrate without the need for the formation of a protein complex<sup>[81, 86, 87]</sup> or for supporting proteins, e.g. rubber elongation factor<sup>[82-85]</sup>, as described before with regard to the biosynthesis of natural rubber. Moreover, the underlying mechanisms differ from one another, so that the application of such supporting proteins to the ThkCPT reaction might be expected to have no effect on the product formation. However, to produce long-chain polyprenyl diphosphates and their analogs, other enzymes might be considered in the future, e.g. CPTs from guayule (*Parthenium argentatum*) or the Russian dandelion (*Taraxacum koksaghyz*)<sup>[76, 77]</sup>. Here, the set-up of the reaction has to be adjusted as for example rubber elongation factors, CPT proteins and small rubber particle proteins are participating in natural rubber biosynthesis as well<sup>[82-85]</sup>. In future studies, the application of a vesicle system harboring the hydrophobic products could also be applicable for production of long-chain products.

## 4. *Arabidopsis thaliana* CPT

### 4.1. General information

*Arabidopsis thaliana* encodes nine *cis*-prenyltransferase genes, AtCPT1–9 (in reference to the *Arabidopsis* chromosome-based locus identifier) and one CPT-binding protein (CBP), AtLEW1<sup>[87, 138]</sup>. It has been reported that AtCPT2–7 are homologs of the bacterial *M. luteus* CPT, while AtCPT1/8/9 are more homologous to the yeast CPTs<sup>[87]</sup>. Additionally, AtCPT2–7 encode a putative chloroplast-targeting motif in their N-termini, while AtCPT1/8/9 proteins do not have such a motif. This indicates that AtCPT2–7 are likely to be independent prokaryotic type CPTs that localize to the plastids, whereas AtCPT1/8/9 are eukaryotic type CPTs that require the presence of CBP for activity, according to the CPT/CBP protein complex model elaborated for *H. brasiliensis* (section 1.4.2.2.)<sup>[87]</sup> AtCPT4 was shown to be a medium-chain CPT responsible for the formation of a C<sub>50</sub> product while AtCPT1, AtCPT3, AtCPT6, AtCPT8 and AtCPT9 are long-chain CPTs catalyzing the formation of C<sub>70-85</sub> polyisoprenoids<sup>[138]</sup>. Such polyisoprenoids serve e.g. as precursors of glycosyl carrier lipids in the biosynthesis of glycoproteins on endoplasmic reticulum<sup>[138]</sup>.

Within this work, AtCPT3 (AT2G23410, hereinafter referred to as AtCPT), which has been previously studied<sup>[4, 54]</sup>, was used. The enzyme has a molecular mass of ≈35 kDa (303 amino acids) and can be found at high levels in roots<sup>[54]</sup>. It catalyzes the formation of polyprenyl diphosphates with predominant carbon number C<sub>120</sub><sup>[4]</sup> and was therefore interesting to analyze. It might be possible that AtCPT is able to form long-chain products even with artificial substrates. Hydrophathy and transmembrane motif analyses showed that AtCPT is hydrophilic and has a N-terminal transmembrane region large enough to span the lipid bilayers<sup>[4]</sup>.

### 4.2. Results and discussion

#### 4.2.1. Truncation of AtCPT

On the basis of the fact that AtCPT contains a N-terminal transmembrane region<sup>[4]</sup>, this part was removed in its coding gene via PCR (section 2.3.6.3.) with the aim to facilitate protein purification. The primers (Table 7, section 2.1.7.) were chosen according to the appropriate UniProt entry (<http://www.uniprot.org/uniprot/O80458>). The obtained fragment from PCR

was then ligated into the pET20b(+) vector (section 2.3.6.3). The truncated AtCPT is designated as AtCPT\_Δ33. The N-terminal transmembrane region was successfully removed as shown by sequencing (Figure A1 in the appendix, section 7.2.).

#### **4.2.2. Production and purification of recombinant AtCPT protein**

For the production of AtCPT, *E. coli* BL21 (DE3) cells harboring both the plasmids for expression of full-length AtCPT and GroESL (heat shock protein family HSP60) were used. As a chaperonin, GroESL facilitates protein folding<sup>[93, 139-141]</sup>. Recombinant expression was then carried out as described in section 2.4.1. The expression vector pET20b(+) confers resistance to ampicillin and the vector pTG10 confers resistance to chloramphenicol. Both possess a T7 expression cassette which enables an IPTG-induced protein production. For protein purification two different strategies were developed (see below).

##### **4.2.2.1. Preparation of periplasmic extracts**

As the recombinant AtCPT produced by expression of pET20b(+)-AtCPT contains a *pelB* signal sequence (Figure A1, appendix section 7.2.) the protein is assumed to be transported into the periplasm of *E. coli* cells<sup>[102]</sup>. Therefore, a periplasmic preparation was carried out after recombinant protein production (sections 2.4.1. and 2.4.5.). The cell lysis steps were controlled by SDS-PAGE (section 2.4.10.) as shown in figure 33. As the *pelB* signal sequence should be removed by a signal peptidase when the protein is directed to the periplasm<sup>[102]</sup> it is assumed that the recombinant protein has a molecular weight of approximately 37 kDa (indicated by arrows in figure 33). The induction of protein biosynthesis is clearly visible (lane 2). The TSE supernatant does not seem to contain the protein of interest as there is no protein band visible at the expected size (lane 3). In contrast, the H<sub>2</sub>O supernatant shows traces of AtCPT (lane 4). Most of the enzyme is still left in the insoluble fraction (remaining cell pellet) which indicates that a periplasmic preparation is not sufficient (lane 5). The residual lysate (soluble fraction) contains a lot of host proteins (not shown).

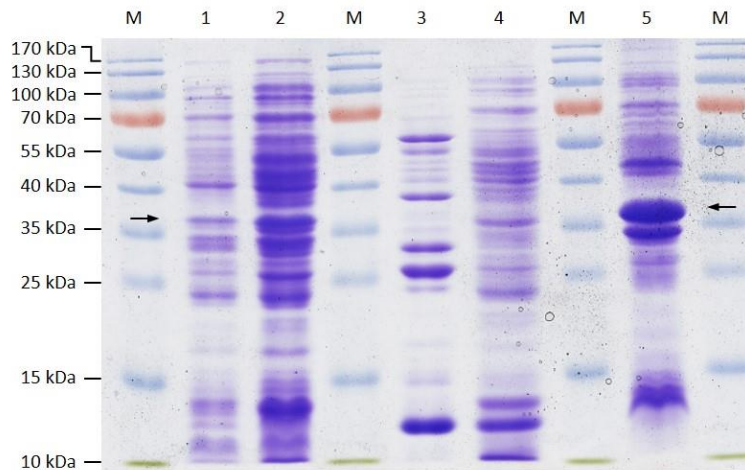


**Figure 33** SDS-PAGE gel with Coomassie staining of the periplasmic preparation steps for enrichment of AtCPT. The AtCPT band is marked with arrows. M: PageRuler™ prestained protein ladder, 1: before IPTG induction, 2: after IPTG induction, 3: TSE supernatant, 4: H<sub>2</sub>O supernatant, 5: insoluble protein fraction (cell pellet after lysis).

#### 4.2.2.2. Cell lysis by ultrasonic treatment and purification of full-length and truncated AtCPT via IMAC

As the periplasmic preparation does not yield sufficient amounts of full-length AtCPT and a large part of the protein is still left in the insoluble fraction, lysis of the cell pellet by ultrasonic treatment was carried out after recombinant protein biosynthesis (sections 2.4.1. and 2.4.2.). Afterwards, the protein was purified via Ni<sup>2+</sup>-mediated IMAC (section 2.4.4.). With regard to further analyses of the protein bands (section 2.5.6.), dialysis (section 2.4.7.) with subsequent concentration of the protein sample (section 2.4.8.) were carried out. The purification steps were checked by SDS-PAGE (section 2.4.10.) as shown in figure 34. The induction of protein biosynthesis can be seen in lane 2. Some of the enzyme remains in the insoluble fraction (lane 3) but the larger part can be found in the soluble fraction (lane 4). During IMAC purification, a certain part of protein did not bind to the column material (lane 5). As the AtCPT binds via its His<sub>6</sub> tag to the Ni-NTA matrix, unbound proteins, e.g. from the expression host, could be washed out (lane 6). Afterwards, the protein of interest was eluted by imidazole containing buffer (lane 7). Buffer exchange and desalting was carried out via SEC (lane 8). Then, the protein sample was dialyzed and concentrated (lane 9). However, the yield of protein was quite low (1.6 mg per liter of liquid culture containing 7% AtCPT, see section 4.2.3.).

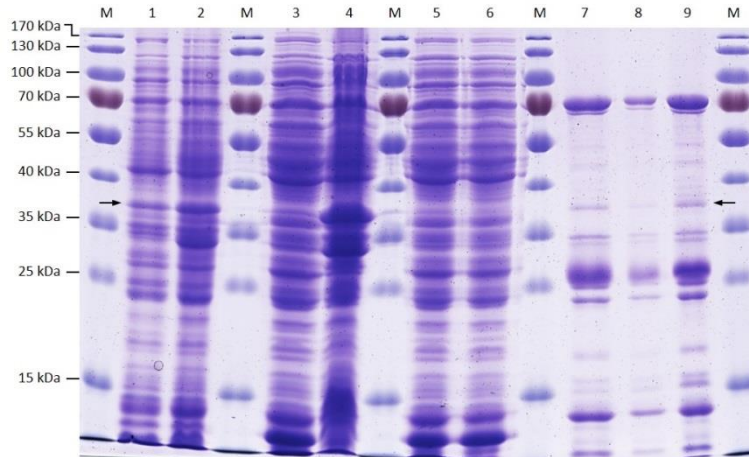


**Figure 34** SDS-PAGE gel with Coomassie staining of the purification steps of AtCPT. The AtCPT band is marked with arrows. M: PageRuler™ prestained protein ladder, 1: before IPTG induction, 2: after IPTG induction, 3: insoluble protein fraction, 4: soluble protein fraction, 5: column flow-through, 6: wash fraction (unbound proteins), 7: eluted protein fraction, 8: desalted protein fraction, 9: protein fraction after dialysis and concentration.

The truncated version AtCPT\_Δ33 was expressed and purified similar to the full-length protein as described above. The purification steps were controlled by SDS-PAGE (section 2.4.10.). AtCPT\_Δ33 has a molecular weight of approximately 33 kDa (including the His<sub>6</sub> tag and excluding the *pelB* signal sequence). Unfortunately, no appropriate protein could be detected after the procedure as seen in lane 8 in figure 35. It is conspicuous that there appears a dominant protein band at a molecular weight of approximately 37 kDa (lanes 2 and 3) which would correspond to the full-length AtCPT. Additionally, another protein band can be seen at a molecular weight of 35 kDa (lanes 2 and 3). This would correspond to AtCPT\_Δ33 with the *pelB* signal sequence still attached to the protein. Maybe the truncated version misfolds what could impede the transport to the periplasm of *E. coli* cells. This in turn would imply that the signal sequence could not be removed by a signal peptidase. However, the protein remains in the insoluble fraction (lane 3) and it was not possible to obtain purified AtCPT\_Δ33. It seems like the formation of inclusion bodies is dominating under these conditions. It is also possible that the truncated version cannot be synthesized as functional protein.

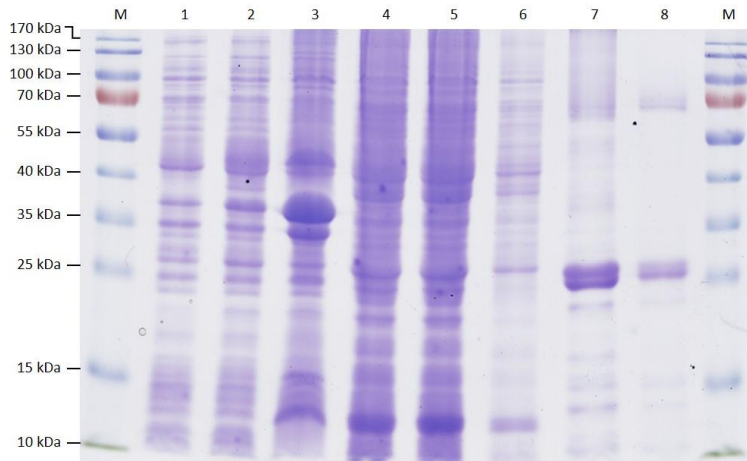


**Figure 35** SDS-PAGE gel with Coomassie staining of the purification steps of AtCPT\_Δ33. M: PageRuler™ prestained protein ladder, 1: before IPTG induction, 2: after IPTG induction, 3: insoluble protein fraction, 4: soluble protein fraction, 5: column flow-through, 6: wash fraction (unbound proteins), 7: eluted protein fraction, 8: desalted protein fraction.

#### 4.2.3. Analysis of AtCPT peptide fragments

As the desalted protein fraction of full-length AtCPT still contains host proteins (Figure 34) the identity of the predominant bands was determined. After dialysis and concentration of the protein sample (sections 2.4.7. and 2.4.8.), it was separated via SDS-PAGE (section 2.4.10.). Four gel bands were chosen and cut out (Figure 36). Additionally, the percentage of full-length AtCPT in the protein solution (after the purification steps) was determined. The samples were evaluated in cooperation with Petra Majovsky and Dr. Wolfgang Hoehenwarter at the IPB Halle. After in-solution and in-gel digestion (sections 2.4.11. and 2.4.12.) with trypsin, the purified and desalted peptides (section 2.4.13.) were analyzed by LC-ESI-MS (section 2.5.6.).

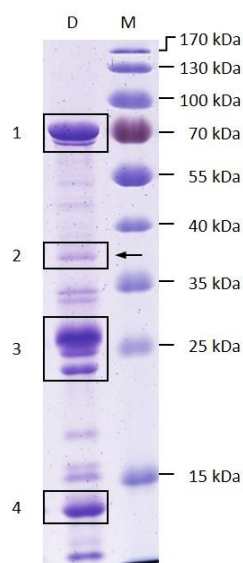


**Figure 36** SDS-PAGE gel with Coomassie staining of the enriched AtCPT fraction. The AtCPT band is marked with an arrow. Cut out protein bands are framed and designated by numbers (1 to 4). D: protein fraction after dialysis and concentration, M: PageRuler™ prestained protein ladder.

It could be shown that AtCPT is the most abundant fraction in gel band 2 (Table A5 in the appendix, section 7.4.). The other three chosen gel bands contain primarily proteins from the expression host *E. coli* (most abundant protein in band 1: bifunctional polymyxin resistance protein ArnA, 3: cAMP-activated global transcriptional regulator CRP, 4: RNA-binding protein Hfq). In solution, AtCPT constitutes only 7 % of total protein in the sample (Table A5 in the appendix, section 7.4.).

#### 4.2.4. Substrate conversion with full-length AtCPT

It is known from literature that AtCPT is able to form polyprenyl diphosphates with a predominant chain length of 120 carbon atoms. In the corresponding study, the product chain length was determined by using FPP and [ $^{14}\text{C}$ ]IPP as elongation substrate. The enzyme exhibits a high affinity for FPP ( $K_m = 0.13 \mu\text{M}$ ) whereas it shows a lower affinity for IPP ( $K_m = 23 \mu\text{M}$ ).<sup>[4]</sup>

Activity assays performed in this thesis were performed with the fractions obtained from the periplasmic preparation (sections 2.4.5. and 4.2.2.1.) which were used for the conversion of FPP and IPP for a first screening for enzymatic activity. These samples were then analyzed by thin layer chromatography (TLC, section 2.5.2.). It has already been described that some CPTs accept artificial starter substrates, e.g. the fluorescent MANT-O-GPP<sup>[3, 112]</sup>. Therefore, additional activity assays were carried out with this alternative allylic substrate, IPP as elongation substrate and “purified” AtCPT as the detection of the labeled products by HPLC is highly sensitive (sections 2.5.1. and 2.5.3.1.). It could be shown that the enzyme is able to convert the artificial starter substrate. Due to the low amount of enriched AtCPT preparations the  $K_m$  value for MANT-O-GPP could not be determined.

##### *i) Conversion of FPP*

The products formed during the conversion of FPP and IPP with the fractions obtained from the periplasmic preparation (sections 2.4.5. and 4.2.2.1.) were analyzed by TLC (section 2.5.2.). The reaction is shown in figure 37. Farnesol ( $\text{C}_{15}\text{H}_{26}\text{O}$ ) and solanesol ( $\text{C}_{45}\text{H}_{74}\text{O}$ ) were used as standards.

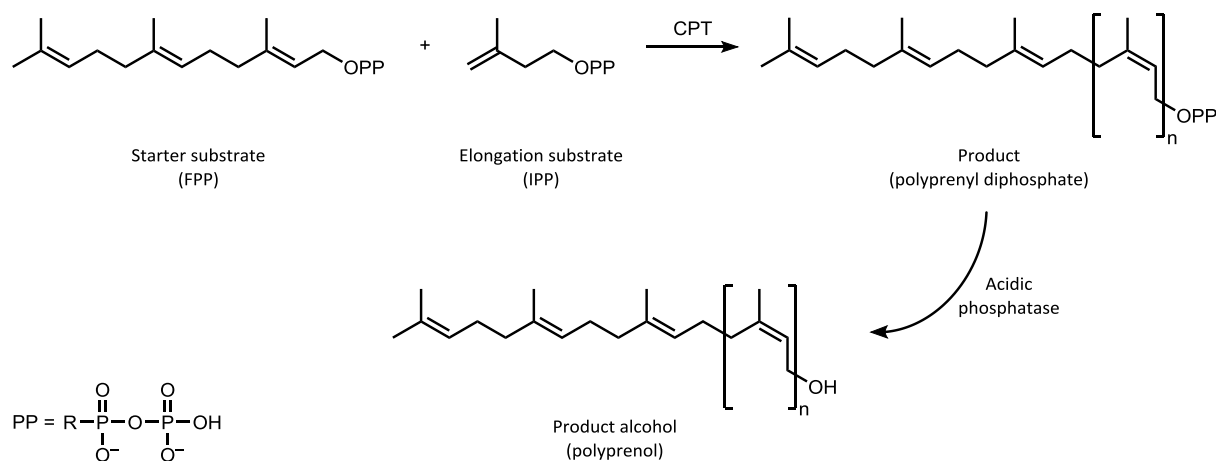


**Figure 37** Reaction scheme of the enzymatic conversion of FPP and IPP, leading to polyprenols with distinct chain lengths.



The activity assay with the TSE and the H<sub>2</sub>O supernatants did not yield any elongated products (Figure 38, lanes 1 to 4). In contrast, in the activity assay with the soluble protein fraction products with a chain length comparable to solanesol (C<sub>45</sub>, C<sub>50</sub>) were formed (lanes 5 and 6). The products formed by the insoluble protein fraction exhibit a chain length of 45 carbon atoms (lanes 7 and 8). As crude extracts were used for the conversion of FPP and IPP, the CPT activity cannot be clearly assigned to AtCPT. It is also possible that the substrates were converted by remaining expression host proteins as the fractions were not purified. Therefore, an activity assay should be carried out in subsequent studies after purified enzyme is obtained with an optimized purification protocol to confirm the results of the assays shown above.

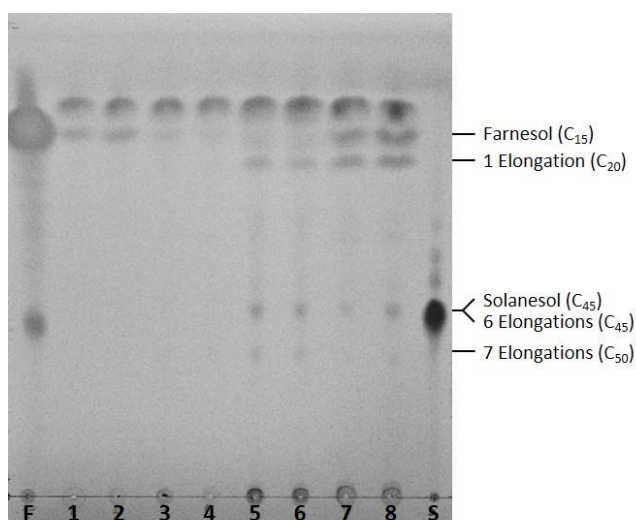


**Figure 38** TLC analysis of the products formed by AtCPT with FPP and IPP as substrates. Reactions were performed at 30°C reaction temperature followed by diphosphate hydrolysis. Stationary phase: RP-18, solvent system: acetone/H<sub>2</sub>O (19:1, v/v), detection agent: iodine fume. F: farnesol, S: solanesol, 1 + 2: assay with the TSE supernatant, 3 + 4: assay with the H<sub>2</sub>O supernatant, 5 + 6: assay with the soluble protein fraction (lysate), 7 + 8: assay with the insoluble protein fraction (cell pellet resuspended in assay buffer).

### ii) Conversion of MANT-O-GPP

The products formed during the conversion of MANT-O-GPP and IPP (see Figure 14, section 3.2.4.2.) by “purified” full-length AtCPT were analyzed by fluorescence-based HPLC (section 2.5.3.1.). As the amount of product was very low, a concentrated sample was applied in the measurements instead of the conventionally used diluted samples (1:3). The enzyme accepts the fluorescent starter substrate and is able to catalyze the elongation with IPP (Figure 39).

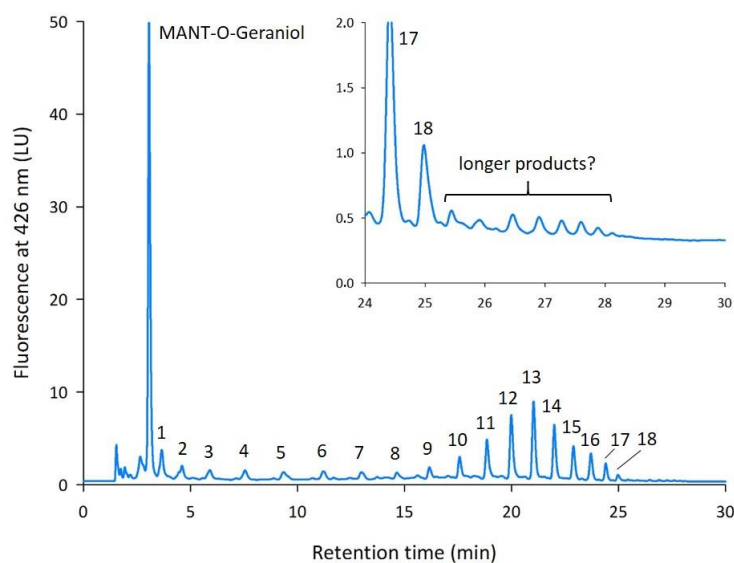


**Figure 39** HPLC chromatogram of the products of an AtCPT reaction with MANT-O-GPP and IPP. Reactions were performed at 30°C reaction temperature followed by diphosphate hydrolysis. After excitation at 359 nm the emission was measured at 426 nm via fluorescence. LU: luminescence units. Numbers indicate the catalyzed elongation steps.

In these reactions, IPP is attached to MANT-O-GPP up to 18 times which corresponds to the formation of a  $C_{105}$  product analog. In the inset in figure 39 it can also be seen that there were additional small peaks detected which may represent even more IPP attachments. The product formed by 13 elongations can be observed as the main product ( $C_{80}$  product analog). In contrast to the obtained product chain length described in literature ( $C_{120}$ )<sup>[4]</sup>, the products observed here exhibit a slightly shorter chain length. Possibly, the used HPLC method has to be modified to detect also the very long-chain products. On the other hand, the AtCPT could only be obtained in low amounts.

### 4.3. Conclusions

The plant *cis*-prenyltransferase from *A. thaliana* was tested for the production of long-chain polyprenyl diphosphates. However, expression and purification have proven to be difficult as the amount of obtained purified enzyme was very low. The application of a *pelB* signal sequence and subsequent periplasmic preparation did not lead to enrichment of the recombinant enzyme. As AtCPT contains a N-terminal transmembrane region<sup>[4]</sup>, a truncated version of the enzyme was prepared (AtCPT\_Δ33). Unfortunately, the purification of this variant was not feasible as the protein remains in the insoluble fraction. In the future, one could also try to process the formed inclusion bodies to obtain soluble protein. However, expression of recombinant full-length AtCPT was successful and cell lysis by ultrasonic followed by purification via IMAC yielded fractions of enriched AtCPT protein. Even though a major part of the enzyme was detected in the soluble protein fraction the yield of purified

AtCPT was quite low. The purified sample still contains impurities from host proteins but it could be shown by analysis of AtCPT peptide fragments via LC-ESI-MS that the corresponding protein band in the gel after SDS-PAGE represents mainly AtCPT. The obtained protein fraction was then used for substrate conversion. The enzyme accepts the fluorescent starter substrate MANT-O-GPP and is able to catalyze the condensation of IPP up to 18 times ( $C_{105}$  product analog) whereby the  $C_{80}$  product analog constitutes the main product. The products exhibit slightly shorter chain lengths than described in literature ( $C_{120}$ )<sup>[4]</sup>. In addition, within this work a new detection method was successfully applied to the products formed by AtCPT.

To fully understand how substrate binding and catalytic activity are achieved by CPT enzymes further investigations have to be carried out. It is already known that the used *cis*-prenyltransferase from *A. thaliana* is homologous to the bacterial *M. luteus* CPT<sup>[87]</sup>. Its amino acid sequence is also highly homologous to several conserved regions in CPTs from *E. coli*, *M. luteus* and yeast<sup>[4]</sup>, suggesting a common catalytic mechanism for chain elongation.

As described before, the used AtCPT is likely to be independent prokaryotic type CPT that does not require the presence of CBP for activity, according to the CPT/CBP protein complex model elaborated for *H. brasiliensis* (section 1.4.2.2.).<sup>[87]</sup> As also discussed for the ThkCPT (section 3.3.), the AtCPT used here was chosen because of this independence from additional factors. For the production of long-chain polyprenyl diphosphates these parameters have to be taken into account.

If it becomes possible to obtain a higher amount of purified enzyme by an optimized method for expression and purification, this enzyme can be used for further experiments with artificial substrates to elucidate if the AtCPT is able to form longer product analogs compared to the ThkCPT.

## 5. Summary

This work comprises the analysis of a medium-chain (*Thermococcus kodakaraensis*, ThkCPT) as well as a long-chain (*Arabidopsis thaliana*, AtCPT) *cis*-prenyltransferase. For a highly sensitive and selective detection of the enzymatically formed products via HPLC, a fluorescent analog of the native substrate FPP (MANT-O-GPP) was used, which is effectively converted by both CPTs.

The thermophilic ThkCPT is able to condense this labeled allylic substrate and the homoallylic native substrate IPP as well as the artificial substrates BPP, Cl-BPP and Br-BPP. IPP is attached up to 13 times to MANT-O-GPP. The halogenated homoallylic substrates Cl-BPP and Br-BPP were condensed up to 8 times each to the fluorescent starter substrate. Such generation of artificial polymers would be attractive for industrial application as several synthetic rubbers contain structurally modified polyisoprenes, e.g. polychloroprene<sup>[119]</sup>.

With BPP as elongation substrate it could be shown in this work that ThkCPT is able to catalyze up to 3 attachments. This is the first time that more than one attachment could be shown for BPP. However, the less voluminous substituent at its C3 position seems to be responsible for the restricted substrate conversion. This was analyzed by using the alternative fluorescent starter substrate MANT-O-nor FPP that was only elongated once in the reaction with BPP. In contrast, long-chain products are formed when IPP is used as second substrate. Until now, such an elongation of an allylic substrate lacking the methyl group at the C3 position has not been reported yet<sup>[115, 133]</sup>. The conversion of BPP could neither be enhanced by mutagenesis studies concerning the active site of ThkCPT.

In contrast, mutagenesis studies concerning positions in the hydrophobic tunnel resulted in a new variant (Y156A) that is able to catalyze up to 21 elongations with IPP. However, the product formation with Cl-BPP could not be altered. This demonstrates that not only the topology of the hydrophobic tunnel is important for product formation. Thus, the conversion of artificial substrates might only be improved if the precise reaction mechanism of CPTs is elucidated.

To regulate the product formation of ThkCPT the influence of the assay conditions was investigated by variation of the incubation time, the solvent system or the bivalent cation involved in the catalytic cycle. It could be demonstrated that the incubation time and the application of a biphasic system influence the product distribution in the reaction with IPP

and Cl-BPP. Furthermore, it was shown that  $Mg^{2+}$  can be substituted by other bivalent cations, e.g.  $Mn^{2+}$ ,  $Co^{2+}$ ,  $Ni^{2+}$ ,  $Cu^{2+}$  or  $Zn^{2+}$ . In the reaction with IPP a changed product distribution and some more attachments to MANT-O-GPP were observed. In contrast, the bivalent cation seems to have a stronger impact on the product formation with Cl-BPP as rather short-chain products were formed and a changed product distribution was observed. Due to a lower turnover rate of artificial substrates, a longer incubation time is necessary in the conversion of Cl-BPP. With these findings it is possible to accumulate the short-chain intermediates that might be used as starting materials in pharmaceutical research and chemical syntheses.

In the presented work the products formed with MANT-O-GPP and IPP or Cl-BPP by ThkCPT were identified by high resolution mass spectrometry. In the future, also products derived from conversions of the native substrate FPP could be analyzed with the developed technique, especially since it proved to be applicable to HPLC-based product fractionation of highly concentrated samples coupled to UV-Vis detection.

It could be shown in this study that cells expressing ThkCPT can be also cultivated in microtiter plate format, followed by protein production in AI medium and the cell lysis by osmotic shock. However, the lower volume of culture seems to influence the enzymatic activity since no product formation could be detected after activity assays. Though, it was demonstrated that *n*-hexane can be replaced by *n*-heptane for the extraction of the product alcohols.

The expression and purification of the plant *cis*-prenyltransferase from *A. thaliana* have proven to be difficult as the amount of obtained enzyme preparation was very low. Nevertheless, analysis of peptide fragments via LC-ESI-MS confirmed that the corresponding protein band consists mainly of AtCPT. In activity assays the AtCPT catalyzed the attachment of up to 18 IPP units to MANT-O-GPP. The products exhibit slightly shorter chain lengths than described in literature (120 carbon atoms)<sup>[4]</sup>. Furthermore, within this work another detection method was successfully applied to the products formed by AtCPT.

## 6. Zusammenfassung

Diese Arbeit umfasst die Untersuchung einer mittelketten (*Thermococcus kodakaraensis*, ThkCPT) und einer langketten (*Arabidopsis thaliana*, ThkCPT) *cis*-Prenyltransferase. Um eine hochempfindliche und selektive Detektion der enzymatisch gebildeten Produkte durch HPLC zu ermöglichen, wurde ein fluoreszierendes Analog des natürlichen Startersubstrates FPP (MANT-O-GPP) verwendet, welches effektiv von beiden CPTs umgesetzt wird.

Die thermophile ThkCPT ist in der Lage, die Kondensation dieses fluoreszenzmarkierten allylischen Substrates und des homoallylischen natürlichen Substrates IPP sowie der artifiziellen IPP-Analoga BPP, Cl-BPP und Br-BPP zu katalysieren. Dabei wird MANT-O-GPP um bis zu 13 IPP-Einheiten bzw. um bis zu jeweils 8 Einheiten der halogenierten homoallylischen Substrate Cl-BPP und Br-BPP verlängert. Eine solche Generierung artifizieller Polymere wäre für industrielle Anwendungen von Interesse, da einige Synthesekautschuke, wie z. B. Polychloropren, strukturell modifizierte Polyisoprene enthalten<sup>[119]</sup>.

In dieser Arbeit konnte gezeigt werden, dass die ThkCPT fähig ist, die Verlängerung des Startersubstrates MANT-O-GPP um bis zu 3 BPP-Einheiten zu katalysieren. Dies ist das erste Mal, dass mehr als eine Verlängerung mit BPP als Elongationssubstrat gezeigt werden konnte. Der weniger voluminöse Substituent an dessen C3-Position scheint für den begrenzten Substratumsatz verantwortlich zu sein. Dies wurde durch die Verwendung eines alternativen fluoreszierenden Startersubstrates (MANT-O-nor FPP) untersucht, welches nur um eine weitere BPP-Einheit verlängert wurde. Im Gegensatz dazu konnte bei der Verwendung von IPP als Elongationssubstrat die Bildung langkettiger Produkte beobachtet werden. Über eine solche Verlängerung eines allylischen Substrates, welches an der C3-Position keine Methylgruppe aufweist, wurde bislang noch nicht berichtet<sup>[115, 133]</sup>. Der Umsatz von BPP konnte auch nicht durch Mutagenese-Studien bezüglich des aktiven Zentrums der ThkCPT gesteigert werden.

Im Gegensatz dazu führten Mutagenese-Studien hinsichtlich des hydrophoben Tunnels des Enzyms zu einer neuen Variante (Y156A), die in der Lage ist, bis zu 21 Verlängerungen mit IPP als Elongationssubstrat zu katalysieren. Jedoch konnte die Produktbildung mit Cl-BPP nicht verbessert werden. Dies zeigt, dass nicht nur die Beschaffenheit des hydrophoben Tunnels für die Produktbildung von Bedeutung ist. Somit kann der Umsatz artifizieller

Substrate möglicherweise nur optimiert werden, wenn der präzise Reaktionsmechanismus von CPTs aufgeklärt wird.

Um die Produktbildung der ThkCPT zu regulieren, wurde der Einfluss der Assay-Bedingungen analysiert. Hierfür wurde die Inkubationszeit variiert, das verwendete Lösungsmittelsystem abgewandelt oder das bivalente Kation, welches in die Katalyse involviert ist, substituiert. Es konnte nachgewiesen werden, dass die Inkubationszeit und die Verwendung eines Zweiphasen-Systems die Produktverteilung bei der Reaktion mit IPP bzw. Cl-BPP beeinflussen. Weiterhin wurde gezeigt, dass  $Mg^{2+}$  durch andere bivalente Kationen, wie z. B.  $Mn^{2+}$ ,  $Co^{2+}$ ,  $Ni^{2+}$ ,  $Cu^{2+}$  oder  $Zn^{2+}$  substituiert werden kann. Bei der Reaktion mit IPP wurden eine veränderte Produktverteilung sowie einige weitere Anlagerungen an MANT-O-GPP beobachtet. Demgegenüber scheint ein alternatives bivalentes Kation eine stärkere Auswirkung auf die Produktbildung mit Cl-BPP als Elongationssubstrat zu haben. Hier wurden vermehrt kurzkettige Produkte und eine veränderte Produktverteilung erfasst. Aufgrund der geringeren Umsatzgeschwindigkeit artifizierlicher Substrate ist zudem bei der Reaktion mit Cl-BPP eine längere Inkubationszeit notwendig. Anhand dieser Erkenntnisse ist es möglich, kurzkettige Intermediate zu akkumulieren, welche möglicherweise als Ausgangsmaterialien in der pharmazeutischen Forschung oder der chemischen Synthese genutzt werden können.

In der vorgestellten Arbeit wurden die aus MANT-O-GPP und IPP bzw. Cl-BPP gebildeten Produkte der ThkCPT durch hochauflösende Massenspektrometrie identifiziert. Zukünftig könnten auch Produkte, die durch den Einsatz des natürlichen Substrates FPP gebildet werden, mithilfe der entwickelten Methode analysiert werden. Insbesondere da sich die HPLC-basierte Produktfraktionierung von hochkonzentrierten Proben kombiniert mit der Detektion via UV-Vis als geeignet erwiesen hat.

In dieser Studie konnte weiterhin gezeigt werden, dass Zellen, die ThkCPT exprimieren, auch in Mikrotiterplatten kultiviert werden können, gefolgt von der Proteinproduktion in AI-Medium und Zellaufschluss durch osmotischen Schock. Allerdings scheint das geringere Kulturvolumen die enzymatische Aktivität zu beeinflussen, da nach der Durchführung von Aktivitätstests keine Produktbildung detektiert werden konnte. Jedoch konnte gezeigt werden, dass *n*-Hexan durch *n*-Heptan bei der Extraktion der gebildeten Produktalkohole ersetzt werden kann.

Die Expression und Reinigung der pflanzlichen *cis*-Prenyltransferase aus *A. thaliana* erwiesen sich als problematisch, die Menge an erhaltenem Enzym war sehr gering. Dennoch bestätigten LC-ESI-MS-Analysen der Peptidfragmente, dass die entsprechende Protein-Bande im Gel nach der SDS-PAGE hauptsächlich AtCPT aufweist. In Aktivitätstests katalysierte die AtCPT die Anlagerung von bis zu 18 IPP-Einheiten an MANT-O-GPP. Die Produkte wiesen geringfügig kürzere Kettenlängen auf als in der Literatur beschrieben ( $C_{120}$ )<sup>[4]</sup>. Darüber hinaus wurde im Rahmen dieser Arbeit eine weitere Detektionsmethode erfolgreich für die Produkte der AtCPT angewandt.



## 7. List of References

- [1] Wessjohann, L. A., Keim, J., Weigel, B. and Dippe, M. (2013) Alkylating enzymes, *Curr Opin Chem Biol*, **17** (2): 229-235.
- [2] Takahashi, S. and Koyama, T. (2006) Structure and function of *cis*-prenyl chain elongating enzymes, *Chem Rec*, **6** (4): 194-205.
- [3] Keim, J. (2014) Biokatalytische Umsetzung von natürlichen und artifiziellen Prenyldiphosphaten (Dissertation), *Martin-Luther-Universität Halle-Wittenberg*, Halle.
- [4] Oh, S. K., Han, K. H., Ryu, S. B. and Kang, H. (2000) Molecular cloning, expression, and functional analysis of a *cis*-prenyltransferase from *Arabidopsis thaliana*. Implications in rubber biosynthesis, *J Biol Chem*, **275** (24): 18482-18488.
- [5] Brandt, W., Brauer, L., Gunnewich, N., Kufka, J., Rausch, F., Schulze, D., Schulze, E., Weber, R., Zakharova, S. and Wessjohann, L. (2009) Molecular and structural basis of metabolic diversity mediated by prenyldiphosphate converting enzymes, *Phytochemistry*, **70** (15-16): 1758-1775.
- [6] Croteau, R., Kutchan, T. M. and Lewis, N. G. (2000) Natural products (secondary metabolites), in: Buchanan, B., Gruissem, W. and Jones, R. (Eds.) *Biochemistry & Molecular Biology of Plants*, Chapter 24: 1250-1318, *American Society of Plant Physiologists*, Maryland (USA).
- [7] Bloch, K. (1992) Sterol molecule: structure, biosynthesis, and function, *Steroids*, **57** (8): 378-383.
- [8] McGarvey, D. J. and Croteau, R. (1995) Terpenoid metabolism, *The Plant Cell*, **7** (7): 1015-1026.
- [9] Rohmer, M. (1999) The discovery of a mevalonate-independent pathway for isoprenoid biosynthesis in bacteria, algae and higher plants, *Nat Prod Rep*, **16** (5): 565-574.
- [10] Skorupinska-Tudek, K., Poznanski, J., Wojcik, J., Bienkowski, T., Szostkiewicz, I., Zelman-Femiak, M., Bajda, A., Chojnacki, T., Olszowska, O., Grunler, J., Meyer, O., Rohmer, M., Danikiewicz, W. and Swiezewska, E. (2008) Contribution of the mevalonate and methylerythritol phosphate pathways to the biosynthesis of dolichols in plants, *J Biol Chem*, **283** (30): 21024-21035.

- [11] Joyard, J., Ferro, M., Masselon, C., Seigneurin-Berny, D., Salvi, D., Garin, J. and Rolland, N. (2009) Chloroplast proteomics and the compartmentation of plastidial isoprenoid biosynthetic pathways, *Mol Plant*, **2** (6): 1154-1180.
- [12] Bloch, K. (1965) The biological synthesis of cholesterol, *Science*, **150** (3692): 19-28.
- [13] Katsuki, H. and Bloch, K. (1967) Studies on the biosynthesis of ergosterol in yeast, *J Biol Chem*, **242** (2): 222-227.
- [14] Lynen, F. (1967) Biosynthetic pathways from acetate to natural products, *Pure Appl Chem*, **14** (1): 137-168.
- [15] Miziorko, H. M. (2011) Enzymes of the mevalonate pathway of isoprenoid biosynthesis, *Arch Biochem Biophys*, **505** (2): 131-143.
- [16] Rohmer, M., Knani, M., Simonin, P., Sutter, B. and Sahm, H. (1993) Isoprenoid biosynthesis in bacteria: a novel pathway for the early steps leading to isopentenyl diphosphate, *Biochem J*, **295**: 517-524.
- [17] Rohmer, M., Seemann, M., Horbach, S., Bringer-Meyer, S. and Sahm, H. (1996) Glyceraldehyde 3-phosphate and pyruvate as precursors of isoprenic units in an alternative non-mevalonate pathway for terpenoid biosynthesis, *J Am Chem Soc*, **118** (11): 2564-2566.
- [18] Jomaa, H., Wiesner, J., Sanderbrand, S., Altincicek, B., Weidemeyer, C., Hintz, M., Türbachova, I., Eberl, M., Zeidler, J., Lichtenthaler, H. K., Soldati, D. and Beck, E. (1999) Inhibitors of the nonmevalonate pathway of isoprenoid biosynthesis as antimalarial drugs, *Science*, **285** (5433): 1573-1576.
- [19] Grawert, T., Groll, M., Rohdich, F., Bacher, A. and Eisenreich, W. (2011) Biochemistry of the non-mevalonate isoprenoid pathway, *Cell Mol Life Sci*, **68** (23): 3797-3814.
- [20] Hale, I., O'Neill, P. M., Berry, N. G., Odom, A. and Sharma, R. (2012) The MEP pathway and the development of inhibitors as potential anti-infective agents, *MedChemComm*, **3** (4): 418-433.
- [21] Perez-Gil, J. and Rodriguez-Concepcion, M. (2013) Metabolic plasticity for isoprenoid biosynthesis in bacteria, *Biochem J*, **452** (1): 19-25.
- [22] Gao, Y., Honzatko, R. B. and Peters, R. J. (2012) Terpenoid synthase structures: a so far incomplete view of complex catalysis, *Nat Prod Rep*, **29** (10): 1153-1175.

- [23] Kumari, S., Priya, P., Misra, G. and Yadav, G. (2013) Structural and biochemical perspectives in plant isoprenoid biosynthesis, *Phytochem Rev*, **12** (2): 255-291.
- [24] Roberts, S. C. (2007) Production and engineering of terpenoids in plant cell culture, *Nat Chem Biol*, **3** (7): 387-395.
- [25] Eisenreich, W., Bacher, A., Arigoni, D. and Rohdich, F. (2004) Biosynthesis of isoprenoids via the non-mevalonate pathway, *Cell Mol Life Sci*, **61** (12): 1401-1426.
- [26] Gershenzon, J. and Dudareva, N. (2007) The function of terpene natural products in the natural world, *Nat Chem Biol*, **3** (7): 408-414.
- [27] Pybus, D. H. and Sell, C. S. (1999) The chemistry of fragrances, *Royal Society of Chemistry*, Cambridge (UK).
- [28] Cragg, G. M. and Newman, D. J. (2005) Plants as a source of anti-cancer agents, *J Ethnopharmacol*, **100** (1-2): 72-79.
- [29] Srivastava, V., Negi, A. S., Kumar, J. K., Gupta, M. M. and Khanuja, S. P. (2005) Plant-based anticancer molecules: a chemical and biological profile of some important leads, *Bioorg Med Chem*, **13** (21): 5892-908.
- [30] Klayman, D. L. (1985) Qinghaosu (artemisinin): an antimalarial drug from China, *Science*, **228** (4703): 1049-1055.
- [31] Wani, M. C., Taylor, H. L., Wall, M. E., Coggon, P. and McPhail, A. T. (1971) Plant antitumor agents. VI. The isolation and structure of taxol, a novel antileukemic and antitumor agent from *Taxus brevifolia*, *J Am Chem Soc*, **93** (9): 2325-2327.
- [32] Miele, M., Mumot, A. M., Zappa, A., Romano, P. and Ottaggio, L. (2012) Hazel and other sources of paclitaxel and related compounds, *Phytochem Rev*, **11** (2-3): 211-225.
- [33] Liu, C., Zhao, Y. and Wang, Y. (2006) Artemisinin: current state and perspectives for biotechnological production of an antimalarial drug, *Appl Microbiol Biotechnol*, **72** (1): 11-20.
- [34] Wang, K. C. and Ohnuma, S. (2000) Isoprenyl diphosphate synthases, *BBA-Mol Cell Biol L*, **1529** (1-3): 33-48.

- [35] Steinbüchel, A. (2003) Production of rubber-like polymers by microorganisms, *Curr Opin Microbiol*, **6** (3): 261-270.
- [36] International Rubber Study Group, Rubber statistical bulletin, April-June 2017 edition, <http://www.rubberstudy.com/statistics.aspx> (lastly opened on 2017-07-18).
- [37] Puskas, J. E., Gautriaud, E., Deffieux, A. and Kennedy, J. P. (2006) Natural rubber biosynthesis - A living carbocationic polymerization?, *Progress in Polymer Science*, **31** (6): 533-548.
- [38] Röthemeyer, F. and Sommer, F. (2013) Kautschuktechnologie: Werkstoff-Verarbeitung-Produkte, 3. Auflage, 54-60, *Carl Hanser Verlag GmbH Co KG*, München.
- [39] Tanaka, Y. and Sakdapipanich, J. T. (2001) Chemical structure and occurrence of natural polyisoprenes, in: Koyama, T. and Steinbüchel, A. (Eds.) Biopolymers, Volume 2: Polyisoprenoids, Chapter 1: 2-21, *Wiley-VCH*, Weinheim.
- [40] van Beilen, J. B. and Poirier, Y. (2007) Establishment of new crops for the production of natural rubber, *Trends Biotechnol*, **25** (11): 522-529.
- [41] Bushman, B. S., Scholte, A. A., Cornish, K., Scott, D. J., Brichta, J. L., Vederas, J. C., Ochoa, O., Michelmore, R. W., Shintani, D. K. and Knapp, S. J. (2006) Identification and comparison of natural rubber from two *Lactuca* species, *Phytochemistry*, **67** (23): 2590-2596.
- [42] da Costa, B. M., Keasling, J. D., McMahan, C. M. and Cornish, K. (2006) Magnesium ion regulation of in vitro rubber biosynthesis by *Parthenium argentatum* Gray, *Phytochemistry*, **67** (15): 1621-1628.
- [43] Park, C. R. (1925) Studies of the physical properties of balata and rubber, *J Ind Eng Chem*, **17** (2): 152-160.
- [44] Hammond, D. S. (2005) Tropical forests of the guiana shield: ancient forests in a modern world, *CABI*, Wallingford (UK).
- [45] Prakash, R., Gopikrishna, V. and Kandaswamy, D. (2005) Gutta-percha - an untold story, *Endodontology*, **17** (2): 32-36.
- [46] Venturi, M., Di Lenarda, R. and Breschi, L. (2006) An *ex vivo* comparison of three different gutta-percha cones when compacted at different temperatures: rheological considerations in relation to the filling of lateral canals, *Int Endod J*, **39** (8): 648-656.

- [47] Liang, P.-H., Ko, T.-P. and Wang, A. H. J. (2002) Structure, mechanism and function of prenyltransferases, *Eur J Biochem*, **269** (14): 3339-3354.
- [48] Zverina, E. A., Lamphear, C. L., Wright, E. N. and Fierke, C. A. (2012) Recent advances in protein prenyltransferases: substrate identification, regulation, and disease interventions, *Curr Opin Chem Biol*, **16** (5-6): 544-552.
- [49] Resh, M. D. (2013) Covalent lipid modifications of proteins, *Curr Biol*, **23** (10): R431-R435.
- [50] Heide, L. (2009) Prenyl transfer to aromatic substrates: genetics and enzymology, *Curr Opin Chem Biol*, **13** (2): 171-179.
- [51] Wessjohann, L. A., Sontag, B. and Dessoy, M. A. (1999) Enzymatic C-C-coupling: the development of aromatic prenylation for organic synthesis, in: Diederichsen, U., Lindhorst, T. L., Wessjohann, L. A. and Westermann, B. (Eds.) *Bioorganic Chemistry – Highlights and New Aspects*, Chapter 79-88, *Wiley-VCH*, Weinheim.
- [52] Kharel, Y. and Koyama, T. (2003) Molecular analysis of *cis*-prenyl chain elongating enzymes, *Nat Prod Rep*, **20** (1): 111-118.
- [53] Sato, M., Sato, K., Nishikawa, S.-I., Hirata, A., Kato, J.-I. and Nakano, A. (1999) The yeast *RER2* gene, identified by endoplasmic reticulum protein localization mutations, encodes *cis*-prenyltransferase, a key enzyme in dolichol synthesis, *Mol Cell Biol*, **19** (1): 471-483.
- [54] Cunillera, N., Arró, M., Forés, O., Manzano, D. and Ferrer, A. (2000) Characterization of dehydrodolichyl diphosphate synthase of *Arabidopsis thaliana*, a key enzyme in dolichol biosynthesis, *FEBS Letters*, **477** (3): 170-174.
- [55] Clarke, C. F., Tanaka, R. D., Svenson, K., Wamsley, M., Fogelman, A. M. and Edwards, P. A. (1987) Molecular cloning and sequence of a cholesterol-repressible enzyme related to prenyltransferase in the isoprene biosynthetic pathway, *Mol Cell Biol*, **7** (9): 3138-3146.
- [56] Ogura, K. and Koyama, T. (1998) Enzymatic aspects of isoprenoid chain elongation, *Chem Rev*, **98** (4): 1263-1276.
- [57] Koyama, T. (1999) Molecular analysis of prenyl chain elongating enzymes, *Biosci Biotech Bioch*, **69** (10): 1671-1676.

- [58] Tarshis, L. C., Yan, M., Poulter, C. D. and Sacchettini, J. C. (1994) Crystal structure of recombinant farnesyl diphosphate synthase at 2.6-Å resolution, *Biochemistry*, **33** (36): 10871-10877.
- [59] Tarshis, L. C., Proteau, P. J., Kellogg, B. A., Sacchettini, J. C. and Poulter, C. D. (1996) Regulation of product chain length by isoprenyl diphosphate synthases, *P Natl Acad Sci USA*, **96** (26): 15018-15023.
- [60] Joly, A. and Edwards, P. A. (1993) Effect of site-directed mutagenesis of conserved aspartate and arginine residues upon farnesyl diphosphate synthase activity, *J Biol Chem*, **268** (36): 26983-26989.
- [61] Koyama, T., Saito, K., Ogura, K., Obata, S. and Takeshita, A. (1994) Site-directed mutagenesis of farnesyl diphosphate synthase; effect of substitution on the three carboxyl-terminal amino acids, *Can J Chem*, **72** (1): 75-79.
- [62] Song, L. and Poulter, C. D. (1994) Yeast farnesyl-diphosphate synthase: site-directed mutagenesis of residues in highly conserved prenyltransferase domains I and II, *P Natl Acad Sci USA*, **91**: 3044-3048.
- [63] Koyama, T., Tajima, M., Sano, H., Doi, T., Koike-Takeshita, A., Obata, S., Nishino, T. and Ogura, K. (1996) Identification of significant residues in the substrate binding site of *Bacillus stearothermophilus* farnesyl diphosphate synthase, *Biochemistry*, **35** (29): 9533-9538.
- [64] Ohnuma, S., Narita, K., Nakazawa, T., Ishida, C., Takeuchi, Y., Ohto, C. and Nishino, T. (1996) A role of the amino acid residue located on the fifth position before the first aspartate-rich motif of farnesyl diphosphate synthase on determination of the final product, *J Biol Chem*, **271** (48): 30748-30754.
- [65] Lu, Y. P., Liu, H. G., Teng, K. H. and Liang, P. H. (2010) Mechanism of *cis*-prenyltransferase reaction probed by substrate analogues, *Biochem Biophys Res Commun*, **400** (4): 758-762.
- [66] Lu, Y. P., Liu, H. G. and Liang, P. H. (2009) Different reaction mechanisms for *cis*- and *trans*-prenyltransferases, *Biochem Biophys Res Commun*, **379** (2): 351-355.
- [67] Shimizu, N., Koyama, T. and Ogura, K. (1998) Molecular cloning, expression, and purification of undecaprenyl diphosphate synthase, *J Biol Chem*, **273** (31): 19476-19481.

- [68] Pan, J. J., Yang, L. W. and Liang, P. H. (2000) Effect of site-directed mutagenesis of the conserved aspartate and glutamate on *E. coli* undecaprenyl pyrophosphate synthase catalysis, *Biochemistry*, **39** (45): 13856-13861.
- [69] Fujihashi, M., Zhang, Y. W., Higuchi, Y., Li, X. Y., Koyama, T. and Miki, K. (2001) Crystal structure of *cis*-prenyl chain elongating enzyme, undecaprenyl diphosphate synthase, *P Natl Acad Sci USA*, **98** (8): 4337-4342.
- [70] The PyMOL Molecular Graphics System, Version 1.8, Schrödinger, LLC.
- [71] Teng, K. H. and Liang, P. H. (2012) Structures, mechanisms and inhibitors of undecaprenyl diphosphate synthase: a *cis*-prenyltransferase for bacterial peptidoglycan biosynthesis, *Bioorg Chem*, **43**: 51-57.
- [72] Ko, T. P., Chen, Y. K., Robinson, H., Tsai, P. C., Gao, Y. G., Chen, A. P., Wang, A. H. and Liang, P. H. (2001) Mechanism of product chain length determination and the role of a flexible loop in *Escherichia coli* undecaprenyl-pyrophosphate synthase catalysis, *J Biol Chem*, **276** (50): 47474-47482.
- [73] Guo, R. T., Ko, T. P., Chen, A. P., Kuo, C. J., Wang, A. H. and Liang, P. H. (2005) Crystal structures of undecaprenyl pyrophosphate synthase in complex with magnesium, isopentenyl pyrophosphate, and farnesyl thiopyrophosphate: roles of the metal ion and conserved residues in catalysis, *J Biol Chem*, **280** (21): 20762-20774.
- [74] Sinko, W., de Oliveira, C., Williams, S., Van Wynsberghe, A., Durrant, J. D., Cao, R., Oldfield, E. and McCammon, J. A. (2011) Applying molecular dynamics simulations to identify rarely sampled ligand-bound conformational states of undecaprenyl pyrophosphate synthase, an antibacterial target, *Chem Biol Drug Des*, **77** (6): 412-420.
- [75] Yamada, Y., Fukuda, W., Hirooka, K., Hiromoto, T., Nakayama, J., Imanaka, T., Fukusaki, E. and Fujiwara, S. (2009) Efficient in vitro synthesis of *cis*-polyisoprenes using a thermostable *cis*-prenyltransferase from a hyperthermophilic archaeon *Thermococcus kodakaraensis*, *J Biotechnol*, **143** (2): 151-156.
- [76] Schmidt, T., Hillebrand, A., Wurbs, D., Wahler, D., Lenders, M., Schulze Gronover, C. and Prüfer, D. (2010) Molecular cloning and characterization of rubber biosynthetic genes from *Taraxacum koksaghyz*, *Plant Mol Biol Rep*, **28** (2): 277-284.
- [77] Schmidt, T., Lenders, M., Hillebrand, A., van Deenen, N., Munt, O., Reichelt, R., Eisenreich, W., Fischer, R., Prüfer, D. and Gronover, C. S. (2010) Characterization of rubber particles and rubber chain elongation in *Taraxacum koksaghyz*, *BMC Biochem*, **11**: 11.

- [78] Cornish, K. and Xie, W. (2012) Natural rubber biosynthesis in plants: rubber transferase, *Methods Enzymol*, **515**: 63-82.
- [79] Takahashi, S., Lee, H.-J., Yamashita, S. and Koyama, T. (2012) Characterization of *cis*-prenyltransferases from the rubber producing plant *Hevea brasiliensis* heterologously expressed in yeast and plant cells, *Plant Biotechnol*, **29** (4): 411-417.
- [80] Cornish, K. (2001) Similarities and differences in rubber biochemistry among plant species, *Phytochemistry*, **57** (7): 1123-1134.
- [81] Qu, Y., Chakrabarty, R., Tran, H. T., Kwon, E. J., Kwon, M., Nguyen, T. D. and Ro, D. K. (2015) A lettuce (*Lactuca sativa*) homolog of human Nogo-B receptor interacts with *cis*-prenyltransferase and is necessary for natural rubber biosynthesis, *J Biol Chem*, **290** (4): 1898-1914.
- [82] Collins-Silva, J., Nural, A. T., Skaggs, A., Scott, D., Hathwaik, U., Woolsey, R., Schegg, K., McMahan, C., Whalen, M., Cornish, K. and Shintani, D. (2012) Altered levels of the *Taraxacum kok-saghyz* (Russian dandelion) small rubber particle protein, TksRPP3, result in qualitative and quantitative changes in rubber metabolism, *Phytochemistry*, **79**: 46-56.
- [83] Hillebrand, A., Post, J. J., Wurbs, D., Wahler, D., Lenders, M., Krzyzanek, V., Pruffer, D. and Gronover, C. S. (2012) Down-regulation of small rubber particle protein expression affects integrity of rubber particles and rubber content in *Taraxacum brevicorniculatum*, *PLoS One*, **7** (7): e41874.
- [84] Post, J., van Deenen, N., Fricke, J., Kowalski, N., Wurbs, D., Schaller, H., Eisenreich, W., Huber, C., Twyman, R. M., Pruffer, D. and Gronover, C. S. (2012) Laticifer-specific *cis*-prenyltransferase silencing affects the rubber, triterpene, and inulin content of *Taraxacum brevicorniculatum*, *Plant Physiol*, **158** (3): 1406-1417.
- [85] Chakrabarty, R., Qu, Y. and Ro, D. K. (2015) Silencing the lettuce homologs of small rubber particle protein does not influence natural rubber biosynthesis in lettuce (*Lactuca sativa*), *Phytochemistry*, **113**: 121-129.
- [86] Epping, J., van Deenen, N., Niephaus, E., Stolze, A., Fricke, J., Huber, C., Eisenreich, W., Twyman, R. M., Pruffer, D. and Schulze Gronover, C. (2015) A rubber transferase activator is necessary for natural rubber biosynthesis in dandelion, *Nature Plants*, **1** (5): Article number 15048.
- [87] Kwon, M., Kwon, E. J. and Ro, D. K. (2016) *cis*-Prenyltransferase and polymer analysis from a natural rubber perspective, *Methods Enzymol*, **576**: 121-145.



- [88] Yamashita, S., Yamaguchi, H., Waki, T., Aoki, Y., Mizuno, M., Yanbe, F., Ishii, T., Funaki, A., Tozawa, Y., Miyagi-Inoue, Y., Fushihara, K., Nakayama, T. and Takahashi, S. (2016) Identification and reconstitution of the rubber biosynthetic machinery on rubber particles from *Hevea brasiliensis*, *eLife*, **5**: e19022.
- [89] Dessoy, M. A. (2003) Synthesis and enzymatic coupling of prenyldiphosphates and benzoates (Dissertation), *Martin-Luther-Universität Halle Wittenberg*, Halle.
- [90] Weber, R. A. (2011) Synthese und biokatalytische Umsetzung von Prenyldiphosphaten (Dissertation), *Martin-Luther-Universität Halle-Wittenberg*, Halle.
- [91] Ludwig, S. (2016) Synthesis and biocatalytic conversion of natural and artificial isoprenoid diphosphates (Dissertation), *Martin-Luther-Universität Halle-Wittenberg*, Halle.
- [92] O'Maille, P. E., Chappell, J. and Noel, J. P. (2004) A single-vial analytical and quantitative gas chromatography-mass spectrometry assay for terpene synthases, *Anal Biochem*, **335** (2): 210-217.
- [93] Thomas, J. G. and Baneyx, F. (1996) Protein misfolding and inclusion body formation in recombinant *Escherichia coli* cells overexpressing heat-shock proteins, *J Biol Chem*, **271** (19): 11141-11147.
- [94] Inoue, H., Nojima, H. and Okayama, H. (1990) High efficiency transformation of *Escherichia coli* with plasmids, *Gene*, **96** (1): 23-28.
- [95] Chovancova, E., Pavelka, A., Benes, P., Strnad, O., Brezovsky, J., Kozlikova, B., Gora, A., Sustr, V., Klvana, M., Medek, P., Biedermannova, L., Sochor, J. and Damborsky, J. (2012) CAVER 3.0: a tool for the analysis of transport pathways in dynamic protein structures, *PLoS Comput Biol*, **8** (10): e1002708.
- [96] Stratec Molecular, Invisorb® spin plasmid mini two, <https://www.molecular.stratec.com/files/inhalte/Manuals/InvisorbSpinPlasmidMiniTwo.pdf> (lastly opened on 2017-06-01).
- [97] Macherey-Nagel, NucleoBond® plasmid DNA purification, [http://www.mn-net.com/Portals/8/attachments/Redakteure\\_Bio/Protocols/Plasmid%20DNA%20Purification/UM\\_pDNA\\_NuBoXtra.pdf](http://www.mn-net.com/Portals/8/attachments/Redakteure_Bio/Protocols/Plasmid%20DNA%20Purification/UM_pDNA_NuBoXtra.pdf) (lastly opened on 2017-06-01).

- [98] Agilent Technologies, QuikChange site-directed mutagenesis, <https://www.agilent.com/cs/library/usermanuals/public/200518.pdf> (lastly opened on 2017-06-01).
- [99] Macherey-Nagel, NucleoSpin® gel and PCR clean-up, [http://www.mn-net.com/Portals/8/attachments/Redakteure\\_Bio/Protocols/DNA%20clean-up/UM\\_PCRcleanup\\_Gelix\\_NSgelPCR.pdf](http://www.mn-net.com/Portals/8/attachments/Redakteure_Bio/Protocols/DNA%20clean-up/UM_PCRcleanup_Gelix_NSgelPCR.pdf) (lastly opened on 2017-06-01).
- [100] Schmitt, J., Hess, H. and Stunnenberg, H. G. (1993) Affinity purification of histidine-tagged proteins, *Mol Biol Rep*, **18** (3): 223-230.
- [101] University of Oklahoma Libraries, OU open educational resources, Norman, Oklahoma (USA), <http://www.ou.edu/OpenEducation/ou-resources/biochemical-methods-v2/lab-8/> (lastly opened on 2017-05-31).
- [102] Singh, P., Sharma, L., Kulothungan, S. R., Adkar, B. V., Prajapati, R. S., Ali, P. S., Krishnan, B. and Varadarajan, R. (2013) Effect of signal peptide on stability and folding of *Escherichia coli* thioredoxin, *PLoS One*, **8** (5): e63442.
- [103] Neu, H. C. and Heppel, L. A. (1965) The release of enzymes from *Escherichia coli* by osmotic shock and during the formation of spheroplasts, *J Biol Chem*, **240** (9): 3685-3692.
- [104] Andrews, P. (1964) Estimation of the molecular weights of proteins by sephadex gel-filtration, *Biochem J*, **91** (2): 222-233.
- [105] GE Healthcare, PD-10 desalting column, <https://cdn.gelifesciences.com/dmm3bwsv3/AssetStream.aspx?mediaformatid=10061&destinationid=10016&assetid=11531> (lastly opened on 2017-06-01).
- [106] Bradford, M. M. (1976) A rapid and sensitive method for the quantitation of microgram quantities of protein utilizing the principle of protein-dye binding, *Anal Biochem*, **72** (1-2): 248-254.
- [107] Roti®-Quant manual, [https://www.carlroth.com/downloads/ba/de/K/BA\\_K015\\_DE.pdf](https://www.carlroth.com/downloads/ba/de/K/BA_K015_DE.pdf) (lastly opened on 2017-06-01).
- [108] Laemmli, U. K. (1970) Cleavage of structural proteins during the assembly of the head of bacteriophage T4, *Nature*, **227**: 680-685.

- [109] Meyer, T. S. and Lamberts, B. L. (1965) Use of coomassie brilliant blue R250 for the electrophoresis of microgram quantities of parotid saliva proteins on acrylamide-gel strips, *Biochim Biophys Acta*, **107** (47): 144-145.
- [110] Fuji, H., Koyama, T. and Ogura, K. (1982) Efficient enzymatic hydrolysis of polyprenyl pyrophosphates, *Biochim Biophys Acta*, **712** (3): 716-718.
- [111] Skorupińska-Tudek, K., Bieńkowski, T., Olszowska, O., Furmanowa, M., Chojnacki, T., Danikiewicz, W. and Swieżewska, E. (2003) Divergent pattern of polyisoprenoid alcohols in the tissues of *Coluria geoides*: a new electrospray ionization MS approach, *Lipids*, **38** (9): 981-990.
- [112] Teng, K. H., Chen, A. P., Kuo, C. J., Li, Y. C., Liu, H. G., Chen, C. T. and Liang, P. H. (2011) Fluorescent substrate analog for monitoring chain elongation by undecaprenyl pyrophosphate synthase in real time, *Anal Biochem*, **417** (1): 136-141.
- [113] Molt, K., Telgheder, U., Berechnung der Verfahrensstandardabweichung und Nachweis-, Erfassungs- und Bestimmungsgrenze aus einer Kalibrierung gemäß DIN 32645, Universität Duisburg-Essen, [https://www.uni-due.de/imperia/md/content/iac/git\\_erw\\_1.pdf](https://www.uni-due.de/imperia/md/content/iac/git_erw_1.pdf) (lastly opened on 2017-09-05).
- [114] Nagaki, M., Sato, S., Maki, Y., Nishino, T. and Koyama, T. (2000) Artificial substrates for undecaprenyl diphosphate synthase from *Micrococcus luteus* B-P 26, *J Mol Catal B: Enzym*, **9** (1): 33-38.
- [115] Nagaki, M., Kimura, K., Kimura, H., Maki, Y., Goto, E., Nishino, T. and Koyama, T. (2001) Artificial substrates of medium-chain elongating enzymes, hexaprenyl- and heptaprenyl diphosphate synthases, *Bioorg Med Chem Lett*, **11** (16): 2157-2159.
- [116] Nagaki, M., Kuwahara, K., Kimura, K., Kawakami, J., Maki, Y., Ito, S., Morita, N., Nishino, T. and Koyama, T. (2003) Substrate specificities of medium-prenylchain elongating enzymes, hexaprenyl- and heptaprenyl diphosphate synthases, *J Mol Catal B: Enzym*, **22** (1-2): 97-103.
- [117] Heaps, N. A. and Poulter, C. D. (2011) Synthesis and evaluation of chlorinated substrate analogues for farnesyl diphosphate synthase, *J Org Chem*, **76** (6): 1838-1843.
- [118] Vattekkatte, A., Gatto, N., Schulze, E., Brandt, W. and Boland, W. (2015) Inhibition of a multiproduct terpene synthase from *Medicago truncatula* by 3-bromoprenyl diphosphates, *Org Biomol Chem*, **13** (16): 4776-4784.

- [119] Carothers, W. H., Williams, I., Collins, A. M. and Kirby, J. E. (1931) Acetylene polymers and their derivatives. II. A new synthetic rubber: chloroprene and its polymers, *J Am Chem Soc*, **53** (11): 4203-4225.
- [120] Maynard, J. T. and Mochel, W. E. (1954) The structure of neoprene. VII. Infrared analysis of configuration, *J Polym Sci Pol Chem*, **13** (69): 251-262.
- [121] Lynch, M. (2001) Manufacture and use of chloroprene monomer, *Chem-Biol Interact*, **135-136**: 155-167.
- [122] International Institute of Synthetic Rubber Producers, Inc., Polybutadiene rubber (BR), Houston, Texas (USA), <https://iisrp.com/synthetic-rubber/> (lastly opened on 2017-09-26).
- [123] K-Zeitung Online (Peters, A.), Elastomerenmarkt mit Perspektive, Hannover, <https://www.k-zeitung.de/elastomerenmarkt-mit-perspektive/150/1193/68340/> (lastly opened on 2017-09-26).
- [124] Hauptmann, S., Graefe, J. and Remane, H. (1976) Lehrbuch der organischen Chemie, 1. Auflage, 171-175, *VEB Deutscher Verlag für Grundstoffindustrie*, Leipzig.
- [125] Pan, J. J., Chiou, S. T. and Liang, P. H. (2000) Product distribution and pre-steady-state kinetic analysis of *Escherichia coli* undecaprenyl pyrophosphate synthase reaction, *Biochemistry*, **39** (35): 10936-10942.
- [126] Pan, J. J., Ramamoorthy, G. and Poulter, C. D. (2013) Dependence of the product chain-length on detergents for long-chain E-polyprenyl diphosphate synthases, *Biochemistry*, **52** (29): 5002-5008.
- [127] Troutman, J. M., Erickson, K. M., Scott, P. M., Hazel, J. M., Martinez, C. D. and Dodbele, S. (2015) Tuning the production of variable length, fluorescent polyisoprenoids using surfactant-controlled enzymatic synthesis, *Biochemistry*, **54** (18): 2817-2827.
- [128] Kamat, S., Beckman, E. J. and Russell, A. J. (1992) Role of diffusion in nonaqueous enzymology. 1. Theory, *Enzyme Microb Tech*, **14** (4): 265-271.
- [129] Pencreac'h, G. and Baratti, J. C. (1996) Hydrolysis of *p*-nitrophenyl palmitate in *n*-heptane by the *Pseudomonas cepacia* lipase: A simple test for the determination of lipase activity in organic media, *Enzyme Microb Tech*, **18** (6): 417-422.

- [130] Lukacin, R., Matern, U., Specker, S. and Vogt, T. (2004) Cations modulate the substrate specificity of bifunctional class I *O*-methyltransferase from *Ammi majus*, *FEBS Lett*, **577** (3): 367-370.
- [131] Fraústo da Silva, J. J. R. and Williams, R. J. P. (2001) The biological chemistry of the elements: the inorganic chemistry of life, 2. Edition, 34-53, *Oxford University Press*, Oxford.
- [132] Texas A&M University, Coordination chemistry - Transition metal complexes, Texas, <http://www.chem.tamu.edu/rgroup/marcetta/chem104/lectures/104-l-w04.pdf> (lastly opened on 2017-10-09).
- [133] Fujikura, K., Maki, Y., Ohya, N., Satoh, M. and Koyama, T. (2008) Kinetic studies of *Micrococcus luteus* B-P 26 undecaprenyl diphosphate synthase reaction using 3-desmethyl allylic substrate analogs, *Biosci Biotechnol Biochem*, **72** (3): 851-855.
- [134] Kelley, L. A., Mezulis, S., Yates, C. M., Wass, M. N. and Sternberg, M. J. E. (2015) The Pyre2 web portal for protein modeling, prediction and analysis, *Nat Protoc*, **10**: 845-858.
- [135] Böttcher, D. and Bornscheuer, U. T. (2006) High-throughput screening of activity and enantioselectivity of esterases, *Nat Protoc*, **1** (5): 2340-2343.
- [136] Hauff, S. and Vetter, W. (2009) Quantification of fatty acids as methyl esters and phospholipids in cheese samples after separation of triacylglycerides and phospholipids, *Anal Chim Acta*, **636** (2): 229-235.
- [137] Christie, W. W., AOCs Lipid Library, HPLC separation of phospholipids, Urbana, Illinois (USA), <http://lipidlibrary.aocs.org/History/content.cfm?ItemNumber=40365> (lastly opened on 2017-10-24).
- [138] Kera, K., Takahashi, S., Sutoh, T., Koyama, T. and Nakayama, T. (2012) Identification and characterization of a *cis,trans*-mixed heptaprenyl diphosphate synthase from *Arabidopsis thaliana*, *FEBS J*, **279** (20): 3813-3827.
- [139] Goloubinoff, P., Gatenby, A. A. and Lorimer, G. H. (1989) GroE heat-shock proteins promote assembly of foreign prokaryotic ribulose biphosphate carboxylase oligomers in *Escherichia coli*, *Nature*, **337**: 44-47.
- [140] Kalbach, C. E. and Gatenby, A. A. (1993) Stable expression plasmid for high-level production of GroE molecular chaperones in large-scale cultures, *Enzyme Microb Tech*, **15** (9): 730-735.

[141] Thomas, J. G. and Baneyx, F. (1996) Protein folding in the cytoplasm of *Escherichia coli*: requirements for the DnaK-DnaJ-GrpE and GroEL-GroES molecular chaperone machines, *Mol Microbiol*, **21** (6): 1185-1196.

[142] Uniterra, Rutherford Online - Lexikon der Elemente 2006, Berlin, <http://www.uniterra.de/rutherford/> (lastly opened on 2017-11-06).

### SPRINGER NATURE LICENSE

Jan 27, 2018

---

This Agreement between Leibniz Institute of Plant Biochemistry -- Pia Schöne ("You") and Springer Nature ("Springer Nature") consists of your license details and the terms and conditions provided by Springer Nature and Copyright Clearance Center.

---

License Number	4277040516151
License date	Jan 27, 2018
Licensed Content Publisher	Springer Nature
Licensed Content Publication	Nature Plants
Licensed Content Title	A rubber transferase activator is necessary for natural rubber biosynthesis in dandelion
Licensed Content Author	Janina Epping, Nicole van Deenen, Eva Niephaus, Anna Stolze, Julia Fricke et al.
Licensed Content Date	Apr 27, 2015
Licensed Content Volume	1
Licensed Content Issue	5
Type of Use	Thesis/Dissertation
Requestor type	academic/university or research institute
Format	print and electronic
Portion	figures/tables/illustrations
Number of figures/tables/illustrations	1
High-res required	no
Will you be translating?	no
Circulation/distribution	<501
Author of this Springer Nature content	no
Title	Enzymatic synthesis of natural and artificial polyprenols

## List of References

---

Instructor name	Prof. Ludger A. Wessjohann
Institution name	Leibniz Institute of Plant Biochemistry
Expected presentation date	Jun 2018
Order reference number	15048
Portions	Figure 6
Requestor Location	Leibniz Institute of Plant Biochemistry Weinberg 3 Halle, Saxony-Anhalt 06120 Germany Attn: Leibniz Institute of Plant Biochemistry
Billing Type	Invoice
Billing Address	Leibniz Institute of Plant Biochemistry Weinberg 3 Halle, Germany 06120 Attn: Leibniz Institute of Plant Biochemistry
Total	0.00 EUR

## 8. Appendix

### 8.1. MANT-O-Geraniol calibration line (calculations)

The calculations were done according to Molt & Telgheder (University Duisburg-Essen)<sup>[113]</sup>.

**Table A1** Values used for preparation of the MANT-O-Geraniol calibration line. Concentration of the samples ( $\mu\text{M}$ ) comprise the x values, mean areas (determined from 3 measurements each) comprise the y values.

$x_i$ (c [ $\mu\text{M}$ ])	$y_i$ (mean area)	Standard deviation
18	1633.233154	2.78475E-13
15	1416.704224	0
12.5	1026.067749	0.169888767
6.25	504.0344035	0.225755639
3.125	243.5442454	0.345347886
1.56	118.5839767	0.166640862
0.78	58.09387207	0.102421973
0.39	27.81133842	0.016601726
0.195	13.88676325	0.056174378
0.098	6.681236744	0.038317261

**Table A2** Values of the terms used (for description see section 2.5.3.1.).

Term	b	n	m	i	f	$\alpha$	$t_{f,\alpha}$	$\bar{x}$
Value	90.97	10	3	1-10	8	0.05	1.86	5.7898



**Table A3** Calculated values for  $\hat{y}_i$ ,  $y_i - \hat{y}_i$  and  $(y_i - \hat{y}_i)^2$ . The values for  $\hat{y}_i$  (= calculated value for y) are determined according to the equation obtained from the MANT-O-Geraniol calibration line (equation 2 in section 2.5.3.1., substitution of  $x_i$  values into equation).

$x_i$	$y_i$	$\hat{y}_i$	$y_i - \hat{y}_i$	$(y_i - \hat{y}_i)^2$
18	1633.233154	1615.61	17.623154	310.5755569
15	1416.704224	1342.7	74.004224	5476.62517
12.5	1026.067749	1115.275	-89.20725098	7957.933627
6.25	504.0344035	546.7125	-42.67809652	1821.419922
3.125	243.5442454	262.43125	-18.8870046	356.7189427
1.56	118.5839767	120.0632	-1.479223254	2.188101436
0.78	58.09387207	49.1066	8.98727207	80.77105927
0.39	27.81133842	13.6283	14.18303842	201.158579
0.195	13.88676325	-4.11085	17.99761325	323.9140829
0.098	6.681236744	-12.93494	19.61617674	384.79439

$$s_{y,x} = \sqrt{\frac{\sum_{i=1}^n (y_i - \hat{y}_i)^2}{n - 2}}$$

$$s_{y,x} = \sqrt{\frac{16916.09943}{8}} = 45.9838279$$

**Equation A1** Determination of the residual standard deviation.

$$Q_{xx} = \sum_{i=1}^n x_i^2 - \frac{(\sum_{i=1}^n x_i)^2}{n}$$

$$Q_{xx} = 757.319854 - \frac{3352.178404}{10} = 422.1020136$$

**Equation A2** Determination of the ordinary least squares of x values of the calibration.

$$x_{LOD} = \frac{s_{y,x} \cdot t_{f,\alpha}}{b} \sqrt{\frac{1}{n} + \frac{1}{m} + \frac{\bar{x}^2}{Q_{xx}}}$$

$$x_{LOD} = \frac{45.9838279 \cdot 1.86}{90.97} \sqrt{\frac{1}{10} + \frac{1}{3} + \frac{33.52178404}{422.1020136}} = 0.673244096$$

**Equation A3** Determination of the limit of detection  $x_{LOD}$ .

$$x_{MDL} = 2 \cdot x_{LOD}$$

$$x_{MDL} = 2 \cdot 0.673244096 = 1.346488193$$

**Equation A4** Determination of the method detection limit  $x_{MDL}$ .

Due to the unit of the used  $x_i$  values the calculated limits have the same unit ( $\mu\text{M}$ ).

## 8.2. Amino acid sequences

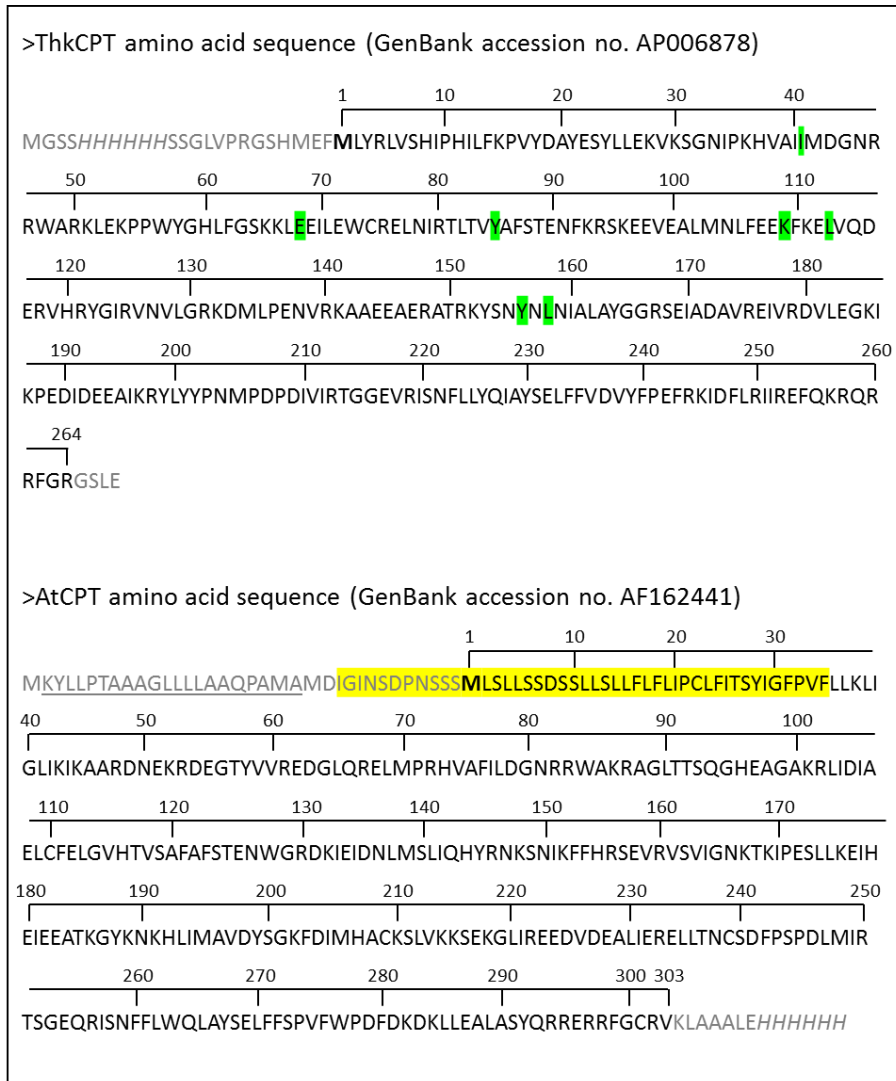


**Figure A1** Amino acid sequences of the used *cis*-prenyltransferases. Bold **M** indicates the start of the native protein sequence, N- and C-terminal tags incl. His<sub>6</sub> and *pelB* signal sequences are shown in grey, native protein sequence is shown in black, poly-histidine tags are written in italic and the *pelB* signal sequence is underlined. The amino acid residues of the native protein sequences are numbered. Positions for mutagenesis in ThkCPT are highlighted in green. The section that was deleted in AtCPT to remove the N-terminal transmembrane region is highlighted in yellow.

### 8.3. Characteristics of the used bivalent cations

**Table A4** Summary of the characteristics of the used bivalent cations and the most abundant chain length of products as stated in the corresponding text in section 3.2.5.1. pm: pikometer.

Ion	Ionic radius [pm] <sup>[142]</sup>	Geometry <sup>[131, 132]</sup>	Preferred donor atom <sup>[131, 132]</sup>	Most abundant chain length of products	
				IPP	CI-BPP
Mg <sup>2+</sup>	78	Octahedral	O (phosphate)	8-10	6-7
Mn <sup>2+</sup>	91	Octahedral	O (phosphate)	8-10	1/3-6
Co <sup>2+</sup>	82	Octahedral	S, N, O (carboxylate)	8-9	3-5
Ni <sup>2+</sup>	78	Octahedral	S, N	8-9	6-7
Cu <sup>2+</sup>	72	Tetragonal	S, N, O (carboxylate)	7-8	1
Zn <sup>2+</sup>	83	Tetrahedral or octahedral	S, N, O (carboxylate)	8-9	1-3

### 8.4. Proportion of full-length AtCPT in gel bands and in solution

The parameters for the determination of the percentage of full-length AtCPT are listed in table A5. As the sample of the gel band is less complex, a mascot significance threshold of 0.05 was chosen as error control. In contrast, a false discovery rate (FDR) of 0.01 was used as error control for the protein solution as this sample is more complex.

**Table A5** Proportion of AtCPT in gel band 2 and in solution. PSM: peptide spectrum match, FDR: false discovery rate.

	#Unique peptides	#PSMs	Fraction most abundant	Fraction total PSMs	Error control
<b>Gel band 2</b>	23	193	100%	18%	Mascot significance threshold 0.05
<b>Solution</b>	17	54	7%	1%	FDR threshold 0.01

## 8.5. HPLC analyses (fractions after SPE)

In preparation for the HR-ESI-MS measurements, the IPP product fractions were prepared via SPE (section 2.5.4.). After several washing steps, the solvents from HPLC analytics [SV A (MeOH/H<sub>2</sub>O/isopropanol 12:1:8 (v/v/v)) and SV B (*n*-hexane/isopropanol 7:3 (v/v))] were used to elute the products from the SPE column material. The collected fractions were then analyzed via HPLC (2.5.3.1.) and it was shown that the products are present in the SPE fractions eluted with HPLC SV B (Figures A2 and A3) which were subsequently used for HR-ESI-MS analyses.

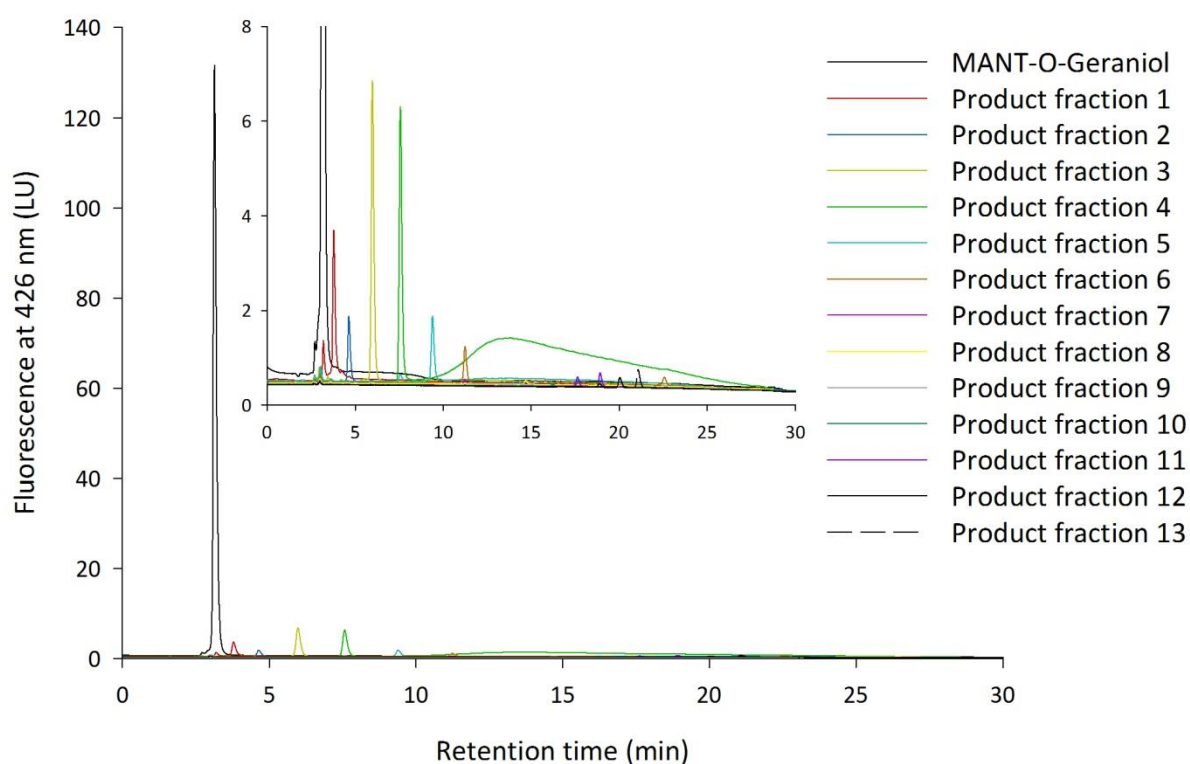


**Figure A2** HPLC chromatogram of ThkCPT products recovered from SPE extraction. Reactions were performed with MANT-O-GPP and IPP at 65°C reaction temperature followed by diphosphate hydrolysis. Elution from the SPE column material was performed with MeOH/H<sub>2</sub>O/isopropanol 12:1:8 (v/v/v). Essentially, residual MANT-O-Geraniol (corresponding alcohol from the starter substrate) is observed in these fractions (elongated products were only detected in very low levels under these conditions). LU: luminescence units.

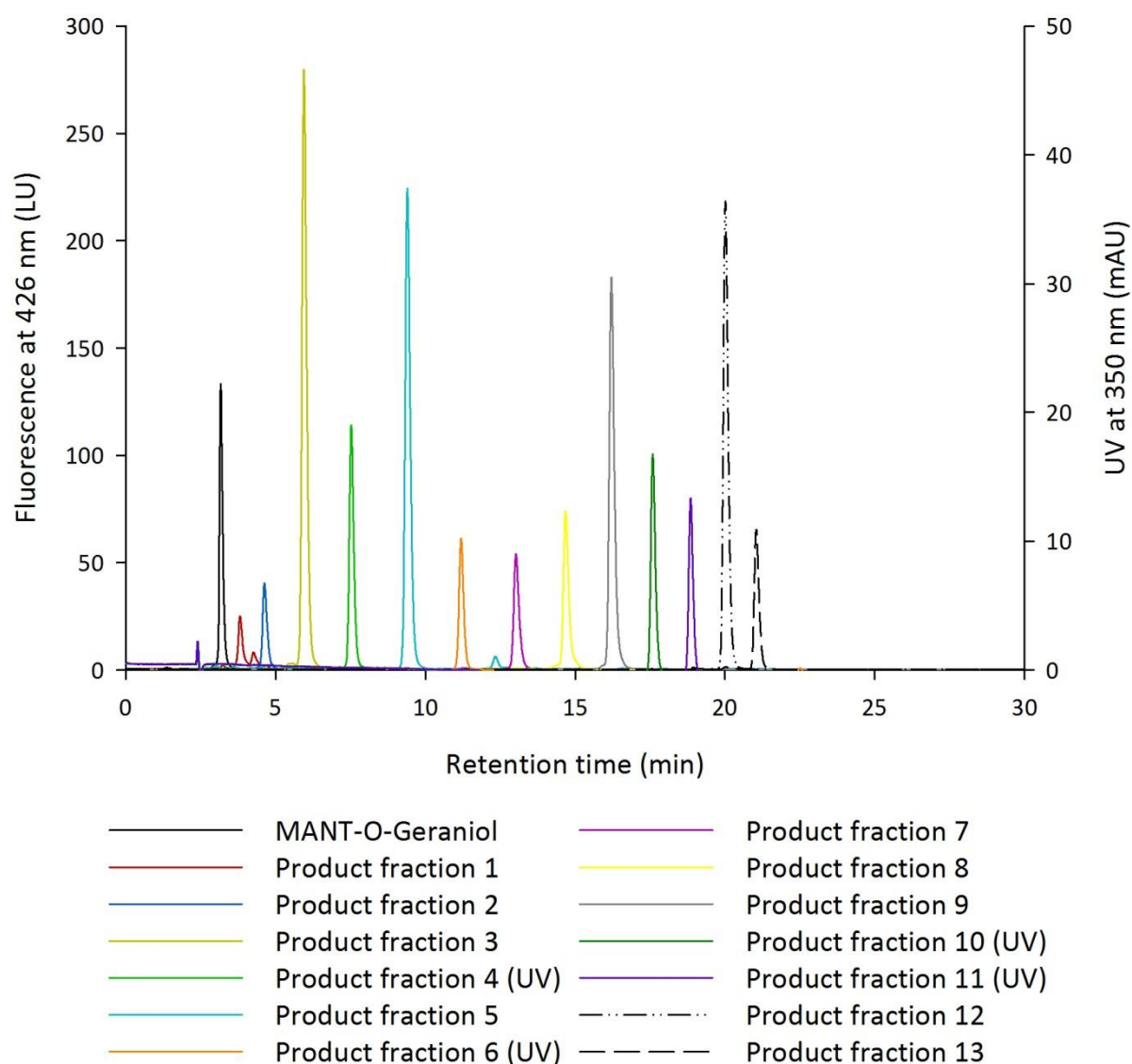


**Figure A3** HPLC chromatogram of ThkCPT products recovered from SPE extraction. Reactions were performed with MANT-O-GPP and IPP at 65°C reaction temperature followed by diphosphate hydrolysis. Elution from the SPE column material was performed with *n*-hexane/isopropanol 7:3 (v/v). Under these conditions, the elongated products were recovered in high levels from the SPE column. For the products 4, 6, 10 and 11 the detection by UV is shown as the fluorescence signal was too high for detection. LU: luminescence units, AU: absorption units.







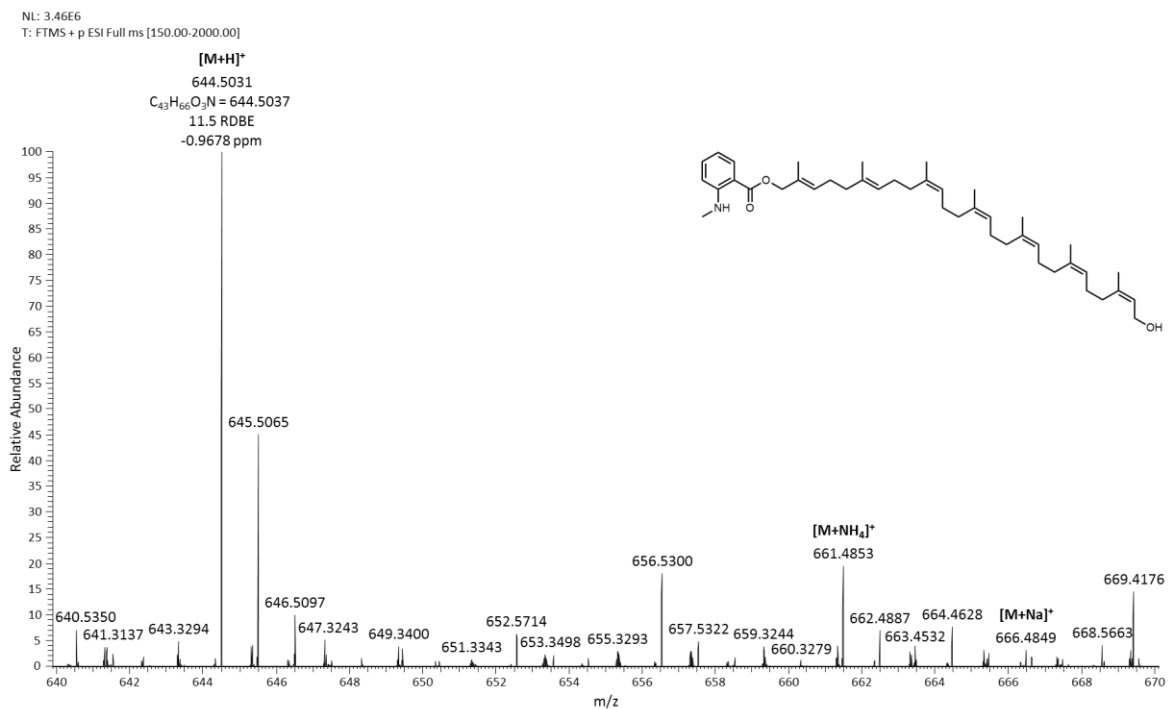


**Figure A8** HR-ESI-MS spectrum of SPE product fraction 5 of the ThkCPT reaction with MANT-O-GPP and IPP which shows the  $[M+H]^+$  ion (C<sub>43</sub>H<sub>66</sub>O<sub>3</sub>N) corresponding to the 5-fold elongated reaction product. The reaction was performed at 65°C reaction temperature followed by diphosphate hydrolysis. Additionally, the ammonium and the sodium adducts and the isotopic pattern can be seen.

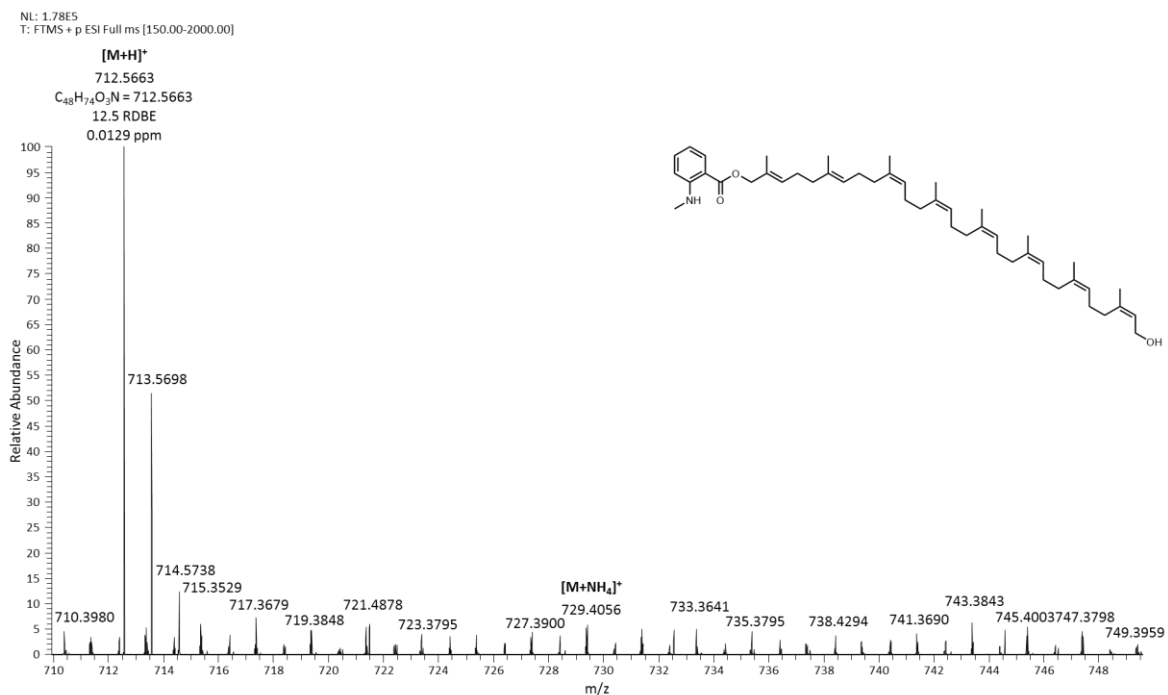


**Figure A9** HR-ESI-MS spectrum of SPE product fraction 6 of the ThkCPT reaction with MANT-O-GPP and IPP which shows the  $[M+H]^+$  ion (C<sub>48</sub>H<sub>74</sub>O<sub>3</sub>N) corresponding to the 6-fold elongated reaction product. The reaction was performed at 65°C reaction temperature followed by diphosphate hydrolysis. Additionally, the ammonium adduct and the isotopic pattern can be seen.

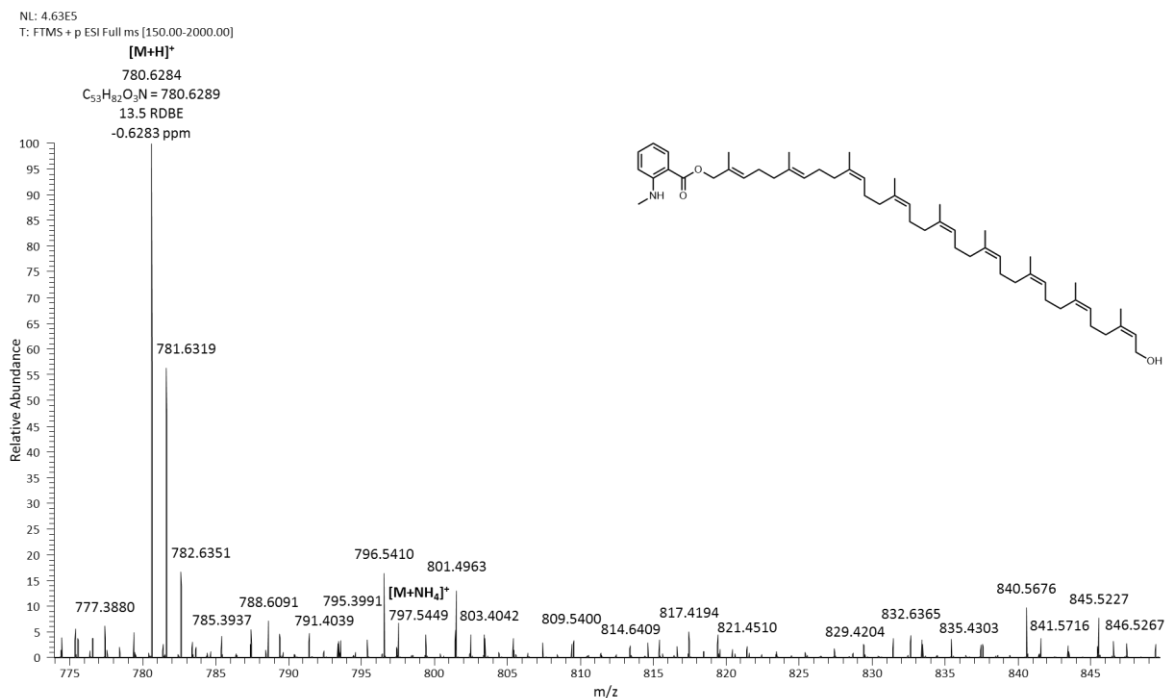


**Figure A10** HR-ESI-MS spectrum of SPE product fraction 7 of the ThkCPT reaction with MANT-O-GPP and IPP which shows the [M+H]<sup>+</sup> ion (C<sub>53</sub>H<sub>82</sub>O<sub>3</sub>N) corresponding to the 7-fold elongated reaction product. The reaction was performed at 65°C reaction temperature followed by diphosphate hydrolysis. Additionally, the ammonium adduct and the isotopic pattern can be seen.

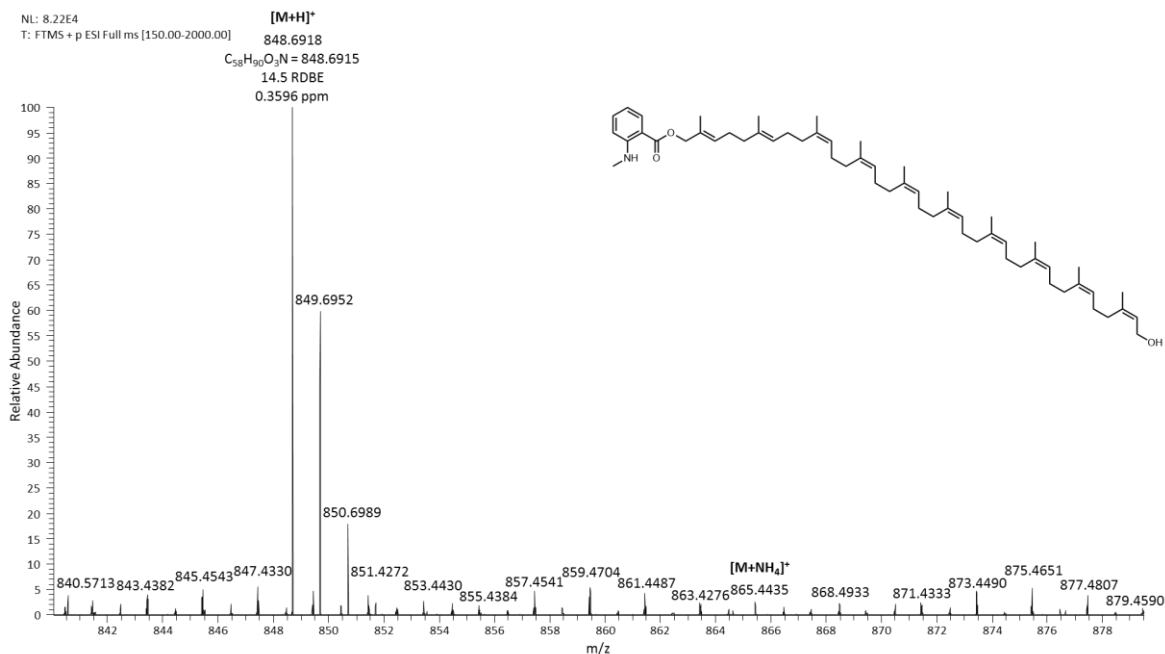


**Figure A11** HR-ESI-MS spectrum of SPE product fraction 8 of the ThkCPT reaction with MANT-O-GPP and IPP which shows the [M+H]<sup>+</sup> ion (C<sub>58</sub>H<sub>90</sub>O<sub>3</sub>N) corresponding to the 8-fold elongated reaction product. The reaction was performed at 65°C reaction temperature followed by diphosphate hydrolysis. Additionally, the ammonium adduct and the isotopic pattern can be seen.

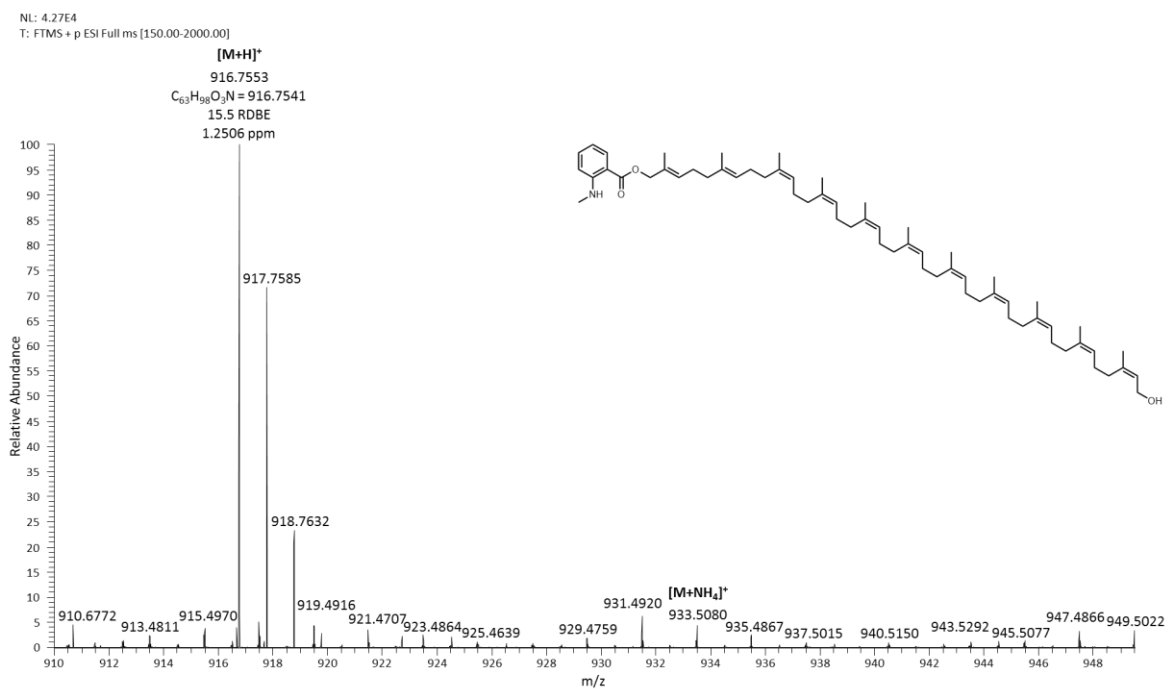


**Figure A12** HR-ESI-MS spectrum of SPE product fraction 9 of the ThkCPT reaction with MANT-O-GPP and IPP which shows the  $[M+H]^+$  ion (C<sub>63</sub>H<sub>98</sub>O<sub>3</sub>N) corresponding to the 9-fold elongated reaction product. The reaction was performed at 65°C reaction temperature followed by diphosphate hydrolysis. Additionally, the ammonium adduct and the isotopic pattern can be seen.

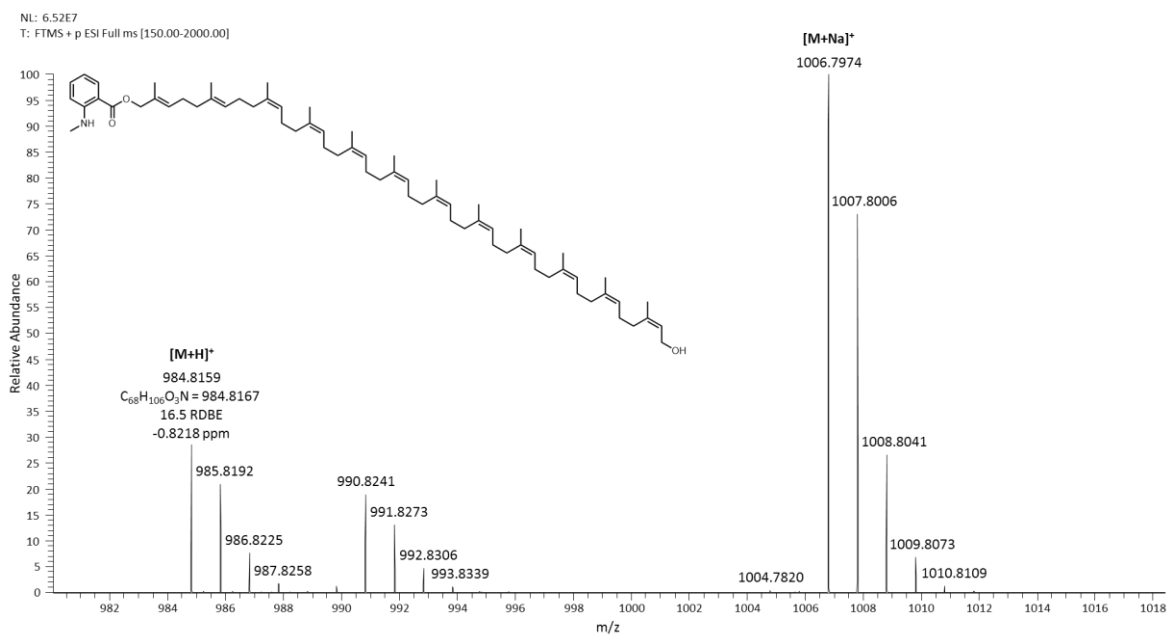


**Figure A13** HR-ESI-MS spectrum of SPE product fraction 10 of the ThkCPT reaction with MANT-O-GPP and IPP which shows the  $[M+H]^+$  ion (C<sub>68</sub>H<sub>106</sub>O<sub>3</sub>N) corresponding to the 10-fold elongated reaction product. The reaction was performed at 65°C reaction temperature followed by diphosphate hydrolysis. Additionally, the sodium adduct and the isotopic pattern can be seen.

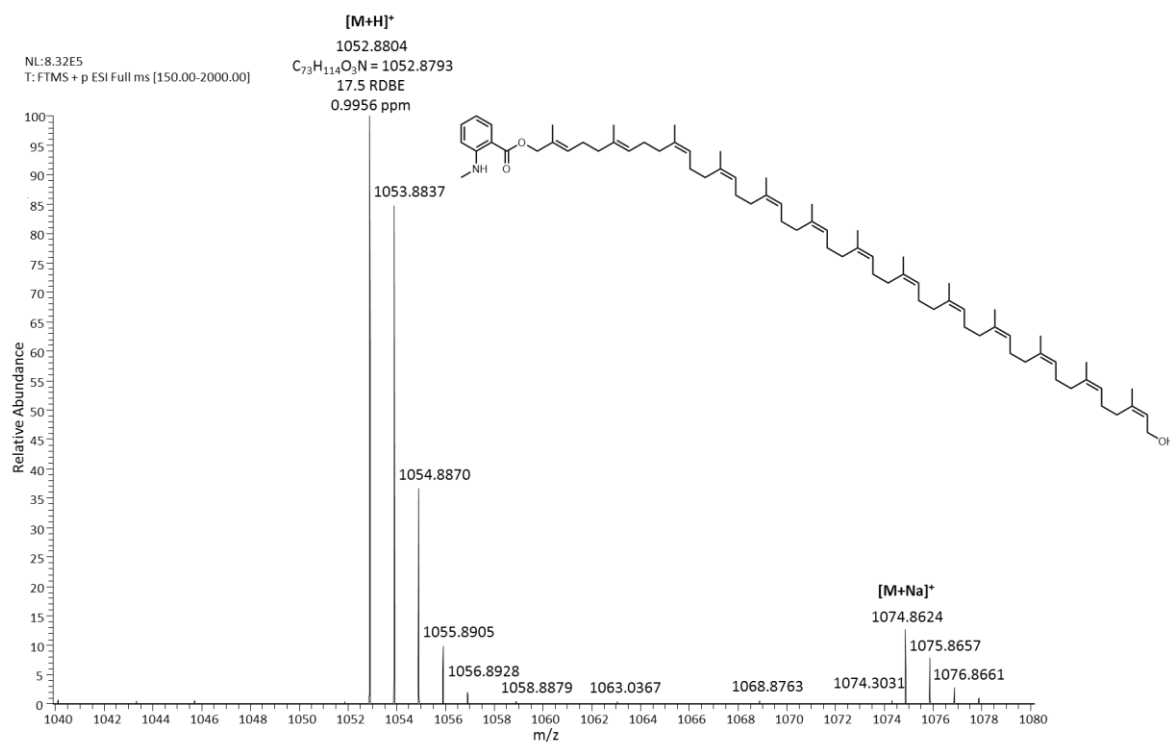


**Figure A14** HR-ESI-MS spectrum of SPE product fraction 11 of the ThkCPT reaction with MANT-O-GPP and IPP which shows the  $[M+H]^+$  ion ( $C_{73}H_{114}O_3N$ ) corresponding to the 11-fold elongated reaction product. The reaction was performed at 65°C reaction temperature followed by diphosphate hydrolysis. Additionally, the sodium adduct and the isotopic pattern can be seen.

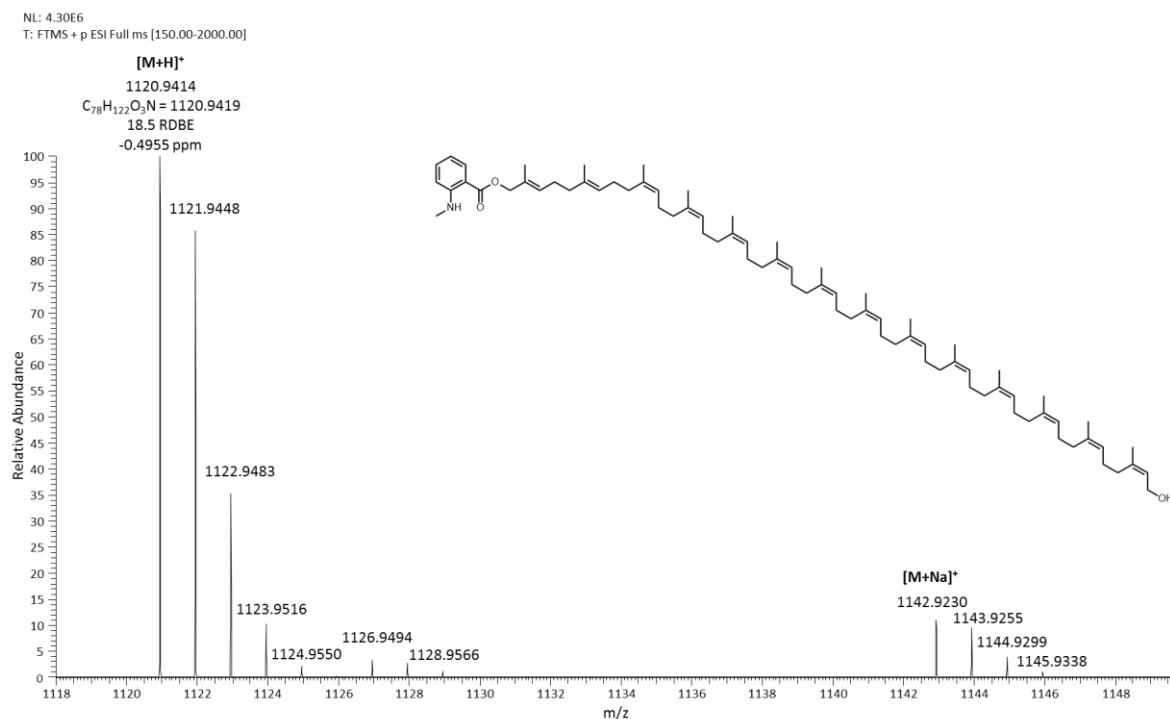


**Figure A15** HR-ESI-MS spectrum of SPE product fraction 12 of the ThkCPT reaction with MANT-O-GPP and IPP which shows the  $[M+H]^+$  ion ( $C_{78}H_{122}O_3N$ ) corresponding to the 12-fold elongated reaction product. The reaction was performed at 65°C reaction temperature followed by diphosphate hydrolysis. Additionally, the sodium adduct and the isotopic pattern can be seen.

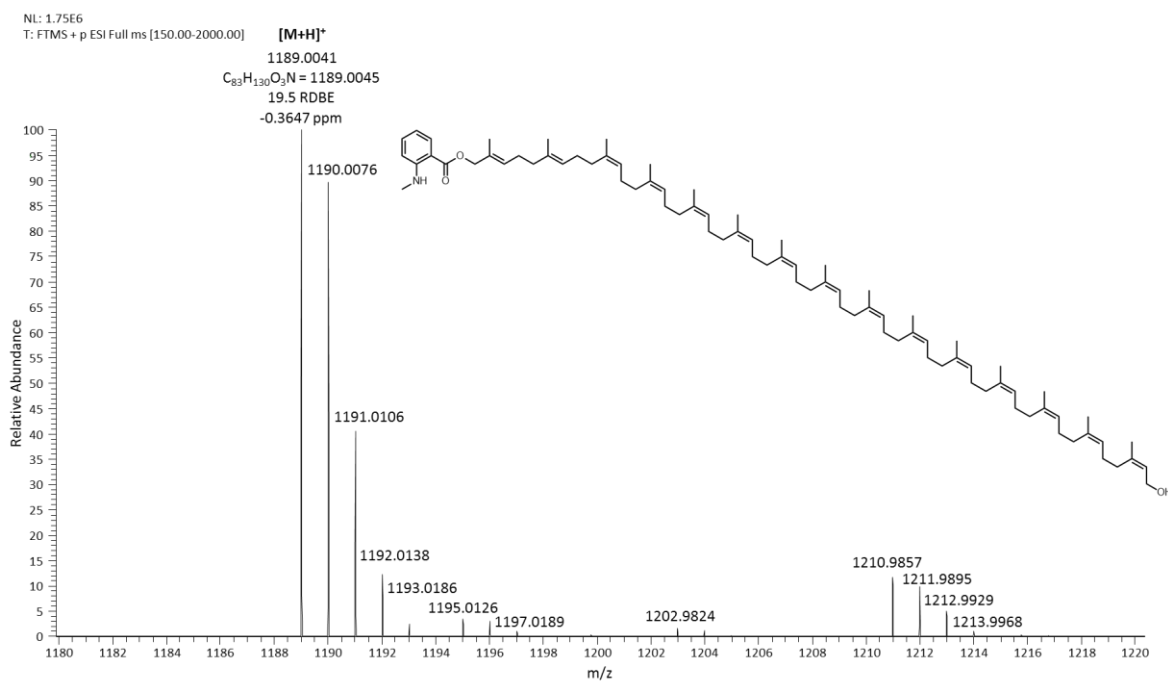


**Figure A16** HR-ESI-MS spectrum of SPE product fraction 13 of the ThkCPT reaction with MANT-O-GPP and IPP which shows the  $[M+H]^+$  ion ( $C_{83}H_{130}O_3N$ ) corresponding to the 13-fold elongated reaction product. The reaction was performed at 65°C reaction temperature followed by diphosphate hydrolysis. Additionally, the isotopic pattern can be seen.

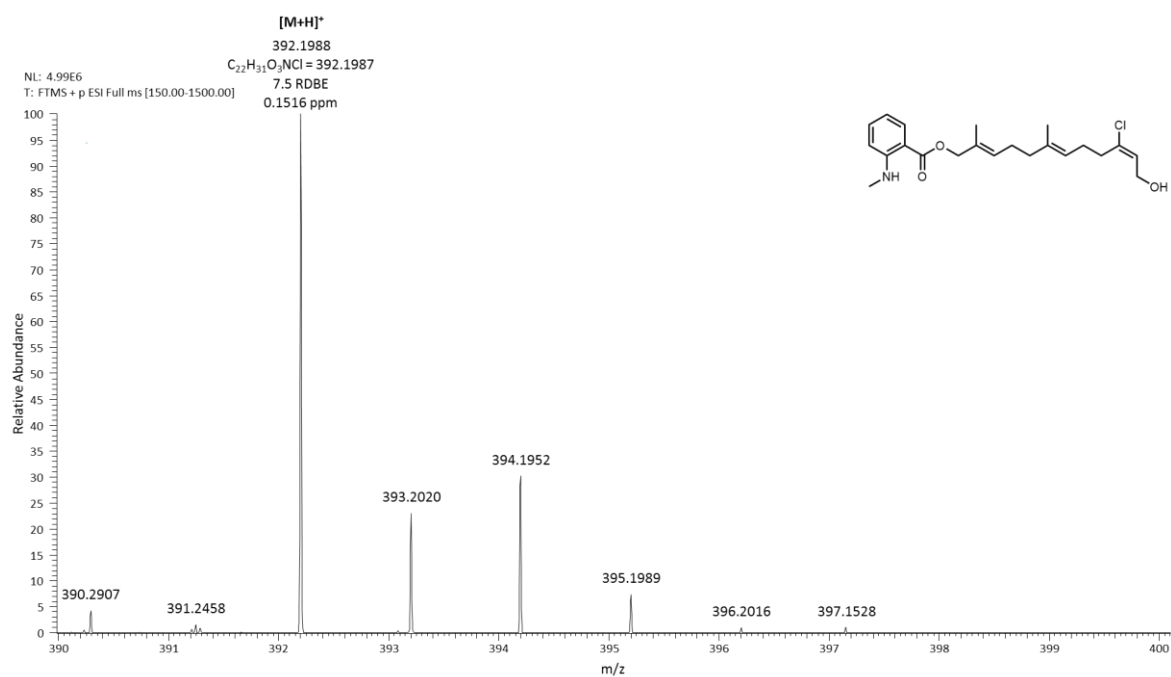


**Figure A17** HR-ESI-MS spectrum of the  $[M+H]^+$  ion ( $C_{22}H_{31}O_3NCl$ ) of the ThkCPT reaction with MANT-O-GPP and Cl-BPP constituting the 1-fold elongated product. The reaction was performed at 65°C reaction temperature followed by diphosphate hydrolysis. Additionally, the isotopic pattern can be seen.

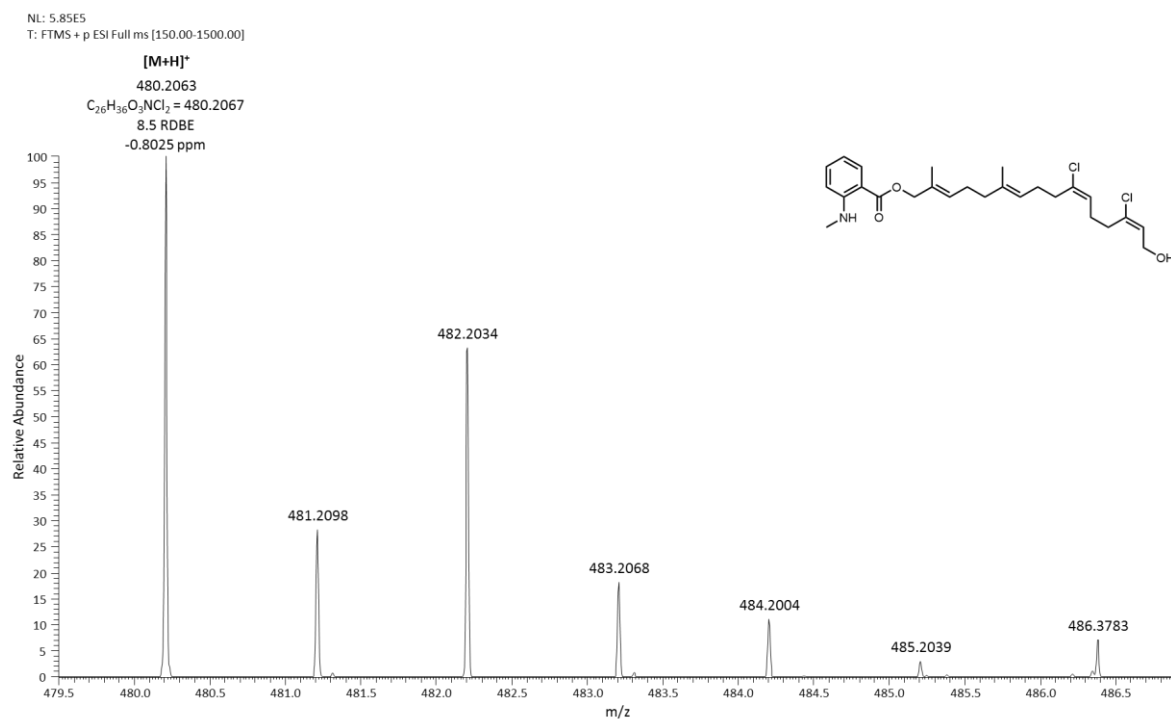


**Figure A18** HR-ESI-MS spectrum of the  $[M+H]^+$  ion ( $C_{26}H_{36}O_3NCl_2$ ) of the ThkCPT reaction with MANT-O-GPP and Cl-BPP constituting the 2-fold elongated product. The reaction was performed at 65°C reaction temperature followed by diphosphate hydrolysis. Additionally, the isotopic pattern can be seen.

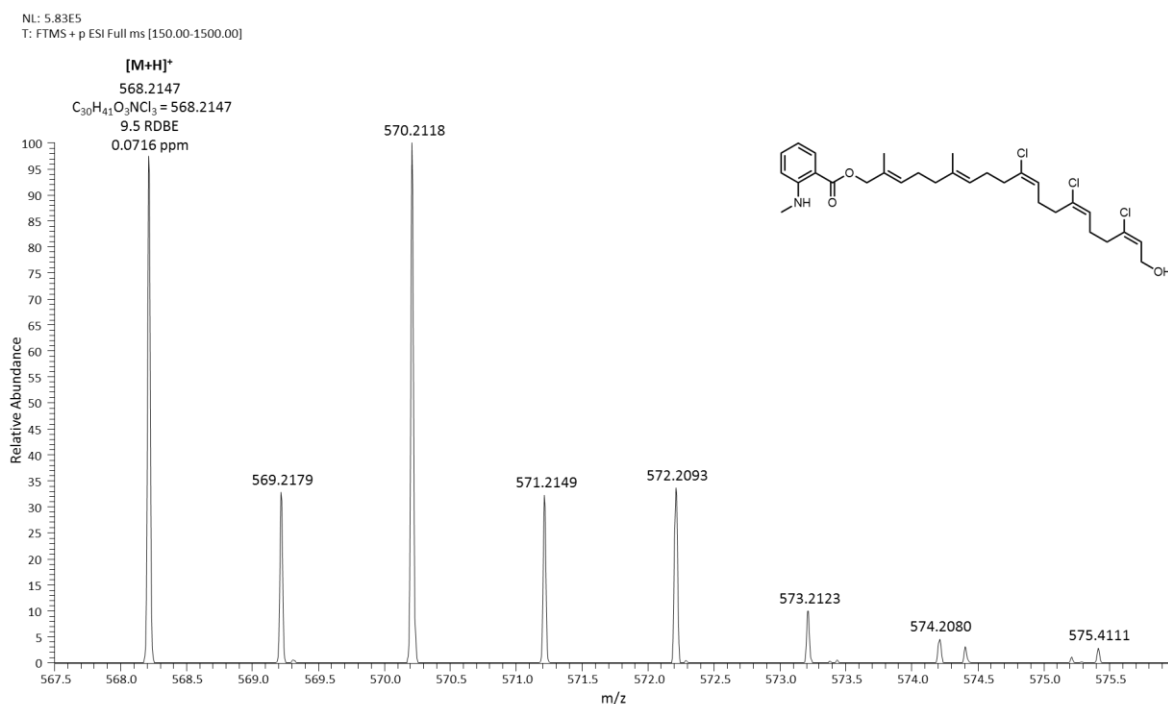


**Figure A19** HR-ESI-MS spectrum of the  $[M+H]^+$  ion ( $C_{30}H_{41}O_3NCl_3$ ) of the ThkCPT reaction with MANT-O-GPP and Cl-BPP constituting the 3-fold elongated product. The reaction was performed at 65°C reaction temperature followed by diphosphate hydrolysis. Additionally, the isotopic pattern can be seen.

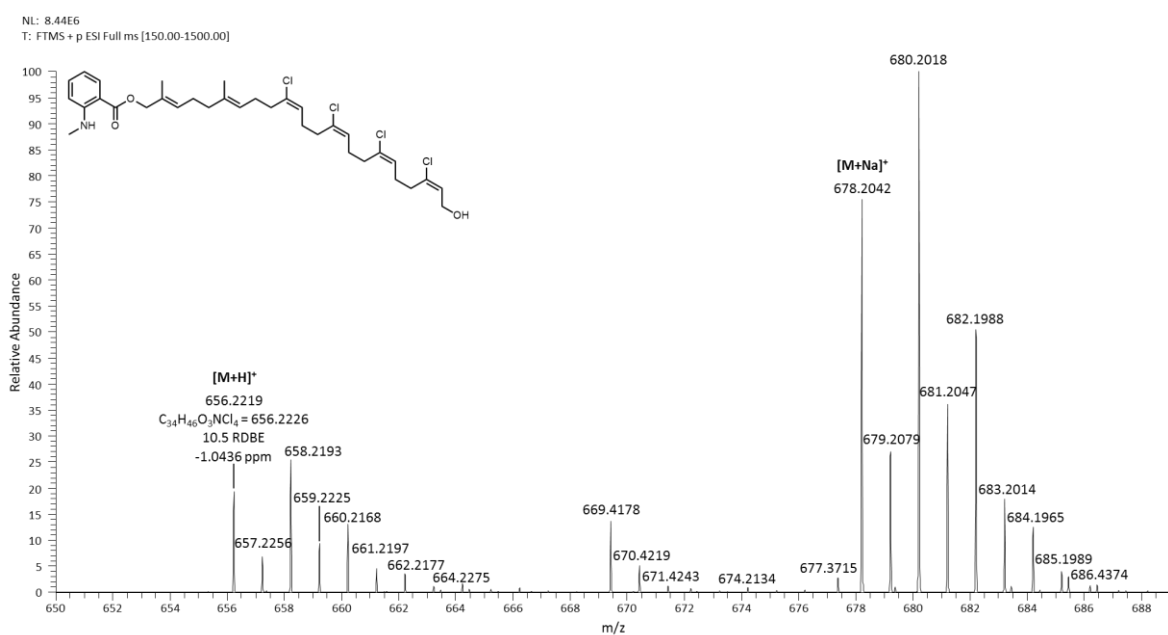


**Figure A20** HR-ESI-MS spectrum of the  $[M+H]^+$  ion ( $C_{34}H_{46}O_3NCl_4$ ) of the ThkCPT reaction with MANT-O-GPP and Cl-BPP constituting the 4-fold elongated product. The reaction was performed at 65°C reaction temperature followed by diphosphate hydrolysis. Additionally, the sodium adduct and the isotopic pattern can be seen.

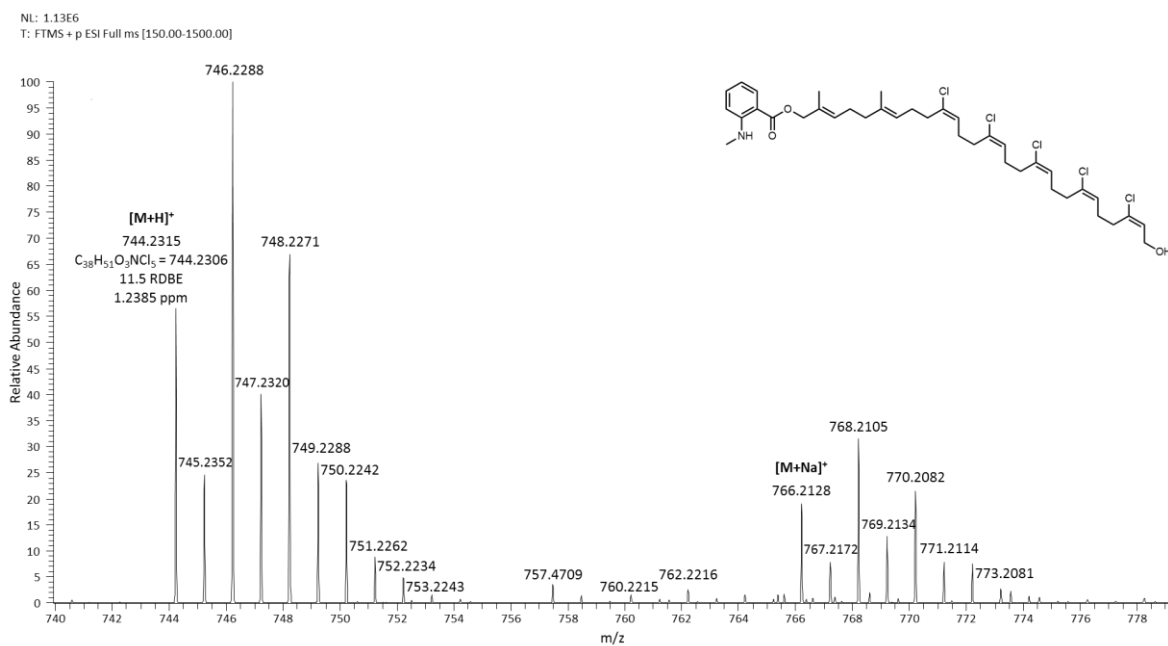


**Figure A21** HR-ESI-MS spectrum of the  $[M+H]^+$  ion ( $C_{38}H_{51}O_3NCl_5$ ) of the ThkCPT reaction with MANT-O-GPP and Cl-BPP constituting the 5-fold elongated product. The reaction was performed at 65°C reaction temperature followed by diphosphate hydrolysis. Additionally, the sodium adduct and the isotopic pattern can be seen.

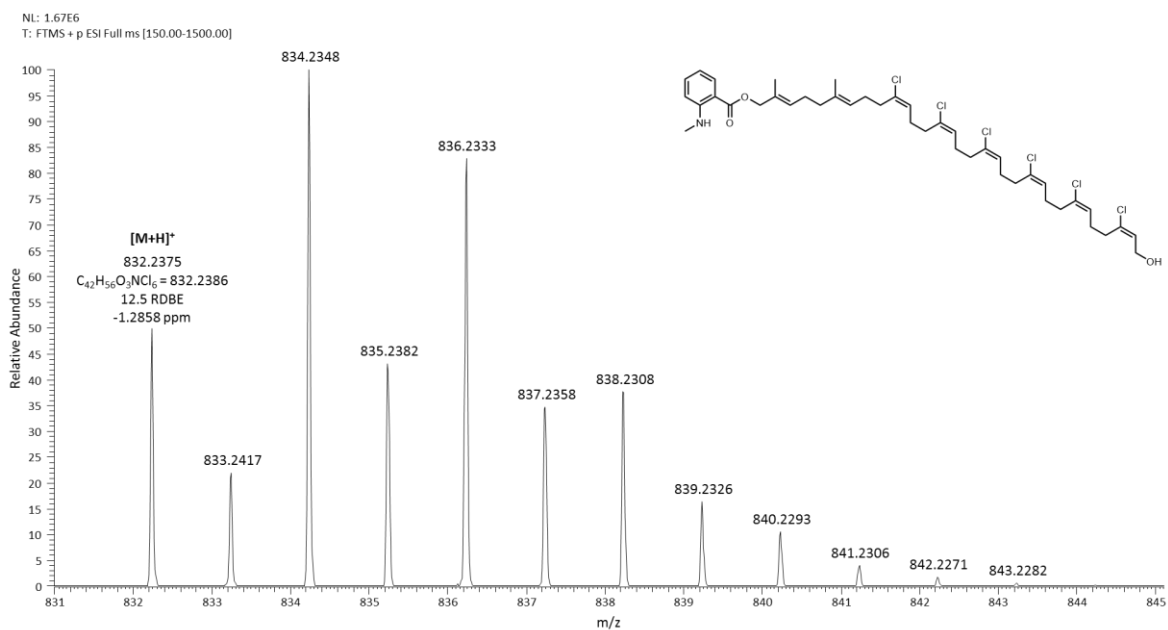


**Figure A22** HR-ESI-MS spectrum of the  $[M+H]^+$  ion ( $C_{42}H_{56}O_3NCl_6$ ) of the ThkCPT reaction with MANT-O-GPP and Cl-BPP constituting the 6-fold elongated product. The reaction was performed at 65°C reaction temperature followed by diphosphate hydrolysis. Additionally, the isotopic pattern can be seen.



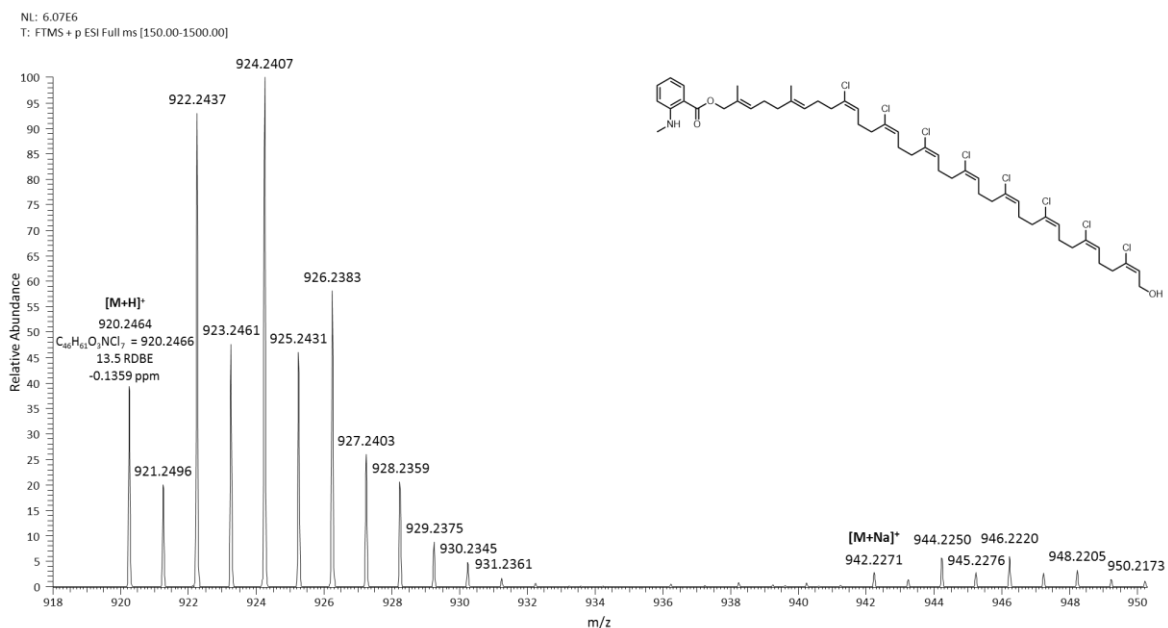


**Figure A23** HR-ESI-MS spectrum of the  $[M+H]^+$  ion ( $C_{46}H_{61}O_3NCl_7$ ) of the ThkCPT reaction with MANT-O-GPP and Cl-BPP constituting the 7-fold elongated product. The reaction was performed at 65°C reaction temperature followed by diphosphate hydrolysis. Additionally, the sodium adduct and the isotopic pattern can be seen.

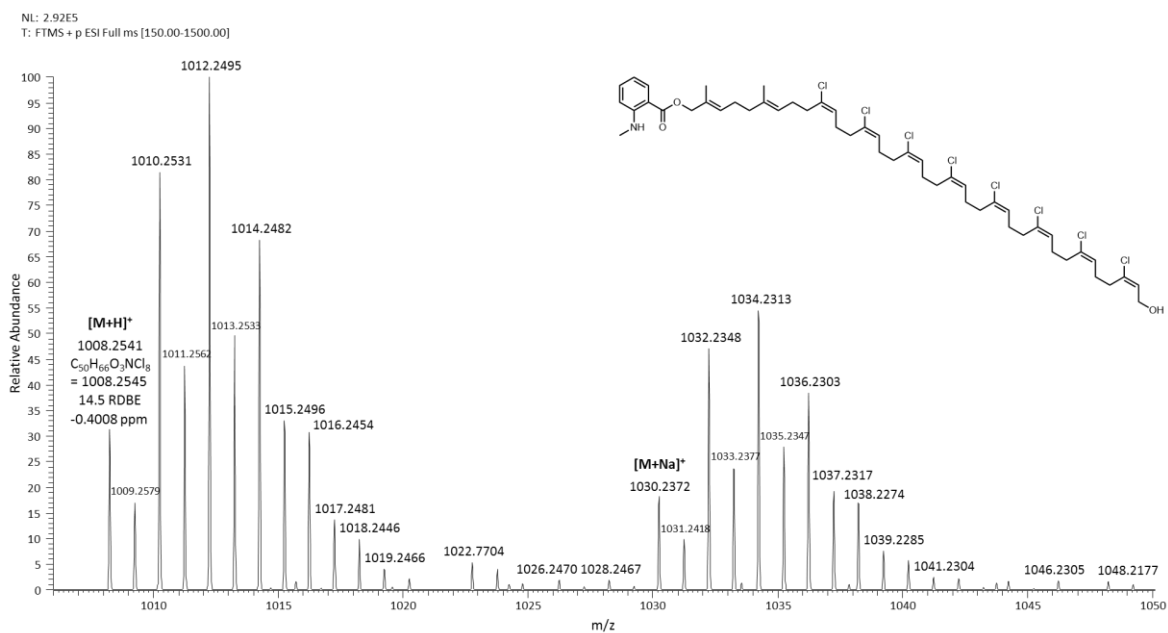


**Figure A24** HR-ESI-MS spectrum of the  $[M+H]^+$  ion ( $C_{50}H_{65}O_3NCl_8$ ) of the ThkCPT reaction with MANT-O-GPP and Cl-BPP constituting the 8-fold elongated product. The reaction was performed at 65°C reaction temperature followed by diphosphate hydrolysis. Additionally, the sodium adduct and the isotopic pattern can be seen.

## 8.7. In-house designation of experiments

**Table A6** Overview of the experiments carried out and their in-house code.

Experiment name	In-house code
Plasmid preparation	PSP163, PSP269, PSP281, PSP322, PSP325, PSP358, PSP366, PSP368, PSP375, PSP384, PSP388, PSP390, PSP392, PSP398, PSP400
Transformation	PSP163, PSP268, PSP279, PSP280, PSP282, PSP284, PSP324, PSP354, PSP360, PSP367, PSP389, PSP427
Site-directed mutagenesis	PSP163, PSP353, PSP356, PSP363, PSP386, PSP387
Colony PCR	PSP163, PSP365, PSP388, PSP390
Truncation of AtCPT (PCR)	PSP323
Agarose gel electrophoresis	PSP163, PSP323, PSP353
Recombinant protein production - ThkCPT	PSP174, PSP190, PSP198, PSP235, PSP238, PSP314, PSP346, PSP359, PSP364, PSP369, PSP399, PSP401, PSP404, PSP408, PSP413, PSP418, PSP428, PSP430
- AtCPT	PSP265, PSP270, PSP285, PSP288, PSP303, PSP304, PSP326, PSP331, PSP339
- in MTP	PSP391
Cell lysis by osmotic shock	PSP347, PSP350
Immobilized metal ion affinity chromatography (IMAC) - ThkCPT	PSP167, PSP177, PSP206, PSP207, PSP209, PSP236, PSP239, PSP316, PSP405, PSP409; PSP410, PSP414, PSP417, PSP420, PSP426, PSP429, PSP431, PSP433, PSP435
- AtCPT	PSP272, PSP286, PSP296, PSP305, PSP309, PSP317, PSP327, PSP328, PSP332, PSP333, PSP340, PSP343
Preparation of periplasmic extracts	PSP289

Dialysis	PSP252, PSP255
Concentrating of protein samples	PSP295
SDS-PAGE	PSP291, PSP318, PSP327, PSP434
Activity assay for the CPTs	
- standard conditions	PSP224, PSP232, PSP290, PSP297, PSP307, PSP310, PSP312, PSP315, PSP319, PSP329, PSP335, PSP337, PSP341, PSP344, PSP376, PSP411, PSP436
- time dependence	PSP202, PSP212
- without Triton X-100	PSP222
- biphasic system	PSP260
- alternative bivalent cations	PSP240, PSP244, PSP256
- crude extracts	PSP348, PSP351, PSP381
- in MTP	PSP393
- ThkCPT variants	PSP370, PSP402, PSP406
Thin layer chromatography	PSP292, PSP298, PSP396
Fluorescence-based HPLC	
- dependence on Triton X-100	PSP223
- alternative substrates	PSP225, PSP321
- alternative bivalent cations	PSP257
- biphasic system	PSP262
- MANT-O-Geraniol calibration line	PSP294, PSP302
- ThkCPT variants	PSP371, PSP403
- AtCPT	PSP302
Product fractionation (HPLC)	
- CI-BPP	PSP226
- IPP	PSP437
Solid phase extraction	PSP440
HR-ESI-MS	
- CI-BPP	PSP233
- IPP	PSP442

## Acknowledgement

First of all, I would like to thank Prof. Dr. Ludger Wessjohann for the opportunity to prepare my thesis in the department of Bioorganic Chemistry at the Leibniz Institute of Plant Biochemistry and for the supply of the interesting topic as well as for guidance and editing of the thesis. I am also grateful for the possibility to take part in several national and international conferences.

I thank Dr. Jeanette Ludwig, née Keim, for her advice and the helpful instructions at the beginning of my doctoral studies. I also thank Dr. Steve Ludwig for the synthesis of the prenyl diphosphates used in this study.

I am very grateful for a lot of scientific discussions and encouragement during my doctoral studies I received from Dr. Danilo Meyer, Dr. Martin Dippe and the whole Biocatalysis working group. Your advices for experiments, talks, presentations or posters were greatly appreciated. I also thank Dr. Martin Dippe for a first proofreading and for his support at the end of my thesis.

For the support concerning the analytics I thank Dr. Jürgen Schmidt, Dr. Andrej Frolov and Annegret Laub for the HR-ESI-MS measurements as well as the data evaluation. I thank Dr. Andrea Porzel for her help with NMR measurements (even if the results are not written down in the thesis). And I am very grateful for the support I received from Anja Ehrlich with the HPLC. She was always very helpful and had an open ear for upcoming questions. Furthermore, I thank Dr. Wolfgang Hoehenwarter, Petra Majovsky and Domenika Thieme for their help with the analysis of the AtCPT peptide fragments via LC-ESI-MS.

I thank PD Dr. Wolfgang Brandt for his help with the computational chemistry and for generating and analyzing the homology model of the ThkCPT for following mutagenesis studies.

I thank Prof. Dr. Uwe Bornscheuer for the opportunity to work in his group at the University of Greifswald during a short-term stay. There, I learned much about automated processes and directed evolution (error prone PCR). I also thank Dr. Dominique Böttcher and Dr. Mark Dörr for their support during my stay. Furthermore, I thank Hubert Kasprowski for the tunnel analysis of the ThkCPT homology model.

I thank the whole Bioorganic Chemistry department for the pleasant atmosphere and a lot of help and discussions - also apart from the daily working routine. I have enjoyed working with you and it was fun, spending summer and Christmas parties with you. A huge thank also goes to the technical staff - without you, nothing would work.

I thank Michelle Kammel, Pauline Stark, Sarah Scharfenberg, Robert Berger and David Edeler for helpful scientific discussions and Sarah for her help to fully understand the calculations of the limit of detection. Besides that I also thank you for a lot of nice lunch breaks, funny leisure activities and overall good times.

I also thank Rica Patzschke, Frank Lange and Henrik Teuscher for all the nice lunch and coffee breaks we spend together and also for their support concerning the scientific part.

I especially thank Annegret Laub, Katharina Wolf and Susann Herrmann. The time flew by and we had a lot of nice moments together. Both, professionally and privately, you were always there and made the world a better place.

I also thank my friends from school time, Anne Guhra, Sandra Ihme and Christiane Rohr, for distraction from everyday life. I am very happy that we are still in contact and meet as often as possible.

Most notably I thank my parents and my whole family - you enabled my education and the following doctorate and you always supported me, with no ifs and buts. Without you this would not have been possible. I love you!

Last but not least I thank Felix Ölke who was always able to put a smile on my face :)

## Curriculum vitae

### Personal details

Name Pia Schöne  
Date of Birth 04.02.1989  
Place of Birth Halle (Saale)  
Nationality German

### Professional experience

07/2018 - present **Research associate**  
Formulation of nanoparticulate drug delivery systems  
Lipocalyx GmbH, Halle (Saale)

### Higher education

11/2013 - 12/2017 **PhD thesis**  
*Enzymatic synthesis of natural artificial polyprenols*  
Leibniz Institute of Plant Biochemistry, Halle (Saale)  
Department of Bioorganic Chemistry  
Supervisor: Prof. Ludger A. Wessjohann

03/2013 - 10/2013 **Master thesis**  
*Investigation of enzymatic reactions by NMR spectroscopy*  
Leibniz Institute of Plant Biochemistry, Halle (Saale)  
Department of Bioorganic Chemistry  
Supervisor: Dr. Andrea Porzel

10/2011 - 02/2013 **Master's program in biochemistry**  
Martin-Luther-Universität Halle-Wittenberg, Halle (Saale)  
Degree: Master of Science

04/2011 - 08/2011 **Bachelor thesis**  
*Phytochemical studies on *Suillus* species with different mass spectrometric methods*  
Leibniz Institute of Plant Biochemistry, Halle (Saale)  
Department of Bioorganic Chemistry  
Supervisor: Dr. Jürgen Schmidt

10/2007 - 03/2011 **Bachelor's program in biochemistry**  
Martin-Luther-Universität Halle-Wittenberg, Halle (Saale)  
Degree: Bachelor of Science

### School education

09/2001 - 07/2007 **Abitur**  
Burg-Gymnasium Wettin, Wettin

### Additional work

08/2011 - 06/2012 **Student assistant**  
Leibniz Institute of Plant Biochemistry, Halle (Saale)  
Department of Bioorganic Chemistry

### Postgraduate training

10/2014 User Training LC + ChemStation (Agilent Technologies), Halle (Saale)  
09/2014 22<sup>nd</sup> Conference on Isoprenoids, Prague  
07/2014 GMP Training Course (SFI Halle), Halle (Saale)  
01/2014 User Training Orbitrap Elite, Halle (Saale)  
10/2011 Multivariate Data Analysis for "Omics"

### Publications

2015 Michels, K., Heinke, R., Schöne, P., Kuipers, O. P., Arnold, N. and Wessjohann, L. (2015) A fluorescence-based bioassay for antibacterials and its application in screening natural product extracts, *The Journal of Antibiotics*, **68**: 734-740. doi: 10.1038/ja.2015.71

2014 Heinke, R., Schöne, P., Arnold, N., Wessjohann, L., Schmidt, J. (2014) Metabolite profiling and fingerprinting of *Suillus* species (Basidiomycetes) by electrospray mass spectrometry, *European Journal of Mass Spectrometry*, **20**: 85-97. doi: 10.1255/ejms.1235

### Posters

06/2015 11<sup>th</sup> Plant Science Student Conference, Halle (Saale)  
08/2016 8<sup>th</sup> International Congress on Biocatalysis, Hamburg-Harburg

**Talks**

- 04/2016            51<sup>st</sup> Naturstofftreffen, Bayreuth  
09/2016            23<sup>rd</sup> Conference on Isoprenoids, Minsk  
06/2017            13<sup>th</sup> Plant Science Student Conference, Halle (Saale)

---

Place, Date

---

(Pia Schöne)



## **Statutory declaration/Eidesstattliche Erklärung**

I declare that I have authored this thesis independently, that I have not used other than the declared sources/resources, and that I have explicitly marked all material which has been quoted either literally or by content from the used sources. Additionally, I declare that this is the first time I apply for the acquisition of the doctoral degree with the present scientific work.

Hiermit erkläre ich, dass ich die vorliegende Arbeit selbstständig und ohne fremde Hilfe verfasst habe. Andere als die von mir angegebenen Quellen und Hilfsmittel habe ich nicht benutzt und die den benutzten Werken wörtlich oder inhaltlich entnommenen Stellen habe ich als solche kenntlich gemacht. Außerdem erkläre ich, dass ich mich mit der vorliegenden wissenschaftlichen Arbeit erstmals um die Erlangung des Doktorgrades bewerbe.

---

Place, Date

---

(Pia Schöne)